



Investigation of the effects of star-disc encounter on protoplanetary disc size

Masterarbeit in Astrophysik

von
Asmita Bhandare

angefertigt im Institut

Max-Planck-Institut für Radioastronomie, Bonn

vorgelegt der

Mathematisch-Naturwissenschaftlichen Fakultät

der

Rheinische Friedrich-Wilhelms-Universität Bonn

October 2015

Gutachterin 1: Prof. Dr. Susanne Pfalzner

Gutachter 2: Prof. Dr. Pavel Kroupa

Declaration of Authorship

I, Asmita Bhandare, hereby declare that this thesis titled, "Investigation of the effects of star-disc encounter on protoplanetary disc size" was formulated by myself and the work presented in it are my own. I confirm that:

- This work was done wholly or mainly while in candidature for a Masters degree at the University of Bonn.
- Where I have consulted the published work of others, this is always clearly attributed.
- Where I have quoted from the work of others, the source is always given. With the exception of such quotations, this thesis is entirely my own work.
- I have acknowledged all main sources of help.

Signed:

Date:

Abstract

Most, if not all, young stars are initially surrounded by protoplanetary discs. Owing to the preferential formation of stars in stellar clusters, the protoplanetary discs around these stars may be affected by the cluster environment. Various works have investigated the influence of stellar fly-bys on discs, although most of them consider only the effects due to parabolic, coplanar encounters, which is only a special case. The few studies that do consider inclined encounters focus mainly on the disc mass loss and angular momentum loss. Here, the first parameter study of the effect of *inclined* encounters on the **disc size** is presented. This is important because the disc size determines the maximum extent of the potentially forming planetary systems. We perform numerical simulations to study the fate of protoplanetary discs due to the impact of parabolic star-disc encounter for the less investigated case of inclined and retrograde encounters. Here, we concentrate on the disc size after such encounters at different periastron distances and for different mass ratios between the perturber and the central star. With this study we cover the parameter space relevant for typical cluster environments. We find that despite the prograde encounters having the strongest effect on the disc size, inclined and even the least destructive retrograde encounters mostly also have a considerable effect, especially for close periastron passages. We find a nearly linear dependence of the disc size on the orbital inclination for the prograde encounters but the situation is more complex for the retrograde cases. These results can be applied directly to cluster simulations to determine the disc size distribution in different cluster environments. We also determine the final orbital parameters of the particles in the disc such as eccentricities, inclinations and semi-major axes. Using this information the presented study can not only be used to describe the fate of discs but also that of planetary systems after inclined encounters. In a follow up study we will investigate the possible connection between inclined encounters and Sedna-like objects in our solar system.

Acknowledgements

Success in any endeavor depends a lot on the support, guidance and encouragement received from our guides, friends and parents. The desire to excel and get close to perfection helps us motivate ourselves into giving the best in our means.

I firstly would like to express my deep gratitude to my supervisor, Prof. Dr. Susanne Pfalzner. I would like to thank her for the constant guidance and motivation throughout the entire thesis. Her encouragement and patience has definitely helped my academic growth and made me a better student. I would like to thank Prof. Dr. Pavel Kroupa for agreeing to be the second supervisor for the Master thesis and for his timely inputs and suggestions during this period. I would also like to thank Prof. Dr. Karl Menten for giving me the opportunity to work in the Minerva Research group of the sub-millimeter group at the Max Planck Institute for Radioastronomy (MPIfR, Bonn). I would like to thank my entire group, Kirsten Vincke, Andreas Breslau, Dr. Meng Xiang-Gruess and Mai Xiang for providing me with a co-operative and enthusiastic work environment. I have to extend my thanks to Andreas Breslau who helped me during the initial phase of the thesis with the numerical setup used for this project and for all the discussions to solve the physical complexities of the problem. I am truly grateful to Kirsten Vincke who has always been available and equally excited for discussions and for her valuable inputs and constant support throughout this year.

I would like to thank all my fellow master students and friends in Bonn for their suggestions and opinions which has helped me remain passionate about my work. My stay in Bonn has been an enjoyable learning experience both academically and otherwise. This experience has surely granted me a glimpse of the “bigger picture”, a deeply rewarding one.

I am personally indebted to my parents, sister and all my friends back home for their constant love, support and encouragement over all these years which has always given me the freedom and inspired me to strive towards my goals. Lastly, I would like to thank everyone who has believed in my abilities and more importantly those who have challenged them.

Contents

Declaration of Authorship	v
Abstract	vii
Acknowledgements	ix
List of Figures	xiii
List of Tables	xv
1 Introduction	1
2 Overview and Background	3
2.1 From clouds to discs	3
2.1.1 Developmental stages of protoplanetary discs	4
2.2 Protoplanetary disc structure	9
2.3 Influence of cluster environment	13
2.3.1 External Photoevaporation	14
2.3.2 Stellar Encounters	15
2.4 Motivation and Aim	18
3 Method	19
3.1 Numerical Method	19
3.1.1 Initial Setup	20
3.1.2 Initial conditions for inclined encounters	23
3.2 Disc-size determination	25
4 Results	29
4.1 Dependence on orbital inclination	31
4.1.1 Prograde vs Retrograde Encounters	31
4.1.2 Coplanar vs Inclined Encounters	33
4.2 Dependence on orbital orientation	41
4.3 Dependence on mass ratio and periastron distance	45
4.4 Dependence on initial disc size	49
5 Discussion	51
5.1 Limitations of the model	51

5.2 Comparisons to previous work	55
6 Summary and Conclusion	57
Appendices	61
A Numerical Recipe for star-disc encounters	63
B Disc sizes after encounter by a perturber on an orbit with $aop = 0^\circ$	67
C Disc sizes after encounter by a perturber on an orbit with $aop = 45^\circ$	71
D Disc sizes after encounter by a perturber on an orbit with $aop = 90^\circ$	75
E Disc size as a function of orbital inclination	79
Bibliography	83

List of Figures

2.1	Formation stages of protoplanetary discs	4
2.2	Schematic picture of a spectral energy distribution of a protoplanetary disc	5
2.3	Evolutionary stages of young stellar objects	7
2.4	Protoplanetary disc structure	9
2.5	ALMA & Hubble images of protoplanetary discs	10
3.1	Timeline of a star-disc encounter	21
3.2	Orientations of the perturber orbit	23
3.3	Surface density profiles of a disc before and after an encounter	26
4.1	Disc size as a function of orbital inclinations for prograde and retrograde encounters at different periastron distances	30
4.2	Disc size as a function of orbital inclinations for encounters by a perturber on orbits with different orientations	32
4.3	Face-on and edge-on view showing particle inclinations for prograde and retrograde encounters	34
4.4	Face-on and edge-on view showing particle eccentricities for prograde and retrograde encounters	36
4.5	Schematics explaining the effect of angular momentum	38
4.6	Disc size as a function of orbital inclinations for different mass ratios . .	39
4.7	Disc size comparison for different orientations of the perturber orbit . .	40

4.8	Face-on view of discs showing particle inclinations after an encounter by a perturber on orbits with different orientations	42
4.9	Face-on view of discs showing particle eccentricities after an encounter by a perturber on orbits with different orientations	43
4.10	Disc-size change as a function of periastron distance for different mass ratios	44
4.11	Face-on view of discs after an encounter for different mass ratios	46
4.12	Face-on view of discs after an encounter at different periastron distances	48
4.13	Final disc size comparison for different initial disc sizes	50
5.1	Disc size comparison with previous work	54
5.2	Disc size comparison for different inclinations of the perturber orbit . . .	56

List of Tables

2.1	Observational classification of young stellar objects	6
3.1	Parameter ranges of the simulated star-disc encounters	25
B.1	Disc sizes for encounter parameters: $aop = 0^\circ$ and $m_{12} = 0.3$	68
B.2	Disc sizes for encounter parameters: $aop = 0^\circ$ and $m_{12} = 0.5$	68
B.3	Disc sizes for encounter parameters: $aop = 0^\circ$ and $m_{12} = 1$	68
B.4	Disc sizes for encounter parameters: $aop = 0^\circ$ and $m_{12} = 2$	69
B.5	Disc sizes for encounter parameters: $aop = 0^\circ$ and $m_{12} = 5$	69
B.6	Disc sizes for encounter parameters: $aop = 0^\circ$ and $m_{12} = 10$	69
B.7	Disc sizes for encounter parameters: $aop = 0^\circ$ and $m_{12} = 20$	70
B.8	Disc sizes for encounter parameters: $aop = 0^\circ$ and $m_{12} = 50$	70
C.1	Disc sizes for encounter parameters: $aop = 45^\circ$ and $m_{12} = 0.3$	72
C.2	Disc sizes for encounter parameters: $aop = 45^\circ$ and $m_{12} = 0.5$	72
C.3	Disc sizes for encounter parameters: $aop = 45^\circ$ and $m_{12} = 1$	72
C.4	Disc sizes for encounter parameters: $aop = 45^\circ$ and $m_{12} = 2$	73
C.5	Disc sizes for encounter parameters: $aop = 45^\circ$ and $m_{12} = 5$	73
C.6	Disc sizes for encounter parameters: $aop = 45^\circ$ and $m_{12} = 10$	73
C.7	Disc sizes for encounter parameters: $aop = 45^\circ$ and $m_{12} = 20$	74
C.8	Disc sizes for encounter parameters: $aop = 45^\circ$ and $m_{12} = 50$	74

D.1	Disc sizes for encounter parameters: $aop = 90^\circ$ and $m_{12} = 0.3$	76
D.2	Disc sizes for encounter parameters: $aop = 90^\circ$ and $m_{12} = 0.5$	76
D.3	Disc sizes for encounter parameters: $aop = 90^\circ$ and $m_{12} = 1$	76
D.4	Disc sizes for encounter parameters: $aop = 90^\circ$ and $m_{12} = 2$	77
D.5	Disc sizes for encounter parameters: $aop = 90^\circ$ and $m_{12} = 5$	77
D.6	Disc sizes for encounter parameters: $aop = 90^\circ$ and $m_{12} = 10$	77
D.7	Disc sizes for encounter parameters: $aop = 90^\circ$ and $m_{12} = 20$	78
D.8	Disc sizes for encounter parameters: $aop = 90^\circ$ and $m_{12} = 50$	78

Chapter 1

Introduction

The discoveries of extrasolar planets and recent observations of protoplanetary discs surrounding stars in stellar clusters have been milestones in understanding some of the most fundamental questions regarding the formation and evolution of planetary systems in addition to our own solar system. In order to formulate planet formation theories and understand the physical mechanisms involved in the evolutionary processes, it is important to investigate the properties of protoplanetary discs which provide the basic material required for the formation of such planetary systems.

In accordance with the currently accepted star formation scenarios, most young stars are not formed in isolation but as a part of a star cluster. These stars formed due to gravitational collapse of dense cores in molecular clouds, are at least initially surrounded by protoplanetary discs as a consequence of conservation of angular momentum.

The cluster environment might have significant effects on the protoplanetary discs and hence it is important to parameterize the disc properties like disc mass, angular momentum, energy, disc size etc. Stellar encounters in such environments can truncate the protoplanetary discs and most matter beyond this truncation radius can become unbound. The truncation radius hence proves to be useful to constrain the region within which enough matter would be available for planet formation.

In this thesis we investigate the effects of gravitational interaction during fly-bys on the disc size. Almost all the investigations done so far to estimate the disc sizes have been restricted to equal-mass, parabolic, coplanar encounters. Here the main aim is to extend the parameter space to investigate the effects due to inclined as well as retrograde encounters and study the dependence of the final disc size on the inclinations and orientations of the perturber orbit, mass of the perturbing star and the periastron distance.

An overview of the formation and evolution of stars and their surrounding discs is presented in chapter 2. Chapter 3 provides a detailed discussion of the numerical setup

involved in the simulations performed for the studies done here. The disc size definition used to determine the disc sizes for different encounter scenarios is also presented. In chapter 4, the effects of inclined prograde and retrograde encounters are compared to the most widely studied case of coplanar encounters. Further, the dependence of the disc size on the mass ratio between the perturber mass and mass of the central star, periastron distance, inclination and orientation of the perturber orbit is also discussed in this chapter. The limitations of the numerical model used in the studies presented here and the comparison to the previous work is detailed in chapter 5. Lastly, the results obtained from the studies done here for different encounter scenarios is summarized in chapter 6.

Chapter 2

Overview and Background

This chapter gives an overview on the current knowledge of protoplanetary discs. In § 2.1, particularly, the formation and evolution stages of young stars and the surrounding protoplanetary discs is discussed briefly, followed by a summary of the properties and structure of the disc relevant to this work in § 2.2. Owing to the preferential formation of stars in stellar clusters, the cluster environment might have an effect on protoplanetary discs. Hence, in § 2.3, the potential influence of the cluster environment on these discs is detailed and the motivation and goals of this thesis are presented in § 2.4.

2.1 From clouds to discs

Protoplanetary discs provide the basic material in the form of gas and dust, required for the formation of planetary systems. As illustrated in Fig. 2.1, protoplanetary discs are formed around most stars during the early stages of star formation as a consequence of conservation of angular momentum during the collapse of a molecular cloud core. Usually such star-disc systems exist not in isolation but as a part of a star cluster [Clarke et al., 2000, Lada and Lada, 2003, Porras et al., 2003]. These star clusters are formed due to gravitational collapse of dense, cool clumps in molecular clouds. With an extent of tens of parsecs, low temperature (~ 10 K), low density ($n \sim 10^2 \text{ cm}^{-3}$), masses in the range $10^4 - 10^6 M_{\odot}$, lifetime $\sim 10^6$ yr, and composed mainly of molecular hydrogen (H_2) these molecular clouds, mostly found in the spiral arms of galaxies, are highly structured, consisting of numerous filaments, clumps, and dense cores [André et al., 2014]. It is in these dense cores ($n \sim 10^5 \text{ cm}^{-3}$) with masses $\sim 1 - 2 M_{\odot}$ and of scales ~ 0.1 pc where the star formation processes occur [Larson, 2003]. The next section describes the formation and evolution stages of stars and their surrounding discs.

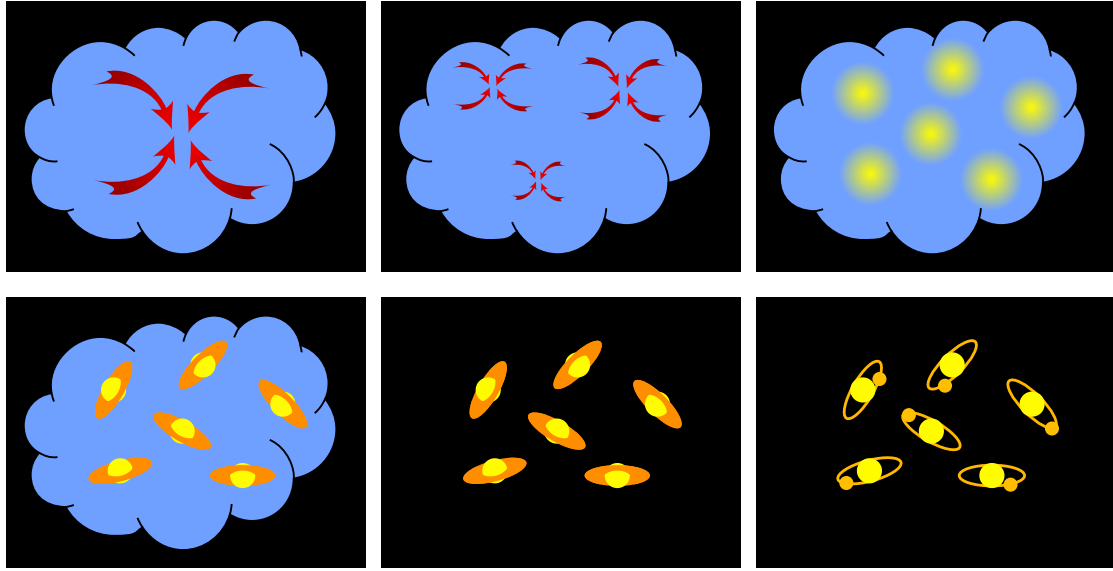


FIGURE 2.1: Formation stages of protoplanetary discs around stars in stellar clusters (image courtesy: Andreas Breslau).

2.1.1 Developmental stages of protoplanetary discs

The first stage of star formation corresponds to turbulent fragmentation of the molecular clouds into gravitationally bound cores which are initially supported against gravity by a combination of thermal, turbulent, and magnetic pressure forces. These gravitationally bound cores become unstable and collapse to form hydrostatic protostellar objects surrounded by a rapidly rotating accretion disc embedded in an infalling envelope of dust and gas. The minimum mass required to obtain gravitationally unstable density fluctuations, known as the Jeans mass, is given by

$$M_J = \frac{5.57 c_s^3}{G^{3/2} \rho^{1/2}}. \quad (2.1)$$

In the above equation, ρ is the uniform density, G is the gravitational constant ($\approx 6.67 \times 10^{-11} \text{ m}^3 \text{ kg}^{-1} \text{ s}^{-2}$) and the isothermal sound speed c_s ¹ = $\sqrt{k_B T / m}$ where m is the average particle mass, T is the gas temperature and k_B is the Boltzmann constant ($\approx 1.38 \times 10^{-23} \text{ J/K}$).

The general understanding is that due to the rotation of the parent cloud and the embedded star, the infall is not spherically symmetric but the surrounding matter forms a disc geometry before being transported onto the stellar surface. These accretion discs play a major role in the redistribution of angular momentum via disk instabilities as well as by shear in a differentially rotating disc. Gradually the central core gains mass via disc accretion due to infall of the collapsing material and develops a collimated bipolar outflow (for an overview of the accretion processes see Hartmann [2009] and

¹ $c_s \approx 344 \text{ m/s}$ in dry air at 20° C.

references therein). The surrounding disc is thought to dissipate over a disc lifetime of 3 - 10 Myr as most of the material is accreted onto the central star or forms planets via gravitational instability² or core accretion³. For an overview of processes involved in the formation and evolution of stars and protoplanetary discs from giant molecular clouds see Lada, Andre et al. [2000], Larson [2003], Cesaroni et al. [2007], Armitage [2009], Williams and Cieza [2011], Li et al. [2014], Armitage [2015] and references therein.

An increasing observational evidence from the optical, infrared and millimeter photometry of young stellar objects indicates the presence of discs around pre-main sequence stars observed either as optically resolved images or as excess emission over the stellar photospheric contribution. A schematic picture of a spectral energy distribution (SED) illustrating the components from different regions of the disc emitting at different wavelength regimes is shown in Fig. 2.2.

Depending on the infrared (IR) excess in their spectral energy distribution, the young stellar objects (YSOs) can be classified in to four classes based on the slope of the SED,

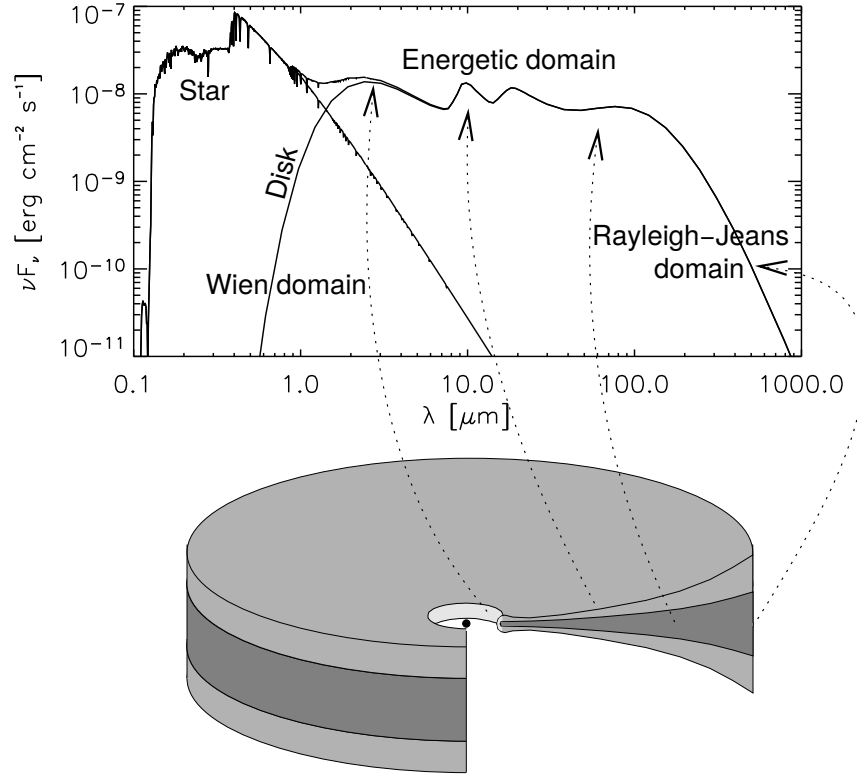


FIGURE 2.2: Schematic picture of a spectral energy distribution of a protoplanetary disc [Dullemond et al., 2007].

²Gravitational instability is a single-step process that leads to growth of small bodies to planetesimals which is driven by the gravitational collapse of large portions of the unstable disk.

³Core accretion involves formation of protoplanetary cores via a multistage process of dust coagulation.

TABLE 2.1: Observational classification of young stellar objects

Class	Phase	IR spectral index	Physical Properties	Observational Characteristics
Class 0	Young Accreting Protostar	–	$M_{\text{env}} > M_* > M_{\text{disc}}$, $T_{\text{bol}} < 70 \text{ K}$	Far-IR or sub-millimeter emission, no optical or near-IR emission
Class I	Evolved Accreting Protostar	$\alpha_{\text{IR}} > 0.3$	$M_* > M_{\text{env}} \sim M_{\text{disc}}$, $T_{\text{bol}} \sim 70 - 650 \text{ K}$	Near-IR and mid-IR emission, optically obscured
Flat Spectrum Sources	–	$-0.3 < \alpha_{\text{IR}} \leq 0.3$	–	Intermediate class between Class I and II
Class II	Classical T Tauri Star ⁴	$-1.6 \leq \alpha_{\text{IR}} \leq -0.3$	$M_{\text{disc}} \sim 0.01M_*$, $M_{\text{env}} \sim 0$, $T_{\text{bol}} \sim 650 - 2880 \text{ K}$	Accreting disc, strong H α and UV emission
Class III	Weak T Tauri Star	$\alpha_{\text{IR}} \leq -1.6$	$M_{\text{disc}}/M_* \ll 1\%$, $M_{\text{env}} \sim 0$, $T_{\text{bol}} > 2880 \text{ K}$	Passive disc, weak accretion

defined by the magnitude of the infrared spectral index (α_{IR}) which can span a wavelength range from 2 μm (near-infrared) - 25 μm (mid-infrared). These classes illustrated in Fig. 2.3 signify the different evolutionary stages of the protostar starting from the prestellar molecular cloud cores until the zero-age main sequence (ZAMS) [Lada and Wilking, 1984, Lada, 1987]. The infrared spectral index is given by

$$\alpha_{\text{IR}} = \frac{d \log(\lambda F_\lambda)}{d \log \lambda}, \quad (2.2)$$

where λ is the wavelength and F_λ is the observed flux.

The first class, Class 0, corresponds to the least evolved phase of YSOs observed during the earliest stages of cloud collapse when the protostar is embedded in an optically thick cloud of gas and dust. Class 0 objects further evolve into Class I objects which correspond to the YSOs still embedded in an envelope of remnant material of the initial cloud and surrounded by a circumstellar disc which is formed as a result of the angular momentum of the infalling material. The circumstellar material can be heated externally by radiation from the protostar and internally via viscous dissipation. This is seen as the excess emission at longer wavelengths in the spectral energy distribution for Class I objects in the left panel of Fig. 2.3 in addition to the emission from the central star which is observed since the circumstellar disc is flat. Outflows and jets are also often detected from these sources.

As the disc evolves, matter is accreted onto the central star which leads to a decrease in the infrared excess. At this stage, the YSOs are classified as Class II sources which are

⁴T Tauri stars are optically visible pre-main sequence stars with masses $M_* \leq 2 M_\odot$.

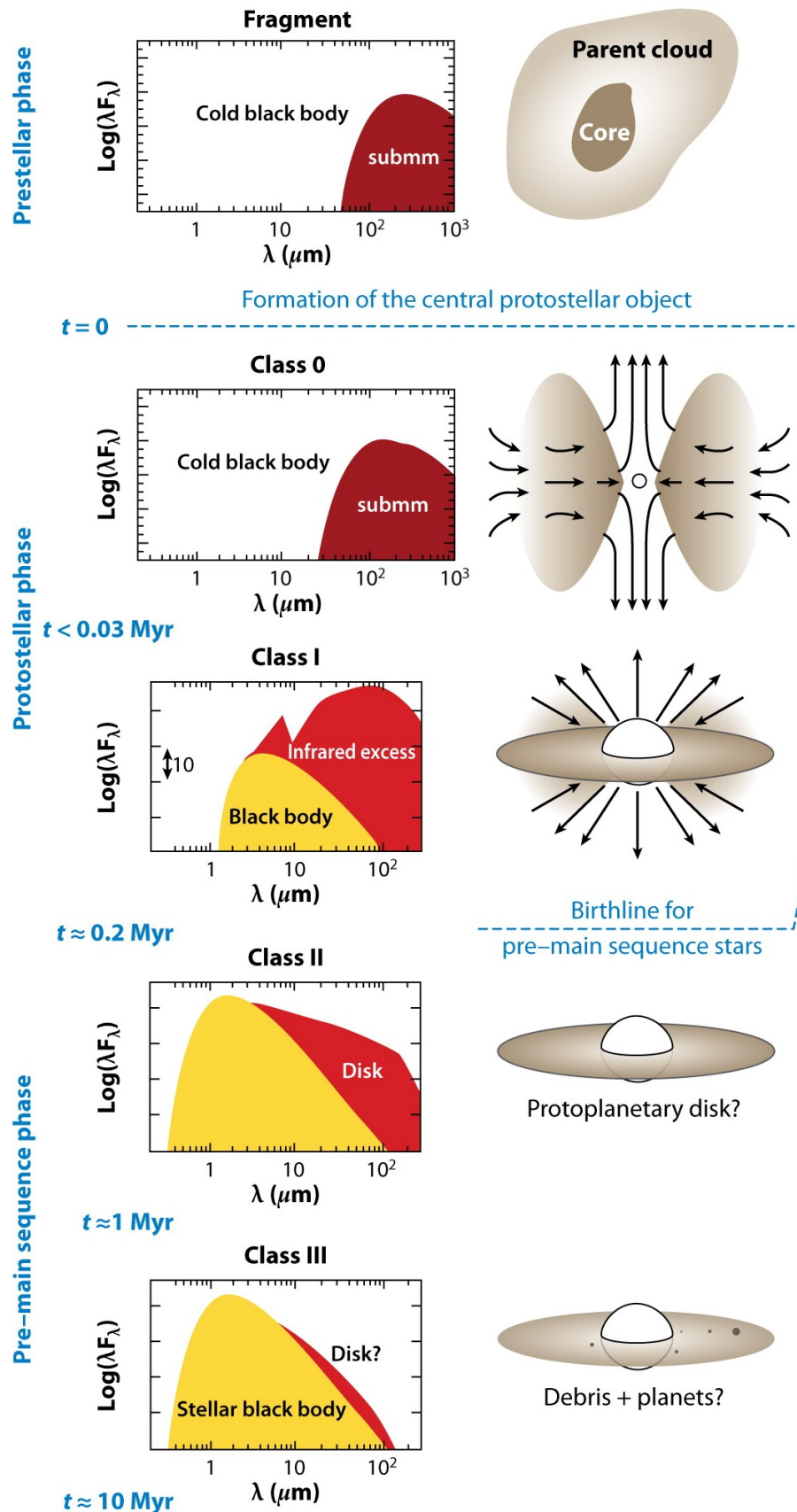


FIGURE 2.3: Evolution stages of young stellar objects. The left panel shows the spectral energy distributions for the different evolutionary stages and the right panel shows the corresponding geometry (adapted from André [2002]).

characterised by a pre-main sequence (PMS) star surrounded by an optically thick disc. In this phase most of the matter from the surrounding envelope either falls onto the disc or is blown away due to the feedback processes from the young central pre-main sequence star. The transfer of angular momentum to large radial distances in the disc leads to accretion of material onto the central star. It is mainly these Class II objects that we model in this thesis.

As more matter gets accreted onto the central PMS due to disc accretion, the protoplanetary disc begins losing gas and becoming optically thin. This final stage of YSOs thus comprising of a pre-main sequence star with little or no evidence of surrounding dust corresponds to the Class III stage of YSOs. The emission from the remnant of the surrounding disc (debris disc⁵ or transitional disc⁶) is negligible. Class III stars are distinguished from the main sequence (MS) stars by their location above the main sequence in the Hertzsprung-Russell diagram or by the strong X-ray activity. A similar process of disc formation and evolution can also be seen in intermediate mass ($M_* \sim 2 - 4 M_\odot$) young stars called Herbig Ae/Be stars.

Observations suggest that protoplanetary discs are associated with more than 50% of the classical T Tauri stars in the solar neighbourhood [Kenyon and Hartmann, 1995, Sicilia-Aguilar et al., 2006, Zhang et al., 2015]. Protoplanetary discs set the stage for planet formation and play an important role during the processes of star formation and evolution owing to its significance for gas accretion onto the central star and redistribution of angular momentum. These discs also help constrain the physical properties like initial angular momentum, mass, size etc. of the parent molecular cloud. It is important to understand the structure and evolution of the protoplanetary discs in order to physically interpret the observed SEDs of the different classes.

⁵Debris disc is a gas poor disc where the opacity is dominated by second-generation dust produced by the collision of planetesimals.

⁶Transitional disc is observed as a strong mid to far infrared emission.

2.2 Protoplanetary disc structure

The study of protoplanetary discs requires an understanding of different physical processes in different regions of the disc such as viscous accretion onto the central star, mass loss due to outflow, irradiation by the central star, interaction with the stellar wind and magnetic field, turbulent mixing of material, dust grain growth, gradual settling of the dust towards the disk mid plane, and planetary formation. Peculiar signatures of these processes can be observed in the SED. The difference in the spatial scales, densities and temperatures in the different regions of the disc demand different observational techniques to ensure a detailed study of these different regions. As illustrated in Fig. 2.4, optical and UV observations are used to study the regions very close to the central star ($\sim 0.01 - 0.1$ AU). Near- infrared (NIR) and mid-infrared (MIR) observations using the Spitzer Space Telescope and the Infrared Space Observatory (ISO) can be used to study the regions of the disc extending from the innermost regions of ~ 0.1 AU up to ~ 10 AU whereas the outer regions of the disc from ~ 10 AU to few 100 AU can be probed using longer wavelength telescopes like Hubble Space Telescope (HST), Herschel Space Observatory and Atacama Large Millimeter Array (ALMA) in the far-infrared and millimeter regime. Figure 2.5 shows examples of discs observed using ALMA and HST.

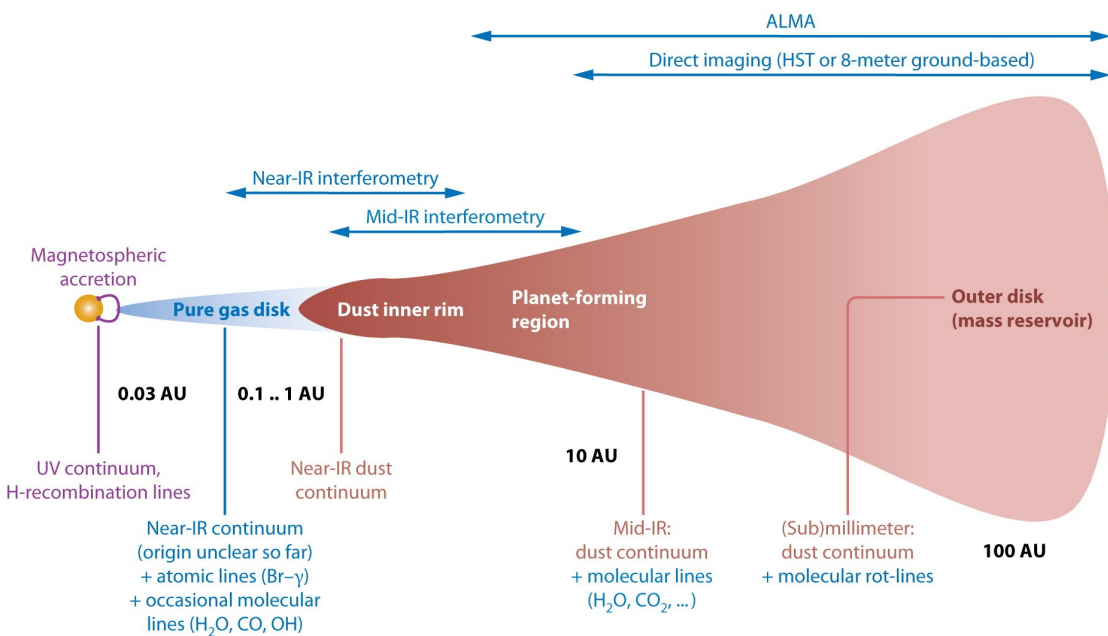


FIGURE 2.4: Protoplanetary disc structure [Dullemond and Monnier, 2010]

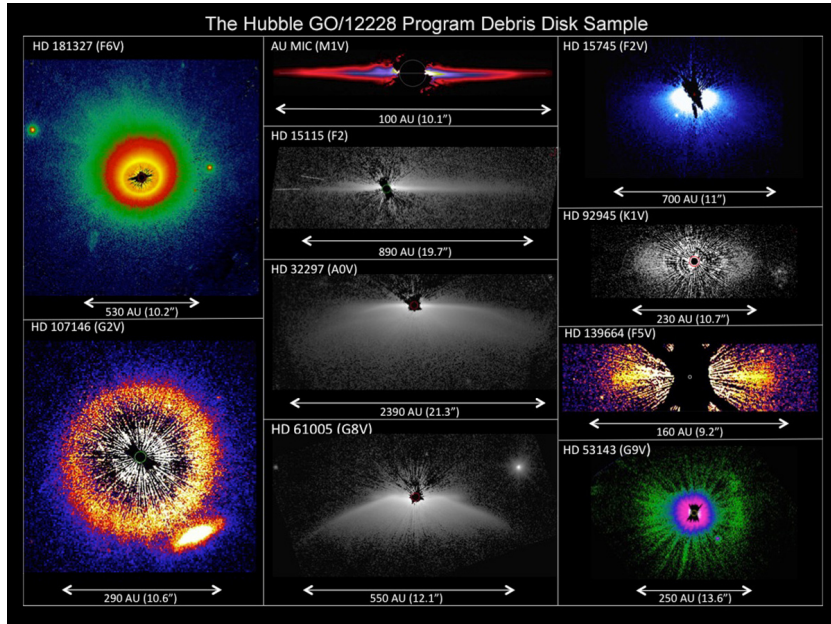
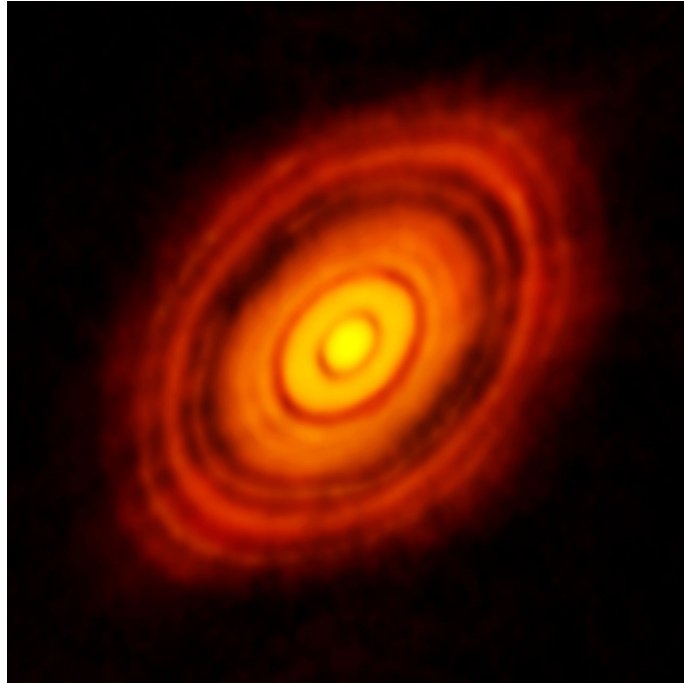


FIGURE 2.5: The sharpest image (top) of the protoplanetary disc surrounding HL Tauri taken by ALMA. It shows the substructures and possible positions of planet forming dark patches within the disc which were resolved for the first time. Image credits: ALMA (ESO/NAOJ/NRAO). Set of images of debris discs (bottom) taken via the Hubble Space Telescope. Image credits: NASA, ESA, G. Schneider (University of Arizona), and the HST/GO 12228 Team ⁷.

⁷retrieved on 13th September, 2015 from <https://www.eso.org/public/images/eso1436a/> and <http://hubblesite.org/newscenter/archive/releases/star/protoplanetary%20disk/2014/44/image/h/>.

The interpretation of the data obtained from observations of discs found in typical star clusters in the solar neighbourhood like the ONC, Trapezium, Arches, Taurus, Auriga and Ophiuchus can then be done by using various theoretical models to study the different properties of the disc.

Observations show that protoplanetary discs typically have radial extents of $\approx 100 - 500$ AU [Vicente and Alves, 2005, Andrews and Williams, 2007a, Moór et al., 2015, Bally et al., 2015] and a lifetime of a few million years [Haisch et al., 2001, Mamajek, 2009, Fedele et al., 2010, Ribas et al., 2014] which corresponds to up to ten million orbits for the inner disc. The disc mass (m_{disc}) obtained from sub-millimeter observations is usually in the range $< 0.01 M_{\odot}$ (low mass) to $> 0.1 M_{\odot}$ (massive). The disc temperature ranges from $10 - 30$ K in the outer disc regions to $\geq 10^3$ K in the inner disc regions. The latter are dominated by viscous heating whereas the outer regions of the disc are dominated by radiative heating due to irradiation of the disc by the central star [Chiang and Goldreich, 1997]. The observational values for these disc properties can be found in Beckwith et al. [1990], McCaughrean and O'dell [1996], Andrews and Williams [2005], Cesaroni et al. [2007], Andrews and Williams [2007b], Eisner et al. [2008], Mann and Williams [2012], Andrews et al. [2013], Joergens et al. [2013], Harsono et al. [2014], Bally et al. [2015], Mann et al. [2015], Beltran and de Wit [2015] and references therein. Due to observational constraints it is difficult to determine a typical surface density for discs. The theoretical estimate of the minimum mass solar nebula [Weidenschilling, 1977] which is constructed by augmenting the current planet masses to match solar abundances, and then smearing those masses into concentric annuli is generally used as a reference point. This yields a surface density which scales as $\Sigma(r) \propto r^{-3/2}$ [Hayashi, 1981]. Furthermore, surface densities have been estimated by fitting theoretical models to observed SEDs. The standard fitting method is based on the assumption that the surface density has a simple power-law dependence of the form

$$\Sigma(r) \propto r^{-p}, \quad (2.3)$$

out to some cut-off radius (r) where p varies in range 0 - 2 [Andrews and Williams, 2007a]. The most widely used model for numerical studies of discs is with the surface density distribution index of $p = 1$ which gives a $1/r$ surface density distribution [Pfalzner et al., 2005b, Olczak et al., 2006, de Juan Ovelar et al., 2012, Steinhäusen et al., 2012]. The time over which the surface density at all radii evolves is described as the viscous time scale which is given as

$$\tau_v = \frac{r^2}{\nu}, \quad (2.4)$$

where ν is the viscosity.

For an isothermal hydrostatic thin-disc (height $h \ll$ radius r), the vertical structure of the disc at a given radius is given by

$$\rho(r, z) = \rho_0 \exp\left(-\frac{z^2}{2h^2(r)}\right). \quad (2.5)$$

In the above equation, ρ_0 is the unperturbed mid-plane particle density on the equatorial plane with $\rho_0 \propto r^{-(b+1)}$ where b is the particle distribution index and $h(r) = 0.05 r$ is the vertical half-thickness of the disc (see Pringle [1981]).

There are a lot of physical processes which play a significant role for disc evolution. The main role of effective viscosity is the redistribution of angular momentum within the disc. This effective viscosity resulting from turbulence in the disc is given by

$$\nu = \alpha c_s h, \quad (2.6)$$

where c_s is the sound speed, h is the vertical scale height and α is a dimensionless parameter that measures how efficient the turbulence is in creating angular momentum transport [Shakura and Sunyaev, 1973]. In most studies involving disc modeling, the α parameter is assumed to be constant.

Another effect seen in discs is the hydrodynamic transport which occurs in cases when self-gravity is important. However, self-gravity probably plays an important role during the early epoch of disc formation only when the disc is massive enough compared to the stellar mass. The instability occurs when

$$\frac{m_{\text{disc}}}{M_*} > \frac{h}{r}, \quad (2.7)$$

where m_{disc} is the disc mass and M_* is the mass of the disc-hosting star.

At later evolutionary stages, it has been observed that for most cases $m_{\text{disc}} \ll M_*$ and hence self-gravity can be neglected in those cases. Self-gravity (at early times) and magnetorotational instability (MRI)⁸ observed in weakly magnetized discs are the two processes that drive turbulent viscosity in the disc and transport angular momentum outwards.

The gravitational stability of the hydrodynamic disc is mainly controlled by two parameters, the ratio of disc mass to the total mass of the system $\mu = m_{\text{disc}}/(m_{\text{disc}} + M_*)$ and the Toomre instability parameter $Q = c_s \Omega / \pi G \Sigma_d$, where Σ_d is the mass surface density, c_s is the sound speed and $\Omega = \sqrt{GM_*/r^3}$ is the Keplerian angular velocity [Toomre, 1964]. For $Q < 1$, thin discs are unstable to the growth of axisymmetric gravitational disturbances. For non-axisymmetric spiral-like disturbances, the discs are unstable for

⁸Instabilities that arise due to the action of magnetic field in a differentially rotating disc which initiate and sustain magnetohydrodynamic turbulence in the disc (for an overview see Hartmann [2009], Armitage [2011]).

$Q \approx 3 - 4$.

In some cases due to disc instabilities, the mass accretion rate increases by more than four orders of magnitude on a timescale of months which can be seen as outbursts. Discs with these FU Orionis outbursts which are powered by the release of gravitational potential energy as gas flows inward are classified as active discs. However, in most cases for T Tauri stars the energy released (\propto accretion rate) is low and the disc is mainly heated by stellar radiation. Such discs are classified as passive discs. Thus the circumstellar discs can be differentiated into these two types, namely active discs and passive discs.

2.3 Influence of cluster environment

As discussed in § 2.1 most stars are not formed in isolation but as a part of a stellar cluster. These star clusters can contain just a few dozen stars (e.g. σ Ori cluster) but can also consist of tens of thousands of stars (e.g. Arches cluster). As a consequence the stellar density in different clusters varies widely. Depending on the stellar density, the cluster environment might have a significant effect on the evolution of the discs surrounding young stars (for an overview see Hollenbach et al. [2000], Williams and Cieza [2011] and references therein). The most widely investigated massive cluster in the solar neighbourhood is the Orion Nebula Cluster (ONC).

The two most investigated processes by which the cluster environment potentially influences the evolution of protoplanetary discs are

- External photoevaporation: Here the strong radiation field of massive O or B stars influences the disc of nearly low mass stars [Johnstone et al., 1998, Adams et al., 2004, Font et al., 2004, Clarke, 2007, Dullemond et al., 2007, Gorti and Hollenbach, 2009, Owen et al., 2010, 2012, Rosotti et al., 2015].
- Gravitational interactions during fly-bys: This process can lead to significant alteration in disc properties due to gravitational influence of passing stars [Clarke and Pringle, 1993, Hall et al., 1996, Kobayashi and Ida, 2001, Pfalzner et al., 2005b, Thies et al., 2005, Malmberg et al., 2011, de Juan Ovelar et al., 2012, Rosotti et al., 2014].

The following sections give an overview of the effects of these two processes on protoplanetary disc properties.

2.3.1 External Photoevaporation

The discovery of *proplyds* (externally ionized protoplanetary discs) has been taken as an evidence of external photoevaporation taking place in the central region of the ONC [McCaughrean and O'dell, 1996, O'dell, 1998, Johnstone et al., 1998, Vicente and Alves, 2005, Bally et al., 2015]. Ultraviolet (UV) radiation from massive O and B stars in these clusters tends to rapidly erode the loosely bound outer regions of protoplanetary discs via external photoevaporation. However, they have negligible effects in the inner disc regions ($r_{\text{disc}} < 50$ AU). It has been studied that the photoevaporation rates of discs around low-mass stars illuminated by massive stars may be either dominated by far-ultraviolet (FUV, $h\nu^9 < 13.6$ eV), extreme ultraviolet (EUV, $h\nu > 13.6$ eV) or X-ray ($h\nu > 100$ eV) photon flux from the massive star. EUV photons ionize the gas which increases the gas temperature up to $T \sim 10^4$ K and the FUV photons dissociate the molecules and heat the photodissociation region (PDR) gas up to $T \sim 10^2 - 10^4$ K. In the inner FUV region, photons dominate the mass loss by heating the disc and causing a neutral flow out to an ionization front. In the outer EUV region there is no neutral flow and the mass-loss rate depends on the EUV flux.

Various studies show that the disc lifetimes and masses are affected only for discs that lie within few tens of parsec from an O star. The disc mass-loss in the FUV and EUV dominated regions is given by

$$\dot{M}_{\text{FUV}} \approx 2 \times 10^{-9} r_{\text{disc}} M_{\odot} \text{ yr}^{-1}, \quad (2.8)$$

$$\dot{M}_{\text{EUV}} \approx 8 \times 10^{-12} r_{\text{disc}}^{3/2} \sqrt{\frac{\Phi_i}{d^2}} M_{\odot} \text{ yr}^{-1}, \quad (2.9)$$

where r_{disc} is the disc radius in AU, Φ_i is the ionizing (EUV) photon luminosity of the massive star in units of 10^{49} s^{-1} , d is the distance to the massive star in parsecs and the column density is assumed to be $5 \times 10^{21} \text{ cm}^{-2}$ from the ionization front of the disc inside a proplyd [Störzer and Hollenbach, 1999, Hollenbach et al., 2000].

The mass-loss rate in the X-ray regime is given as

$$\dot{M} \approx 8 \times 10^{-9} \left(\frac{L_X}{1 \times 10^{30} \text{ erg s}^{-1}} \right) M_{\odot} \text{ yr}^{-1}, \quad (2.10)$$

where L_X is the X-ray luminosity [Owen et al., 2012].

Many studies have predicted the disc size using theoretical models to be equivalent to the observed size of the ionization front. The disc radii usually lie in the range from 10 - 100 AU [Johnstone et al., 1998]. The discs are evaporated from outside in

⁹Planck's constant (h) $\approx 6.626 \times 10^{-34} \text{ J} \cdot \text{s}$ and ν is the frequency.

[Ercolano et al., 2011, Koepferl et al., 2013]. The lower limit (r_{\min}) up to which the disc can be reduced due to external photoevaporation is given by

$$r_{\min} \approx \frac{GM_*}{2c_s^2}, \quad (2.11)$$

where M_* is the stellar mass and c_s is the sound speed in the heated flow [Hollenbach et al., 1994, Scally and Clarke, 2001, Dullemond et al., 2007].

The timescale for FUV-induced photoevaporation is $t_{\text{evap}} = m_{\text{disc}}/\dot{M}_{\text{pe}}$ where \dot{M}_{pe} is the mass-loss rate. It is however important to note that external photoevaporation becomes efficient only when most of the cluster gas is removed meaning that external photoevaporation can only take place when the gas and dust density is relatively low. Hence there are limited observations of this process in clusters like the ONC where the gas blow out has just started in the central cluster areas. In planet formation models, it has been seen that FUV radiation fields produced mainly by massive stars could inhibit giant planet formation depending on dust attenuation. Various studies show that external photoevaporation has very little effect on planets forming within 5 - 10 AU from the central star [Johnstone et al., 1998, Scally and Clarke, 2001, Gorti and Hollenbach, 2009]. This is the region where most of the planets in our solar system are found.

2.3.2 Stellar Encounters

A number of studies have investigated the effect of the cluster environment on protoplanetary discs during stellar fly-bys. These encounters are denoted as star-disc encounters in cases where only one of the stars is surrounded by a disc and disc-disc encounters in cases where both the stars are surrounded by discs. Stellar fly-bys can either cause matter to become unbound, captured by the perturbing star or pushed inwards and potentially be accreted onto the central star. This has a significant effect on the disc mass, angular momentum, energy, and disc size depending on the periastron distance, mass ratio between the perturber mass and mass of the central star, eccentricity and inclination of the perturber orbit and the mass distribution within the disc [Steinhausen et al., 2012].

The frequency for such stellar encounters to truncate a disc to a radius r_{disc} can then be calculated as $t_{\text{SE}} \simeq 1/n_*\sigma v$, where n_* is the density of the stars in a cluster, v is the relative velocity (typically $v \sim 1$ km/s), $\sigma \simeq B\pi r_{\text{disc}}^2$ is the collision cross section where B is a dimensionless factor of the order of unity. The rate at which stars in a cluster undergo encounters with other cluster members is $\Gamma = \langle n_*\sigma v \rangle$.

In the past there have been various numerical and analytical studies to investigate the consequences of stellar encounters on final disc properties like energy, angular momentum, disc mass, and disc size [Clarke and Pringle, 1993, Ostriker, 1994, Heller, 1995,

Hall et al., 1996, Hall, 1997, Kobayashi and Ida, 2001, Pfalzner et al., 2005b, Olczak et al., 2006, de Juan Ovelar et al., 2012, Breslau et al., 2014, Rosotti et al., 2014].

The relative angular momentum loss as derived analytically by Ostriker [1994] can be estimated from,

$$\Delta J \sim \frac{M_2}{M_1 + M_2} \times \exp \left[-\sqrt{\frac{M_1}{M_1 + M_2}} \left(\frac{r_{\text{peri}}}{r_{\text{disc}}} \right)^{3/2} \right] \times \frac{2}{\Omega(r_{\text{disc}})} \cos \left(\frac{\beta}{2} \right)^5, \quad (2.12)$$

where M_1 and M_2 are masses of the two stars, r_{peri} is the periastron distance, $\Omega(r_{\text{disc}})$ is the angular velocity at the outer disc radius and β is the inclination between the disc plane and the orbital plane. Note that the above equation is valid only for distant encounters. The study by Ostriker [1994] was restricted to the linear perturbation theory which only accounts for small perturbations at the outer disc regions. For nearly equal-mass encounters, it is valid only if $r_{\text{peri}} \leq 2 \cdot r_{\text{disc}}$ but can be applied for smaller periastron distances for encounters by low-mass perturbers.

Based on numerical N-body simulations, the most extensive parameter study so far has been done by Olczak et al. [2006], who found the relative disc-mass loss for the case of parabolic, coplanar, prograde encounters to be

$$\begin{aligned} \frac{\Delta M_{\text{disc}}}{M_{\text{disc}}} = & \left(\frac{M_2}{M_2 + 0.5M_1} \right)^{1.2} \times \ln \left[2.8 \left(\frac{r_{\text{peri}}}{r_{\text{disc}}} \right)^{0.1} \right] \\ & \times \exp \left\{ -\sqrt{\frac{M_1}{M_2 + 0.5M_1}} \left[\left(\frac{r_{\text{peri}}}{r_{\text{disc}}} \right)^{3/2} - 0.5 \right] \right\}. \end{aligned} \quad (2.13)$$

The numerical investigations to study mass loss, energy and angular momentum transfer due to coplanar as well as non-coplanar, prograde and retrograde parabolic encounters show that the material remaining bound to the host star plays a dominant role in the transfer of energy and angular momentum for prograde encounters while in case of retrograde encounters, the angular momentum transfer is dominated mainly by the unbound particles after the encounter. It has been shown that the mass loss, energy and angular momentum change has a strong dependence on the periastron distance, mass ratio, eccentricity of the perturber orbit, and mass distribution within the disc [Hall et al., 1996, Pfalzner, 2004, Pfalzner et al., 2005b]. The effects on these disc properties due to prograde encounters are more significant as compared to retrograde encounters.

The effects of stellar encounters on protoplanetary disc sizes has been investigated only in a few studies since the disc sizes were for a long time difficult to observe. This

situation has now changed with the advent of ALMA. However, disc size determination is important given its role in various planet formation models owing to the resulting changes in the disc properties during these fly-bys and the implications on evolution of planetary systems. The perturbations due to fly-bys can lead to planet-planet interaction which may cause ejection of outer planets, capture by the perturber or an increase in the eccentricity resulting in wide-orbit planets [Malmberg et al., 2007, 2011]. Hence in this thesis the study mainly focuses on the effects of star-disc encounters on *disc sizes*. However, the definition of a disc size after an encounter is more complex than for unperturbed systems because of an increase in outer disc particle inclinations and eccentricities due to fly-bys.

Clarke and Pringle [1993] were the first to numerically investigate the disc size after an encounter. They found that for an *equal-mass*, prograde, coplanar, parabolic (eccentricity = 1) encounter the disc is tidally stripped down to 1/2 of the periastron distance and Hall [1997] found 90% of the remaining mass to lie within 1/2 of the periastron distance. For the same case, Kobayashi and Ida [2001] concluded that many particles become unbound outside 1/3 periastron distance after a stellar encounter. Using these disc size estimates, most of the previous studies define the truncation radius to be 1/2 - 1/3 of the periastron distance [Adams et al., 2006, Adams, 2010, Malmberg et al., 2011, Jiménez-Torres et al., 2011, Pfalzner, 2013, Rosotti et al., 2014]. Unfortunately, the dependence of the disc size after an encounter, on the mass ratio $m_{12} = M_2/M_1$ between the perturber mass (M_2) and mass of the central star (M_1) has often been neglected in these studies.

Pfalzner et al. [2005b] investigated the dependence of the disc size on the mass ratio for the case of a parabolic, coplanar, prograde encounter at different periastron distances. They define the disc size to be the radius within which 95% of the disc mass is enclosed. However, their studies were done only for a small parameter range of $m_{12} = 0.1 - 2$. de Juan Ovelar et al. [2012] estimated the disc radius as a function of the periastron distance and mass ratio by transforming the disc-mass loss obtained from numerical simulations by Olczak et al. [2006] (equation 2.13) to a truncation radius under the assumption that the disc is always truncated to the equipotential (Lagrangian) point between the two stars. This is given by

$$r_{\text{disc}}(r_{\text{peri}}, M_1, M_2) = \frac{r_{\text{peri}}}{1 + m_{12}^{1/2}}, \quad (2.14)$$

where r_{disc} is the disc radius which is a function of periastron distance r_{peri} , host mass M_1 and perturber mass M_2 .

However, using the mass loss to find the disc size is especially problematic for distant encounters. It has already been indicated by Hall [1997] that after an encounter, for initial discs $\leq 0.25 \cdot r_{\text{peri}}$, the disc material can lose angular momentum and move

inwards by recircularising at smaller radii, thus suggesting that the disc sizes can be reduced even without a significant mass loss. The loss of disc angular momentum in star clusters was confirmed by Pfalzner and Olczak [2007]. Rosotti et al. [2014] have also concluded from their work on star-disc interactions in young stellar clusters, that the disc size is affected to a larger degree than the disc mass. Scally and Clarke [2001] have shown that a star surrounded by a disc undergoes at least one encounter closer than 1000 AU during the lifetime of a disc ($\approx 10^6$ yrs).

In order to obtain a theoretical disc size that is representative of the observed values, Breslau et al. [2014] performed pure N-body simulations for a larger parameter space of different mass ratios ($m_{12} = 0.3 - 500$) and periastron distances, as compared to the previous studies. They define the disc size using the steepest gradient in the surface density distribution. The disc size (r_{final}) is represented as a function of the periastron distance (r_{peri}) and the mass ratio (m_{12}) by

$$r_{\text{final}} = 0.28 \cdot r_{\text{peri}} \cdot m_{12}^{-0.32}. \quad (2.15)$$

However, this result is still limited to coplanar, prograde encounters on parabolic orbits. The outcome of an encounter not only depends on the periastron distance and the mass ratio between the two stars but also on the orbital eccentricity and relative inclination of the perturber orbit.

2.4 Motivation and Aim

The primary goal of this thesis is to study the effects of stellar fly-bys on protoplanetary *disc sizes*. Most of the previous numerical and analytical studies as discussed in § 2.3.2 to determine disc sizes was mainly restricted to parabolic, coplanar, prograde encounters, most often for the equal-mass case. In this thesis, the focus is on the effects due to both inclined and retrograde encounters in addition to the coplanar, prograde cases for different mass ratios and at different periastron distances, hence covering a wide parameter space. The results for disc sizes after inclined encounters are detailed and the prograde cases are compared to the retrograde ones. The results presented in this thesis indicate the consequences of stellar fly-bys for not only understanding the fate of discs but also that of planetary systems and Sedna-like objects on highly inclined orbits in our solar system.

Chapter 3

Method

In this chapter, an overview of the numerical method and simulations performed to study the effects on protoplanetary disc size due to stellar fly-bys is presented. In § 3.1, the numerical method and procedure to setup the star-disc encounter on coplanar and inclined perturber orbits for a range of mass ratios and periastron distances is described. The disc size definition used to determine and compare disc sizes for different encounter scenarios is then discussed in § 3.2.

3.1 Numerical Method

We consider a star surrounded by a disc which is perturbed by a passing star. In these studies, the protoplanetary discs at the final stage of star formation are considered and hence the disc is assumed to be of low mass, $m_{\text{disc}} \ll M_*$. More massive discs are usually found during the initial stages of formation when processes like infall of the surrounding envelope of dust and gas in molecular clouds onto the disc are still ongoing. Observations show that for most discs it holds that the disc mass is much smaller than the stellar masses, for example $m_{\text{disc}} \approx 0.01 M_*$ [Andrews et al., 2013]. In this case, self-gravity in the disc can be neglected because the forces between the disc particles are much smaller than those from the stars. In addition, viscous forces can also be neglected, because the encounter time is short compared to the viscous timescale. The viscous timescale depends on the gas density which is highest in the central areas of the disc. However, the disc size changes mainly affect the outer disc regions where viscosity effects are negligible. In this case it suffices to study only three-body interactions by considering the gravitational forces between the two stars and each disc particle. Following the work from Hall et al. [1996], Pfalzner [2003], Pfalzner et al. [2005b], Breslau et al. [2014], in order to simplify the problem, this can hence be considered as a

restricted three-body problem (Musielak and Quarles [2014] and references therein). Here, the case where only one of the stars is surrounded by a disc is investigated. Although in reality each of the stars is at least initially surrounded by its own disc. In many cases the results from star-disc encounters can be generalised to disc-disc encounters as the captured mass is deposited usually in the inner disc areas and as such does not influence the final disc size [Pfalzner et al., 2005a], exceptions are discussed in chapter 5.

3.1.1 Initial Setup

Here, numerical simulations are performed on thin discs [Pringle, 1981] using 10 000 mass-less tracer particles. It has been shown in a number of studies that this resolution is sufficient for investigations of the global properties of discs. Kobayashi and Ida [2001] and Pfalzner [2003] showed that simulations with initial 50 000 particles lead to similar results for disc masses and sizes. However, the situation is different for studies of, for example, disc instabilities, where particle numbers of the order of several hundred thousand are required.

The tracer particles initially orbit the host star on circular Keplerian orbits in the counter-clockwise direction. For a particle orbiting around a star with mass M_1 on a radius r , the initial angular velocity (ω) is given by

$$\omega = \sqrt{G \frac{M_1}{r^3}}, \quad (3.1)$$

where G is the gravitational constant. The particle's initial orbital period is $T = 2\pi/\omega$. For each of the particles, the equations of motion are solved numerically. The trajectories of the particles during and after the stellar encounter are integrated with the Runge-Kutta Cash-Karp scheme with the maximum allowed error between the 4th and 5th integration step to be 10^{-7} (see Appendix A). An inner hole of 1 AU is considered to avoid small time steps and to account for matter accreted onto the host star. Fig. 3.1 shows an example of the changes in a disc at different simulation times due to a star-disc encounter for an equal-mass prograde, coplanar case at an encounter distance of $r_{\text{peri}} = 100$ AU.

For measuring the effects on the disc size it is nevertheless advantageous to have a relatively high resolution in the outer regions of the disc. Therefore, an initial constant particle surface density is used and different masses are then assigned to the particles to model different mass surface density distributions in the initial disc [Pfalzner et al., 2005b, Olczak et al., 2006, de Juan Ovelar et al., 2012, Steinhausen et al., 2012]. A typical initial mass surface density is $\Sigma(r) \propto r^{-1}$ ($p = 1$ in equation 2.3), this is the

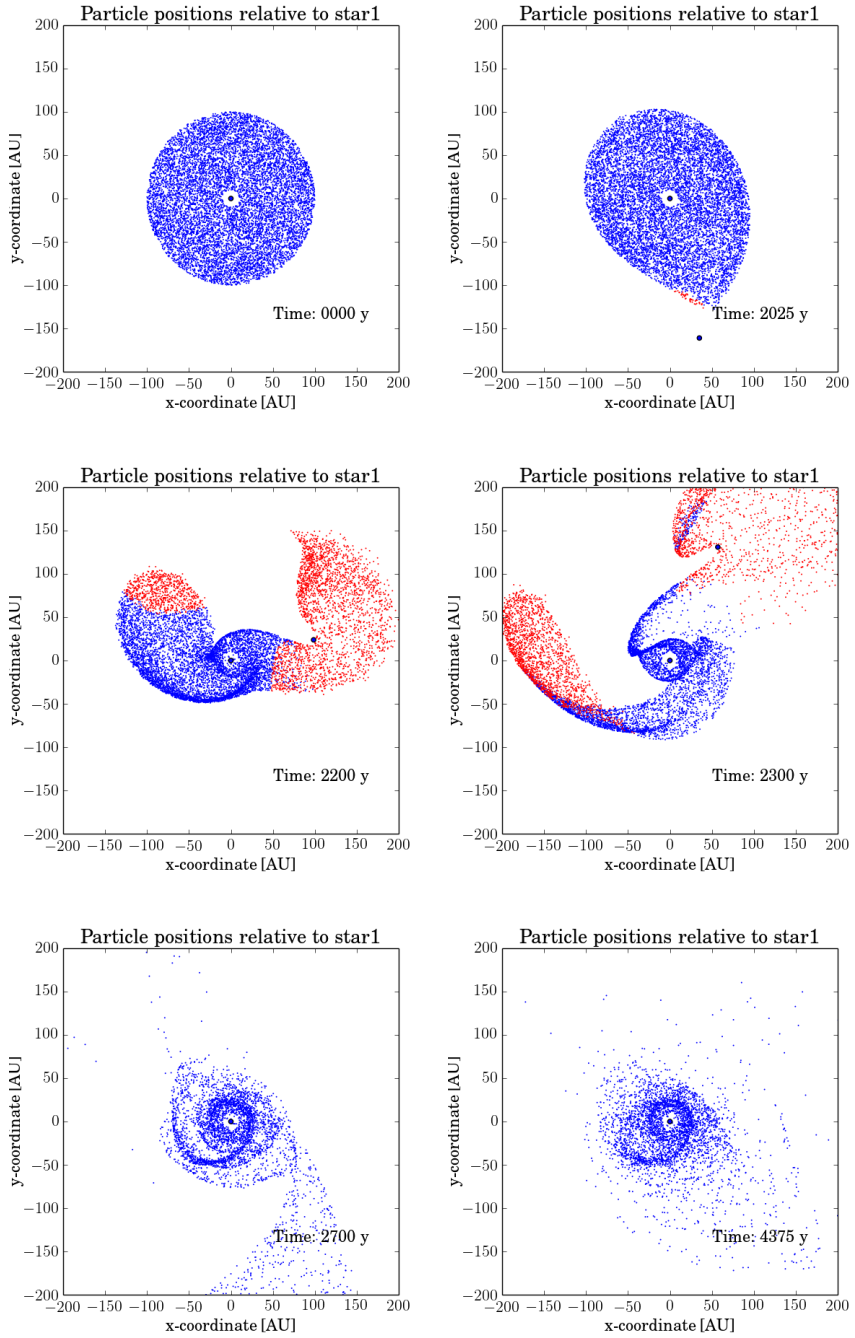


FIGURE 3.1: Face-on view of discs at different time steps after an equal-mass, prograde, coplanar encounter at $r_{\text{peri}} = 100$ AU. The particles bound to the central star are shown in blue. All the other particles i.e. those which are either bound to the perturber, unbound or accreted by either of the stars are shown in red.

most widely used density distribution for theoretical steady-state accretion disc models. As described in § 2.2, the value of the power-law index (p) varies in the range 0 - 2. However, the study of global properties like the disc size is independent of the initial distribution since in the three-body approach the remainder of the disc outside the determined disc size is not important.

For a thin disc ($h \ll r$), as is the case for the disc considered here, the vertical density distribution of the disc at a given radius is given by

$$\rho(r, z) = \rho_0 \exp\left(-\frac{z^2}{2h^2(r)}\right). \quad (3.2)$$

In the above equation, ρ_0 is the unperturbed mid-plane particle density on the equatorial plane with $\rho_0 \propto r^{-(b+1)}$ where b is the particle distribution index and $h(r)$ is the vertical half-thickness of the disc which is here chosen to be $h(r) = 0.05 r$ (also described in § 2.2). This results in particle inclinations of $\leq 5^\circ$ so the disc can still be regarded as thin.

In the here presented simulations, usually the disc has an initial radius (r_{init}) of 100 AU but an additional set of simulations with $r_{\text{init}} = 200$ AU are also performed. Simulations are carried out for different perturber mass to host mass ratios $m_{12} = M_2/M_1$. The host mass (M_1) is always fixed to $1 M_\odot$ and the perturber mass (M_2) is varied in the range $0.3 M_\odot - 50 M_\odot$. These values are typical for a young dense cluster like the ONC [Pfalzner and Olczak, 2007, Weidner et al., 2010]. The lower limit is chosen to be $0.3 M_\odot$, because even for the most destructive prograde coplanar encounters the effects on disc sizes is seen only for very close encounters ($r_{\text{peri}} \leq r_{\text{init}}$) for masses below $0.3 M_\odot$ [Breslau et al., 2014]. For example, for a perturber of mass $0.1 M_\odot$, an initial 100 AU disc remains completely unaffected after encounters at periastron distances greater than ≈ 150 AU. Also in the case of low mass perturbers, the disc mass is not significantly smaller than the mass of the perturbing star and additional effects due to pressure, viscous forces and self gravity should be take into account.

Similarly, periastron distances in the range $r_{\text{peri}} = 30 - 1000$ AU are studied to cover the parameter space from encounters that completely destroy the disc to those having a negligible effect on the disc size. Here completely destroying the disc means the case where less than 5% of the original disc mass remains bound to the central star.

The lower and upper limits for the mass ratio (m_{12}) and periastron distance (r_{peri}) are chosen such that we ensure a disc-size change larger than the typical error in these kind of simulations (i.e. disc-size change > 5 AU). Mathematically, using equation 2.15, this can be represented as

$$0.05 < \frac{r_{\text{final}}}{r_{\text{peri}}} = 0.28 \cdot m_{12}^{-0.32}. \quad (3.3)$$

Here, only the case where the perturber is on a parabolic orbit ($e_p = 1$) is considered. It has been shown that in low-mass clusters and clusters like the ONC this is the dominant type of encounter. However, in denser clusters like for e.g. the Arches cluster this is no longer the case. In these denser environments, hyperbolic encounters with ($e_p > 1$) dominate.

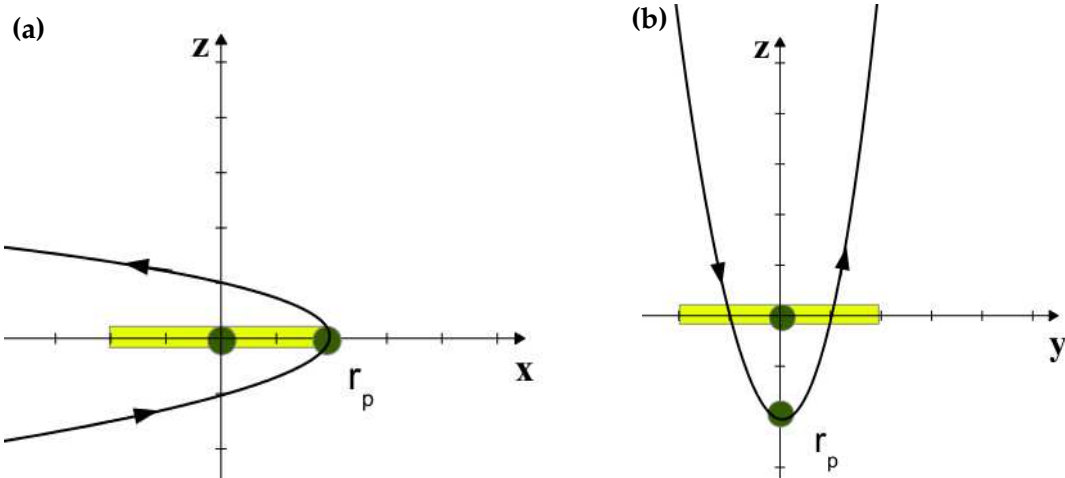


FIGURE 3.2: Encounter orbit with periastron (r_p) (a) in the disc plane ($aop = 0^\circ$) and (b) below the disc plane ($aop = 90^\circ$).

3.1.2 Initial conditions for inclined encounters

In previous studies the effects of the inclination of the perturber orbit has been considered so far for a restricted parameter space and with the aim to determine the disc-mass loss and angular momentum loss. It was pointed out by Heller [1995] that the amount of material that escapes the system depends strongly on the periastron distance *and* the orbital inclination. Hall et al. [1996] also suggested the importance of investigating non-coplanar encounters. Pfalzner et al. [2005b] studied the effects on the disc due to non-coplanar encounters, but concentrated only on the mass and angular momentum loss for a small parameter range. By contrast, here the focus is the effect on the *disc size* for the entire parameter space typically encountered in star clusters.

To incorporate the random motions of stars on parabolic orbits, the effects of orbital inclination as well as orbital orientation [angle of periastron (aop)¹] as illustrated in Fig. 3.2 are therefore considered. Considering the disc to be in the xy plane, in principle the perturber orbit can be inclined in two ways:

- The perturber orbit can be inclined along the x -axis wherein the periastron always lies in the disc plane with $aop = 0^\circ$ (Fig. 3.2a).
- The perturber orbit can be inclined with respect to the xz plane wherein the periastron lies outside the disc plane with $0^\circ < aop < 90^\circ$ (Fig. 3.2b).

For the first case, the angle of periastron is fixed to 0° and the perturber orbit is then inclined along the x -axis with an inclination in the range $0^\circ - 180^\circ$ in steps of 10° . Hence

¹angle between the ascending node and the periapsis, measured in the direction of motion where the ascending node is the point at which the orbit crosses the plane of reference and periapsis is the point of closest approach.

in this case, the periastron would always lie on the x-axis. For the second case, the perturber orbit is first rotated in the xy plane (disc plane) and then inclined along the xz plane. The periastron would then always lie outside the disc plane. For this case, we consider the angle of periastron to be 45° and 90° .

Thus, when studying the effect of orbital orientation, the three cases, $aop = 0^\circ$, $aop = 45^\circ$ and $aop = 90^\circ$ are investigated. In addition, by varying the orbital inclination in the range $0^\circ - 180^\circ$, the entire parameter space to study both coplanar prograde ($i = 0^\circ$) & retrograde ($i = 180^\circ$), non-coplanar prograde ($0^\circ < i < 90^\circ$) & retrograde ($90^\circ < i < 180^\circ$) as well as orthogonal ($i = 90^\circ$) encounters is covered.

For both the cases of inclining the perturber orbit, the direction of motion of the perturber on a prograde ($0^\circ \leq i < 90^\circ$) orbit would be the same as that of the particles in the disc. For example, for the first case of inclination along the x-axis (Fig. 3.2a) the perturber would travel from the front of the disc towards the other side if the particles in the disc are considered to be moving in counter-clockwise sense. In case of a perturber on a retrograde ($90^\circ < i \leq 180^\circ$) orbit, the direction of motion of the perturber would be in the opposite direction compared to the disc particles. For example, for the case of inclination along the x-axis (Fig. 3.2a), the perturber would travel from behind the disc towards the front.

Here we chose that, the simulation starts and ends when it holds for all particles bound to the host that the force of the perturber on the disc particles is less than 0.1% of the force of the host star acting on the particles (i.e. $F_{\text{pert}}/F_{\text{host}} = 0.001$). The covered timespan is usually much longer than in previous investigations. The time after the periastron passage is taken to be equal to the time until or before the periastron passage. After and before this time step, the influence of the perturber is negligible, different initial times would result in almost identical results. The difference in the results is smaller than the numerical errors. This is found to be a reasonable time estimate for the particles to have final stable orbits after the encounter. As an example, the total simulation time for an equal-mass case is of the order of ≈ 4375 years which corresponds roughly to about 24 CPU hours and around 40 orbits for outer most particles and more than 50 orbits for inner particles.

The parameter space covered in the work done here as discussed above is summarized in table 3.1. To cover the entire parameter space spanned by the different mass ratios, orbital inclinations and orbital orientations, 456 different perturber orbits have been considered. Additionally, effects due to the perturber at different periastron distances, for each of these 456 orbits are studied.

TABLE 3.1: Parameter ranges of the simulated star-disc encounters

Mass ratio (m_{12})	0.3 - 50
Periastron distance (r_{peri})	30 AU - 1000 AU
Orbital inclination (i)	$0^\circ - 180^\circ$
Orbital orientation (aop)	$0^\circ, 45^\circ, 90^\circ$
Initial disc radius (r_{init})	100 AU, 200 AU
Simulation time	$\sim 4000 - 5000$ years

3.2 Disc-size determination

There are several ways to define the disc size after an encounter [Clarke and Pringle, 1993, Hall, 1997, Kobayashi and Ida, 2001, Pfalzner et al., 2005b]. Most of the previous attempts to determine disc size have been done for a restricted parameter space of parabolic, coplanar, prograde encounters and often for the equal-mass case. Analytical studies by Kobayashi and Ida [2001] show that after an encounter, most particles become unbound beyond $1/3 \cdot r_{\text{peri}}$ (as discussed in 2.3.2). Most studies hence define the disc size to be $1/3 \cdot r_{\text{peri}}$. However, in their studies using N-body methods, Breslau et al. [2014] have already shown discrepancies in the disc size determined using this definition, especially in case of distant encounters.

Observationally, it is difficult to determine the disc size since it depends on how one is looking at the disc either face-on, edge-on or at different inclinations. Another problem is with the difficulties in observing particles on highly inclined and eccentric orbits. The most common method to determine disc sizes is to fit the observed spectral energy distribution (SED) in the millimeter and sub-millimeter range to truncated power laws or exponential radial density and temperature profiles [Andrews and Williams, 2005, 2007a, Moór et al., 2015]. The disc size is then taken to be the truncation radius. In case of resolved images, the disc size is taken to be the radius beyond which there is an observed luminosity drop [McCaughrean and O'dell, 1996, O'dell, 1998, Vicente and Alves, 2005, Bally et al., 2015]. Since the disc does not have a sharp edge, the disc size is specified in terms of intensity threshold which corresponds to the characteristic radius where the surface density profile begins to steepen [Williams and Cieza, 2011].

Here, the aim is to use a theoretical disc size definition that is representative for the observed values. Therefore, we follow the approach by Breslau et al. [2014] who define the disc size to be the steepest gradient in the surface density (shown by purple dashed line in Fig. 3.3). They use a temporal averaged surface density for the determination of the disc size. This was done by first calculating the particle orbit using the final eccentricity and semi-major axis obtained from the data of the last time step. They then estimated the radial probability distribution for where the particle would be on its orbit

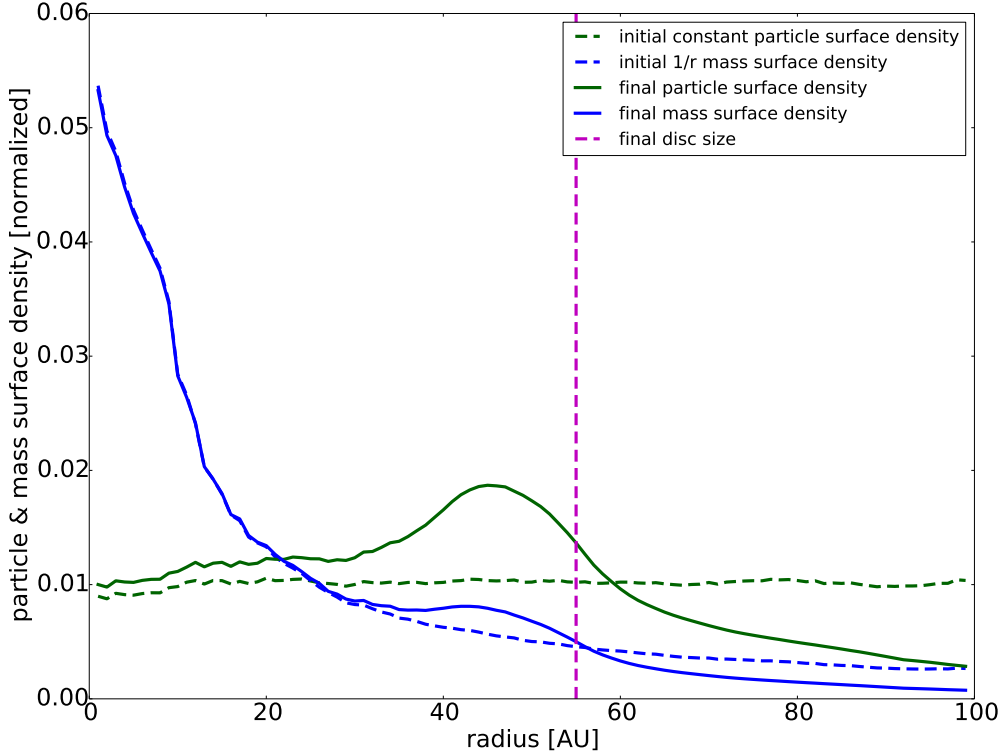


FIGURE 3.3: Surface density for a disc with an initial 100 AU radius around a $1 M_{\odot}$ star perturbed by a $1 M_{\odot}$ perturber at a periastron distance of 200 AU. The vertical purple dashed line shows the final disc radius estimated from the steepest gradient in the surface density profile.

and averaged it over the period of the particle orbit. The sum of the averaged radial probability distributions of all particles then gives the temporal averaged surface density. The reason for using a temporal averaged surface density is to account for particles on highly eccentric orbits. Since the radial distances to the host star for these particles would change with time, the global properties obtained from a snapshot of the particle distribution at the final time step would not necessarily represent the particle distribution in the disc.

Using this disc size definition, for coplanar, prograde encounters, Breslau et al. [2014] found a simple dependence of the final disc size (r_{final}) on the periastron distance (r_{peri}) and mass ratio (m_{12}) of the form

$$r_{\text{final}} = \begin{cases} 0.28 \cdot r_{\text{peri}} \cdot m_{12}^{-0.32}, & \text{for } r_{\text{final}} \leq r_{\text{init}} \\ r_{\text{init}}, & \text{otherwise.} \end{cases} \quad (3.4)$$

The work done in this thesis is an extension to the studies which was restricted to the case of coplanar, prograde encounters by Breslau et al. [2014], to inclined and retrograde encounters. The same method to estimate the disc sizes is adopted. For example, for an equal-mass, coplanar, prograde ($i = 0^\circ$) encounter at $r_{\text{peri}} = 200$ AU, as seen in Fig. 3.3

the disc size is determined using the steepest gradient in the final particle surface density profile (solid green curve). The initial constant particle surface density used in our studies in order to obtain a higher resolution in the outer regions of the disc is shown by the dashed green line. The dashed blue curve indicates the initial r^{-1} surface density. Using either of the initial surface density distributions, for a three-body approach, owing to the disc size definition, there is always going to be some remainder material outside the determined disc size. Hence in this context, the disc size is independent of the initial distribution (as also discussed in § 3.1.1).

Owing to the fact that parabolic encounters have the most significant influence on discs due to the longest interaction time, this study is restricted to only parabolic encounters. Since the main aim of this work, is to study the dependence of disc size on orbital inclination, a parabolic orbit is a reasonable approximation to begin with.

To find the statistical deviations for the disc sizes, 20 simulations for each set of parameters were performed with different initial random seeds for the initial constant particle distribution. An estimate on the mean global error for disc size after encounter due to a perturber on different inclination orbits for a fixed mass ratio was found to be less than 2 AU for grazing and distant encounters ($r_{\text{peri}} \geq 100$ AU) and of the order of $\approx 1 - 5$ AU for penetrating encounters ($r_{\text{peri}} < 100$ AU). The reason for the larger error in case of penetrating encounters is the stronger influence of the perturber on the disc at closer encounter distances and the resulting effects on outer disc particle inclinations and eccentricities which makes it difficult to determine the disc size accurately. Increasing the number of simulation runs did not affect these errors to a great extent and hence 20 runs proved to be sufficient for these studies. Due to the statistical deviations in the data the surface density distributions are smoothed before estimating the disc sizes.

Chapter 4

Results

Most of the previous investigations of the effect of star-disc encounters on protoplanetary disc sizes have been done by considering the perturbing star being on a parabolic coplanar orbit. We extend these investigations to explore the effects on disc sizes due to inclined as well as retrograde orbits of the perturbing star and study the dependence of the disc size on the inclination and orientation of the perturber orbit, the mass ratio and the periastron distance.

In § 4.1, the effects of inclined prograde ($0^\circ < i < 90^\circ$) and retrograde ($90^\circ < i < 180^\circ$) encounters are compared to the mostly widely studied coplanar prograde ($i = 0^\circ$) and retrograde ($i = 180^\circ$) ones. This study also includes the effects due to an encounter with a perturber on an orthogonal ($i = 90^\circ$) orbit. This is an interesting case, since for encounters with $r_{\text{peri}} < r_{\text{init}}$ the perturber passes right through the disc without having interacted much with the disc material before and after it crosses the disc.

Further, in § 4.2 the effects of inclining the perturber orbit along the x-axis are compared to the cases when the perturber orbit is inclined with respect to the xz plane i.e. effects due to different orientations (angle of periastron) of the perturber orbit are compared. In § 4.3 the results for the dependence of disc size on the mass ratio and periastron distance are presented for both coplanar and inclined encounters, followed by the dependence on the initial disc size in § 4.4.

For comparisons a few cases are discussed here. Actual data for the disc size after different encounter scenarios for the entire parameter space can be found in Appendices B, C & D.

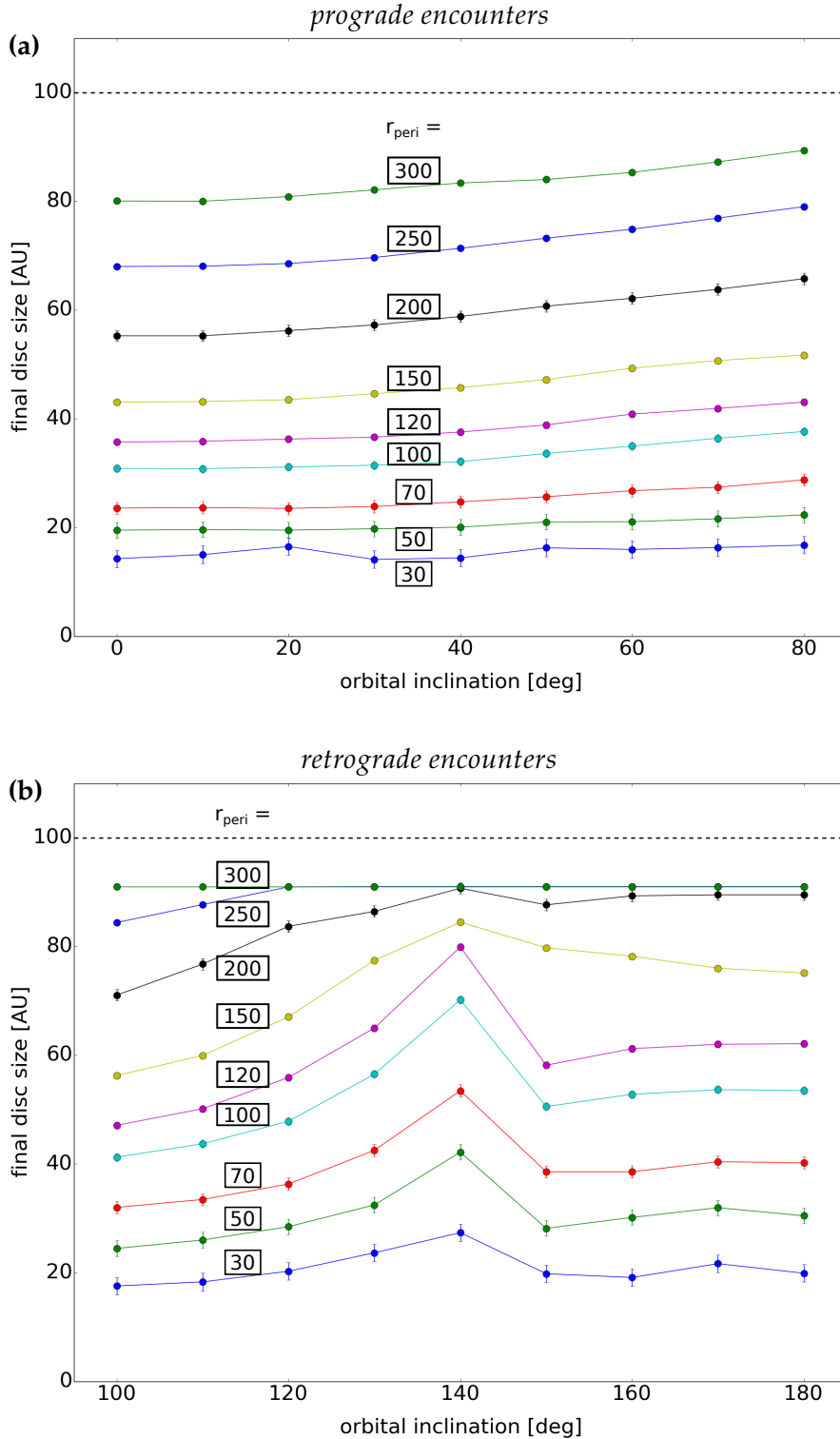


FIGURE 4.1: Final disc size [AU] versus orbital inclination [deg] covering (a) prograde encounters and (b) retrograde encounters. Here, for the equal-mass case, we compare the disc sizes after encounters at different periastron distances (r_{peri}) [AU, in boxes], for a fixed orbital orientation of $aop = 0^\circ$

4.1 Dependence on orbital inclination

In order to emphasise on the significance of retrograde encounters, in § 4.1.1 the effect on the disc size due to retrograde encounters is compared to the prograde ones. Further, in § 4.1.2 the importance of inclined encounters is highlighted.

4.1.1 Prograde vs Retrograde Encounters

Many studies have shown that prograde, coplanar encounters have the strongest influence on the disc in terms of mass loss and angular momentum loss [Clarke and Pringle, 1993, Heller, 1995, Hall et al., 1996, Pfalzner et al., 2005b, Olczak et al., 2006, Pfalzner and Olczak, 2007]. In their numerical studies, Breslau et al. [2014] have already shown a strong effect of prograde, coplanar encounters on the disc size. The studies done here show these results for the prograde **coplanar and inclined** encounters in terms of *disc size*. However, it is seen here for the disc size, that for the retrograde coplanar and inclined encounters, although the effect on the disc size is smaller compared to that in the prograde case, it is still considerable for a wide range of encounter parameters.

In order to first compare the effect on disc size due to **prograde** coplanar and inclined encounters, Fig. 4.1a shows the final disc size for an initial 100 AU disc around a star of mass $M_1 = 1 M_\odot$ perturbed by a star of mass $M_2 = 1 M_\odot$, on different prograde orbits with inclinations in the range $0^\circ \leq i < 90^\circ$ at different periastron distances ([AU], in boxes). Since here for the equal-mass case, encounters with $r_{\text{peri}} > 300$ AU have a negligible effect on the disc size, the cases only in the range $r_{\text{peri}} = 30$ AU - 300 AU are compared. The negligible effect here implies a disc-size change of less than 5% which is smaller than the errors typical for these type of simulations. The lower periastron limit of 30 AU has been chosen because for closer encounters the material remaining bound is less than 5 - 10 % of the initially bound particles which makes it difficult to determine a disc size.

The penetrating and grazing encounters ($r_{\text{peri}} \leq r_{\text{init}}$) destroy most of the disc whereas the distant encounters ($r_{\text{peri}} > r_{\text{init}}$) have an effect only in the outer regions of the disc. As seen in Fig. 4.1a for the prograde encounters, the disc size has an almost linear dependence on the inclination angle. For example, for $r_{\text{peri}} = 70$ AU (red line), the equal-mass coplanar ($i = 0^\circ$) encounter truncates an initial 100 AU disc to 24 AU, an encounter due to a perturber on an orbit with an inclination of 30° truncates the disc to 26 AU whereas a perturber on a highly inclined orbit of 60° reduces the disc to 27 AU. In case of penetrating and grazing encounters ($r_{\text{peri}} \leq 100$ AU), for a fixed periastron distance, the difference in the final disc size due to encounters at different orbital inclinations is less than 5 AU. In case of distant encounters ($r_{\text{peri}} > 100$ AU) where mostly

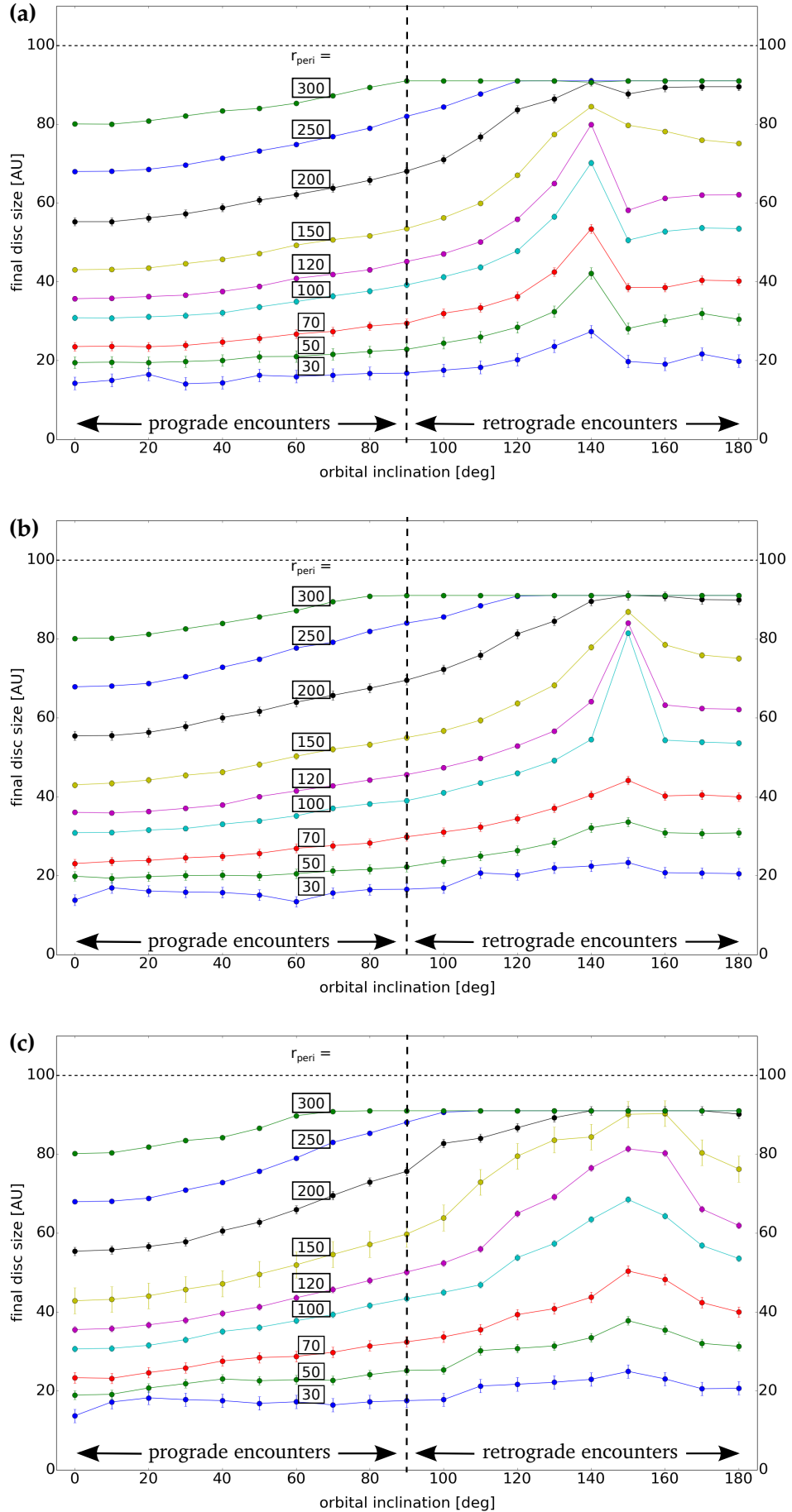


FIGURE 4.2: Final disc size [AU] versus orbital inclination [deg] covering prograde encounters and retrograde encounters. Here, for the equal-mass case, we compare the disc sizes after encounters at different periastron distances (r_{peri}) [AU, in boxes] for fixed orbital orientations of (a) $aop = 0^\circ$, (b) $aop = 45^\circ$ and (c) $aop = 90^\circ$.

only the outer disc particles are affected, this difference is seen to be ≤ 10 AU which is still small compared to the actual initial disc size of 100 AU. Hence these results can be approximated to have a linear dependence.

Figure 4.1b shows a similar plot for the **retrograde** coplanar and inclined encounters. In the case of retrograde encounters, the dependence on the inclination angle is more complex. For the equal-mass case, there is a peak at an inclination of 140° . However, if one compares only the coplanar retrograde ($i = 180^\circ$) case to the prograde cases, the linear dependence seen in case of prograde encounters can be extrapolated up to the coplanar retrograde case. For example, for $r_{\text{peri}} = 70$ AU (red line), the difference between the final disc size of 41 AU due to a perturber on a coplanar retrograde ($i = 180^\circ$) orbit and the mean value obtained from the linear extrapolation is less than ≈ 10 AU.

4.1.2 Coplanar vs Inclined Encounters

Now, in order to compare the disc sizes for all the different orbital inclinations in the range $0^\circ - 180^\circ$ including both the prograde and retrograde cases, Fig. 4.2a shows a similar plot of final disc size as a function of orbital inclination for the equal-mass case after encounters at different periastron distances ([AU], in boxes). Similar plots for all the different mass ratios (m_{12}) considered in this study can be found in Appendix E. Note that here the angle of periastron is fixed to 0° and the inclination of the perturber orbit is defined with respect to the x-axis. The dependence on the orbital inclination for the other two cases of encounters at orbital orientations $aop = 45^\circ$ & 90° where the periastron lies outside the disc plane are shown in Figures 4.2b & 4.2c, respectively. The dependence of disc size on the orbital orientation is discussed later in § 4.2.

In all the three plots it can be clearly seen that although the prograde encounters ($0^\circ \leq i < 90^\circ$) have a stronger influence on the disc leading to smaller disc sizes, even the retrograde encounters ($90^\circ < i \leq 180^\circ$) have a considerable effect. In case of coplanar encounters, for example as seen in Fig. 4.2a for $aop = 0^\circ$, an equal-mass ($m_{12} = 1$), prograde ($i = 0^\circ$) encounter at $r_{\text{peri}} = 100$ AU (sky blue) truncates an initial 100 AU disc to 31 AU. In the retrograde case ($i = 180^\circ$), the disc is reduced to 54 AU. For the case of inclined encounters, it can be seen that although the prograde encounters have a stronger effect on the disc size as compared to the retrograde ones, the effects of retrograde encounters on the disc size are still significant. For example for the equal-mass case, an encounter at $r_{\text{peri}} = 100$ AU on a prograde orbit of $i = 60^\circ$ truncates the initial 100 AU disc to 34 AU whereas in the retrograde case for $i = 120^\circ$, the 100 AU disc is truncated to 48 AU. The difference in the final disc sizes between the prograde and the retrograde cases is seen to be more significant for distant, non-grazing encounters ($r_{\text{peri}} > 100$ AU). These are the type of encounters that dominate in most star cluster

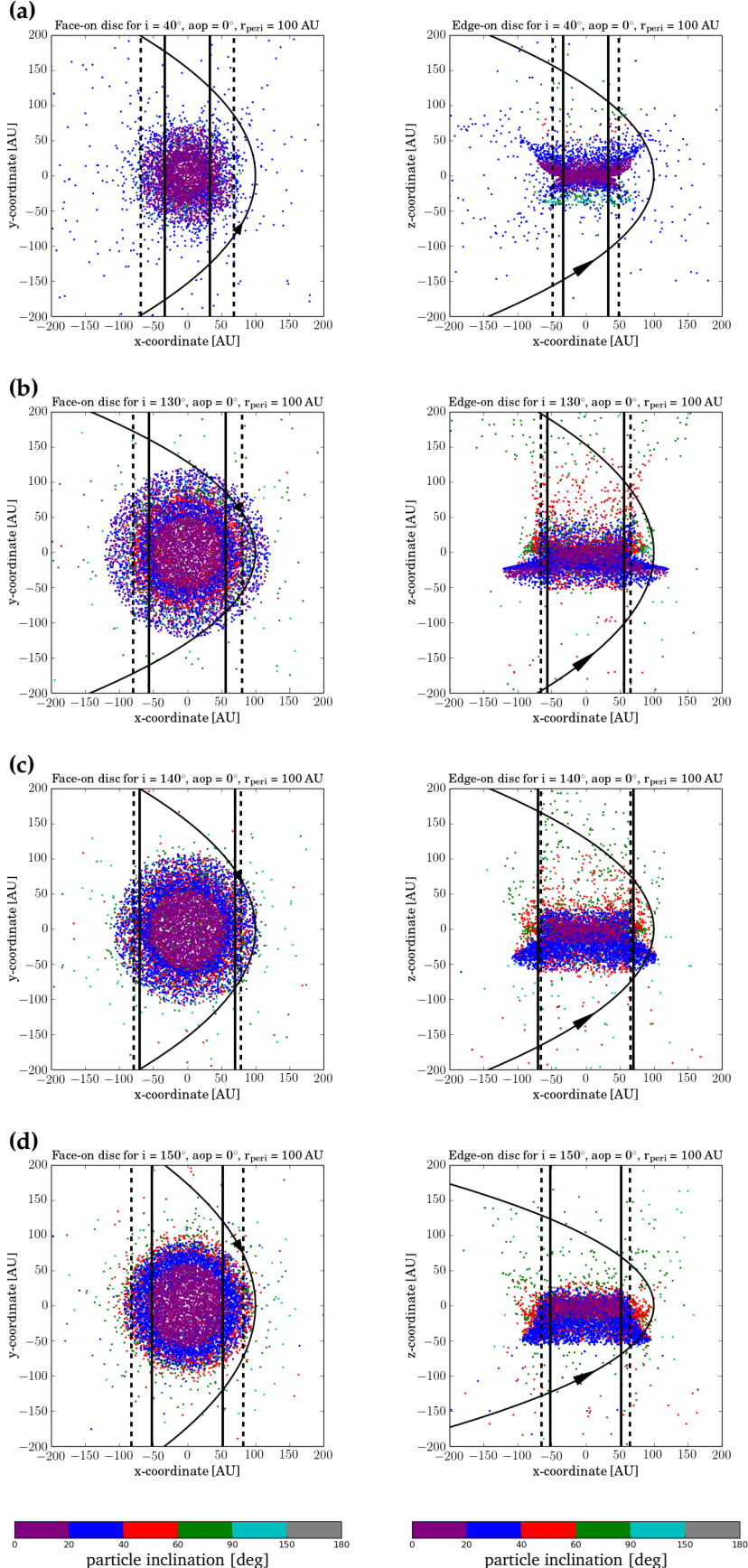


FIGURE 4.3: Face-on and edge-on disc plots at the final time step after an encounter at $r_{\text{peri}} = 100$ AU by a $1 M_{\odot}$ perturber at orbital inclinations (a) $i = 40^\circ$, (b) $i = 130^\circ$, (c) $i = 140^\circ$, (d) $i = 150^\circ$. Vertical solid black line indicates the disc size from steepest gradient in long term averaged surface density profile. Vertical dashed black line indicates the disc size from steepest gradient in projected surface density profile. The different colors indicate **particle inclinations**, the values for which can be found in the legend.

environments [Scally and Clarke, 2001, Olczak et al., 2006].

Here, we would like to emphasise that the effects of *inclined* encounters are **nearly as significant** as compared to the coplanar ones. It has been argued before by Pfalzner et al. [2005b] that inclined encounters do have a considerable effect on the disc mass and angular momentum. However, in their study they found that the effects due to retrograde inclined encounters ($90^\circ < i < 180^\circ$) are significant *only* for penetrating and grazing encounters ($r_{\text{peri}} \leq r_{\text{init}}$). By contrast, in our studies for disc size, we find a considerable effect on the disc size even due to *distant* retrograde, inclined encounters at least up to an encounter distance of $r_{\text{peri}} \approx 5 \cdot r_{\text{init}}$, depending on the perturber mass. Hence it is important to understand that there can be a disc-size change despite of no disc-mass loss or angular momentum loss. The disc-size change is seen an effect of the inward movement of the outer disc particles due to gravitational interactions during stellar fly-bys.

It is also important to note that disc sizes are least susceptible to fly-bys on *inclined* retrograde orbits ($\sim 140^\circ - 160^\circ$) and not for the coplanar retrograde ($i = 180^\circ$) encounter as one would expect. For example, for the equal-mass case an encounter at $r_{\text{peri}} = 150$ AU on a orbit with inclination $i = 140^\circ$ truncates an initial 100 AU disc to 84 AU whereas an encounter due to a perturber on a coplanar retrograde ($i = 180^\circ$) orbit reduces the disc to a comparatively smaller size of 74 AU.

In order to understand if the peak seen at $i = 140^\circ$ is a result of the here used disc size definition, a numerical artifact or a physical effect, it is further investigated by studying the effects of different encounter scenarios on the particle inclinations (Fig. 4.3) and eccentricities (Fig. 4.4) at the final time step and determining the disc size using projected surface densities. The left column of these figures show the face-on view of discs at the final time step after an equal-mass encounter with a perturber on orbital inclinations of $i = 40^\circ$ (a), 130° (b), 140° (c) and 150° (d) whereas the right columns show the corresponding edge-on view. The vertical solid black line indicates the final disc size from steepest gradient in long term averaged surface density profile (discussed in § 3.2). The perturber orbit is shown with the arrow indicating the direction in which the perturber moves on the orbit (note the differences in the prograde and retrograde cases).

Observationally, it is a difficult task to estimate the appropriate disc size due to the dependence on the viewing angle. Depending on how one observes the disc, either face-on, edge-on, or at inclinations in between, not all the particles would be taken into account while estimating the surface density profiles; especially the ones on highly eccentric and/or inclined orbits.

Hence the projected surface densities are calculated in both the xy plane (face-on) and xz plane (edge-on) using the data from the final time step when most of the particles are on stable orbits after the encounter. The final disc sizes are then calculated for both

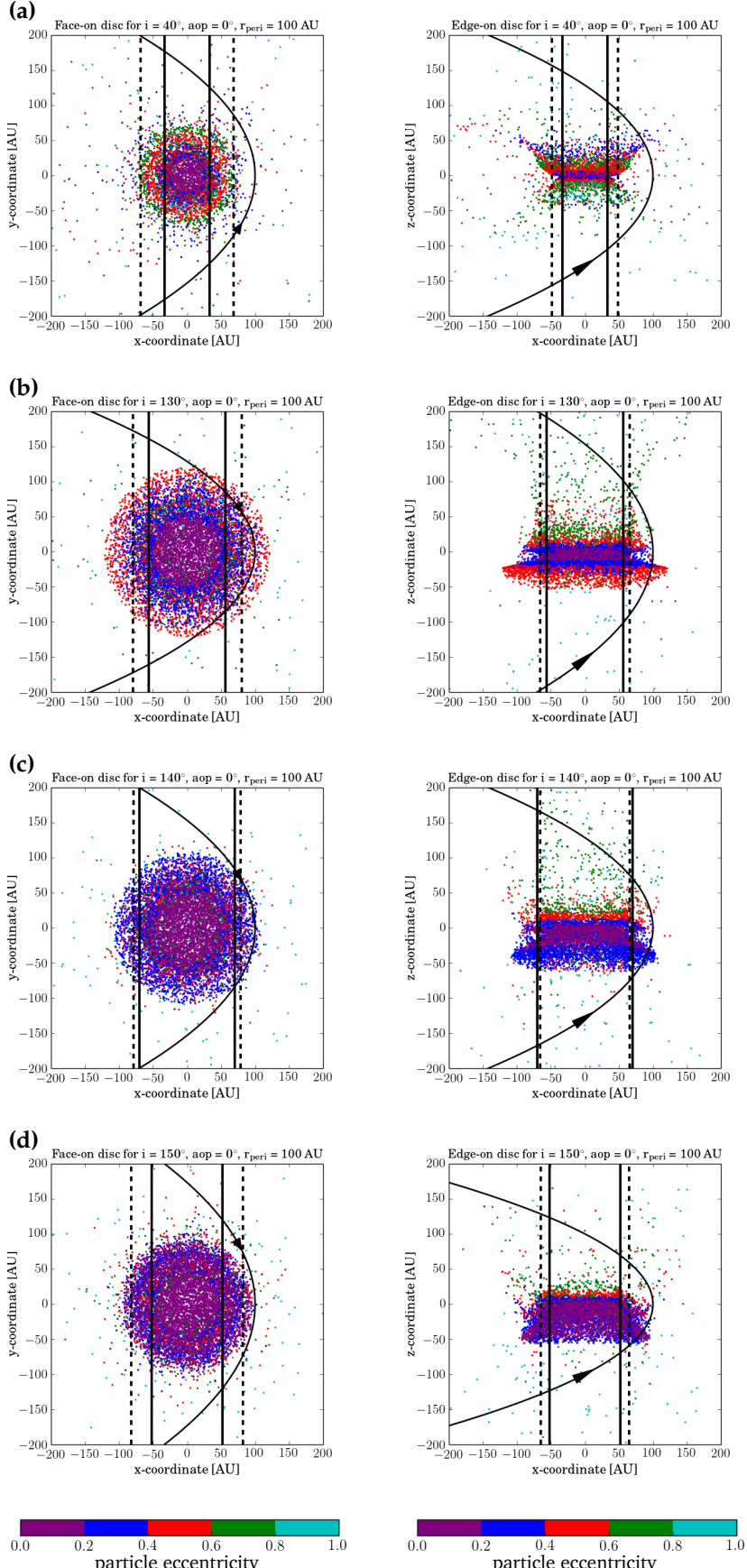


FIGURE 4.4: Face-on and edge-on disc plots at the final time step after an encounter at $r_{\text{peri}} = 100 \text{ AU}$ by a $1 M_\odot$ perturber at orbital inclinations **(a)** $i = 40^\circ$, **(b)** $i = 130^\circ$, **(c)** $i = 140^\circ$, **(d)** $i = 150^\circ$. Vertical solid black line indicates the disc size from steepest gradient in long term averaged surface density profile. Vertical dashed black line indicates the disc size from steepest gradient in projected surface density profile. The different colors indicate **particle eccentricities**, the values for which can be found in the legend.

the cases, using the similar idea of the steepest gradient in the surface density profiles but considering the steepest gradient beyond the limit where at least 80% of the finally bound particles lie within the disc size. These disc sizes can then be considered to be the upper limit and are shown by the vertical dashed lines in Fig. 4.3 & Fig. 4.4.

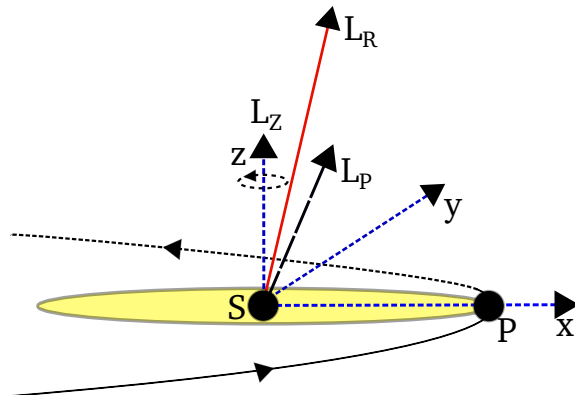
Using either of the disc size definitions one would still observe a gradual increase in the final disc size up to an inclination in the range $i = 140^\circ - 160^\circ$, depending on the mass ratio and periastron distance, and then a decrease for perturber orbital planes closer to the disc plane. Thus the disc size and the fate of the particles initially on circular, coplanar orbits has a strong dependence on the orbital inclination of the perturber.

In Fig. 4.3, particle inclinations have been indicated by different colors, the values for which can be found in the legend. For example, particles having inclinations $\leq 20^\circ$ are shown in purple and those with inclinations in the range $20^\circ - 40^\circ$ are shown in dark blue and so on. Similarly, in Fig. 4.4 particle eccentricities have been indicated by different colors. For example, particles on almost circular orbits with eccentricities in the range 0 - 0.2 are shown in purple and those on orbits tending to parabolic ones with eccentricity > 0.8 are shown in cyan whereas the values for the intermediate cases can be found in the legend.

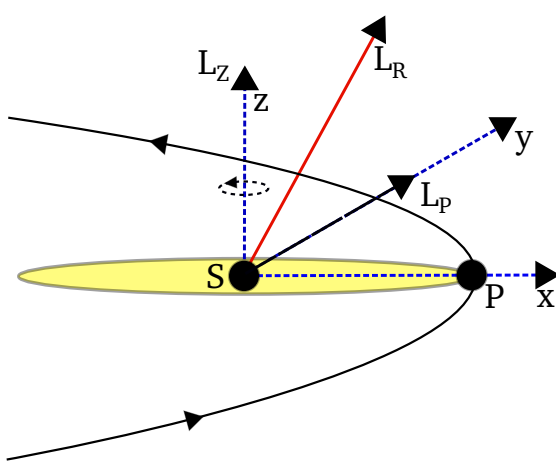
The prograde inclined encounter ($i = 40^\circ$) has a much stronger effect on the disc, truncating it to a relatively smaller disc size in comparison to the retrograde encounters. In all the retrograde cases, the disc is not sharply truncated but the impact of the encounter results in an increase in the outer disc particle inclination and eccentricity as seen in the figures. The disc appears to be more like a torus due to the particles on inclined and/or eccentric orbits.

The particle inclinations and eccentricities can be explained to be a combined effect of the resultant angular momentum due to the torque acting on the disc and the force due to both the stars acting on the particles. Figure 4.5 shows the schematic for the resultant angular momentum of the disc particles in case of a prograde (a), orthogonal (b) and retrograde (c) encounter. Assuming the disc to lie in the xy plane and particles moving in the counter-clockwise direction, the total angular momentum due to the disc particles is always going to be along the z -axis, perpendicular to the disc plane as indicated by L_Z . Depending on the inclination of the perturber orbit, the angular momentum due to the perturber (L_P) points either in the positive or negative yz plane. In case of the prograde encounters, the resultant angular momentum (L_R) lies closer to the z -axis resulting in a small effect on the particle inclinations and eccentricities. The angle between the z -axis and the resultant angular momentum increases with an increase in perturber orbital inclination as indicated for the cases of orthogonal (Fig. 4.5b) and retrograde (Fig. 4.5c) encounters. For the equal-mass case, this angle is maximum ($L_R \perp L_Z$) when the inclination of the perturber orbit is equal to 140° . This effect is seen as an increase in particle inclinations and eccentricities.

(a)



(b)



(c)

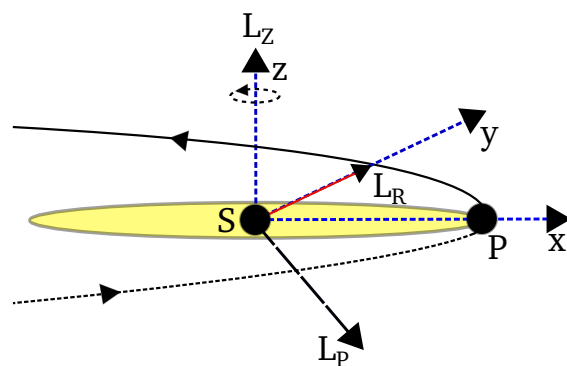


FIGURE 4.5: Schematics showing the resultant angular momentum (L_R) of the disc particles due to (a) prograde, (b) orthogonal and (c) retrograde encounters. L_Z indicates the total angular momentum of the disc particles and L_P indicates the angular momentum of the perturber (P).

In cases where the particles are on inclined and/or eccentric orbits (as seen more clearly in the edge-on plots in Figures 4.3 & 4.4), it is very difficult to define a disc size since one cannot observe a sharp truncation in the disc. In these cases, the disc size determined using the steepest gradient in the surface density profile is smaller than what one would expect since the final disc sizes are estimated considering the non-inclined particles in the disc plane as a result of the disc size definition. As discussed in § 3.2, the particles on highly eccentric orbits would have a small contribution to the overall radial probability distribution. Mostly it is the particles on circular orbits that have a significant contribution to the temporal averaged surface density which is used to determine the resulting disc size. However, the problem is not the here used disc size definition. The large amount of particles on inclined and eccentric orbits is a problem for *any* definition of the disc size. These effects leads to the peak seen at $i = 140^\circ$ for the equal-mass case.

The peak shifts in the range $i = 140^\circ - 160^\circ$ for different mass ratios as indicated by different colors in Fig. 4.6 below. The shift of the peak is a result of the amount of force acting on the disc particles depending on the perturber mass and orbital inclination. A more massive perturber on an orbit closer to the disc plane (i.e. smaller inclinations with respect to the disc plane) will have a stronger effect on the disc leading to an increase in outer disc particle inclinations and eccentricities and hence in turn making it difficult to determine a disc size. The combined effect of the resultant angular momentum (as discussed earlier) and the force of the perturber acting on the disc is then observed as the shift of the peak.

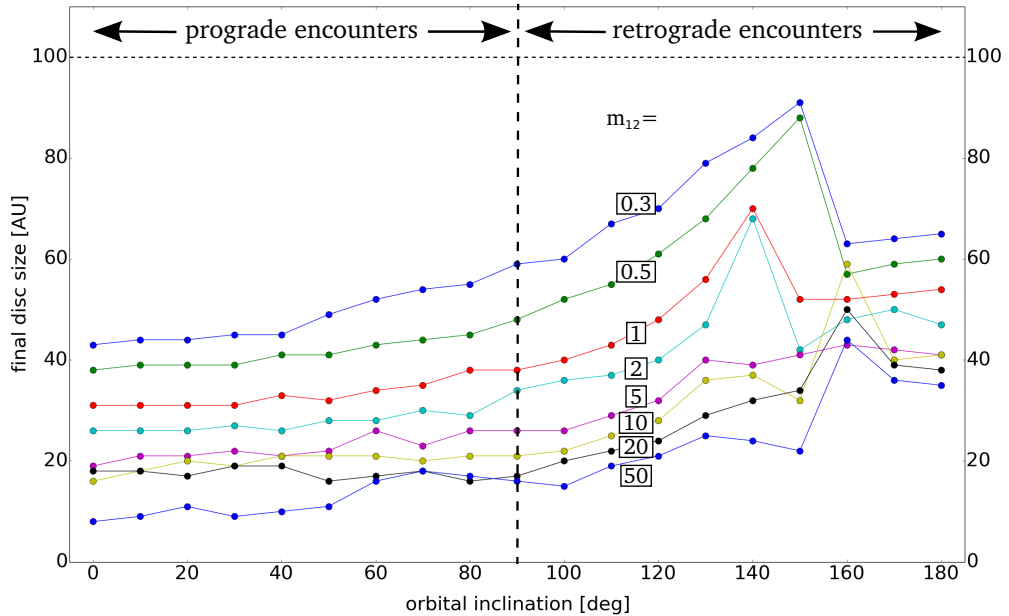


FIGURE 4.6: Final disc size versus orbital inclination [deg] covering prograde and retrograde encounters. Here we compare final disc sizes after an encounter at $r_{peri} = 100$ AU for different mass ratios (m_{12}) [in boxes].

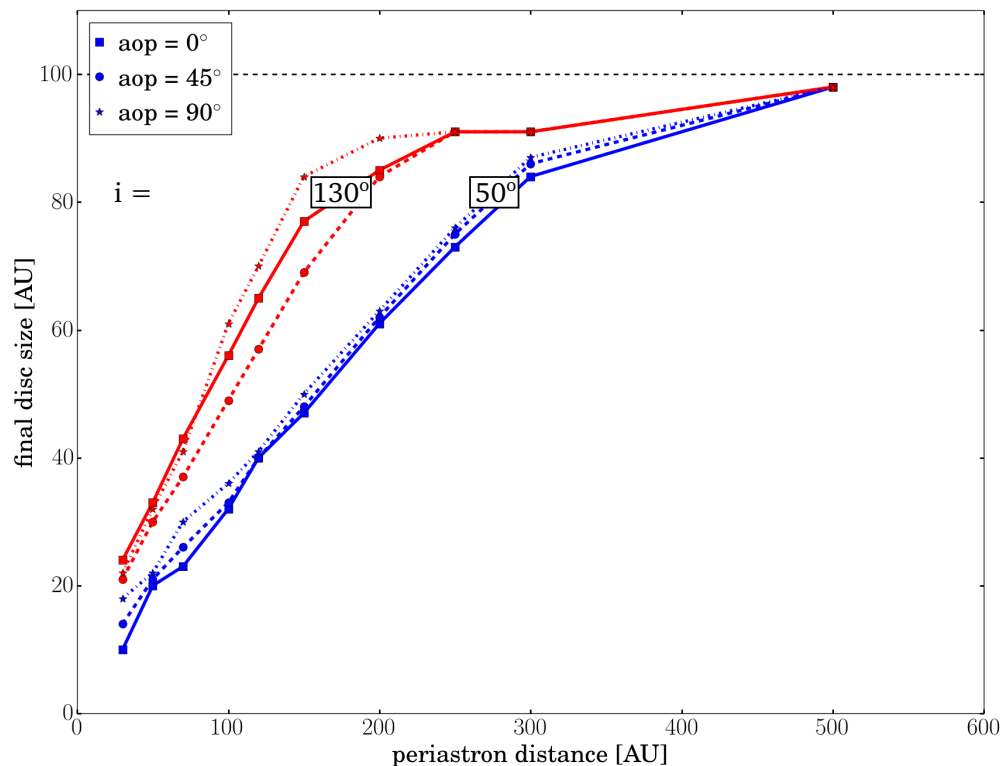


FIGURE 4.7: Final disc size versus periastron distance for a disc with an initial 100 AU radius. Here the equal-mass case is compared for $aop = 0^\circ$ (squares, solid line), $aop = 45^\circ$ (circles, dashed line) and $aop = 90^\circ$ (stars, dotted line). Two cases for a pro-grade encounter $i = 50^\circ$ (blue) and a retrograde encounter $i = 130^\circ$ (red) are shown.

4.2 Dependence on orbital orientation

For three different orientations ($aop = 0^\circ, 45^\circ, 90^\circ$) of the perturber orbit in the xy plane (disc plane) as discussed in § 3.1.2, we have performed similar studies for the entire parameter space (all inclinations, mass ratios and periastron distances). For most of the parameter space, we found a small difference ($\leq 10\%$) in the disc sizes for the different orbital orientations. For example, Fig. 4.7 shows the final disc size versus the periastron distance for $aop = 0^\circ$ (squares, solid line), $aop = 45^\circ$ (circles, dashed line) and $aop = 90^\circ$ (stars, dotted line). Here the dependence of disc size on the aop for two cases of a prograde ($i = 50^\circ$, blue) and a retrograde ($i = 130^\circ$, red) encounter are discussed. For the prograde encounter, we find a linear dependence of the disc size on aop. The disc size differs by ≤ 5 AU. For the retrograde encounter, the dependence of the disc size on aop is more complex. However, the difference in the disc size for the three different orientations is less than 10 AU which is still not very significant.

Hall et al. [1996] stated that they do not expect a substantial difference between orientations with periastron outside the disc plane ($aop = 90^\circ$) and the orientations with periastron in the disc plane ($aop = 0^\circ$). Here, we perform the actual study and confirm their expectation.

Although we do not find a significant difference in the disc size for the different orientations, we do find a difference in the outer disc particle inclinations ($\leq 20^\circ$) and eccentricities for penetrating and grazing encounters. For the case of an equal-mass encounter at a periastron distance of 100 AU, this can be seen in Fig. 4.8 where one can compare the effects on particle inclinations and in Fig. 4.9 which indicates the effects on particle eccentricities for the extreme cases due to different orientations and for different orbital inclinations. For example, in the case for the orthogonal encounter ($i = 90^\circ$, Fig. 4.8c) where the perturber passes through the disc, the disc size (solid black line) after an encounter due to a perturber on the three different orbital orientations differ by less than 5 AU. However as seen in the face-on plots, for the case of $aop = 45^\circ$, at a radius of 120 AU the outer disc particle inclinations are in the range $40^\circ - 60^\circ$ (red particles) whereas in the other two cases of $aop = 0^\circ$ and $aop = 90^\circ$, comparatively fewer highly inclined particles are seen at the radius of 120 AU, and most of them have inclinations in the range $20^\circ - 40^\circ$. A similar effect is seen in case of particle eccentricities (see Fig. 4.9c).

It would hence be interesting to study the consequences of the different encounter scenarios on highly inclined Sedna-like bodies in our solar system as well as for wide-orbit extrasolar planets.

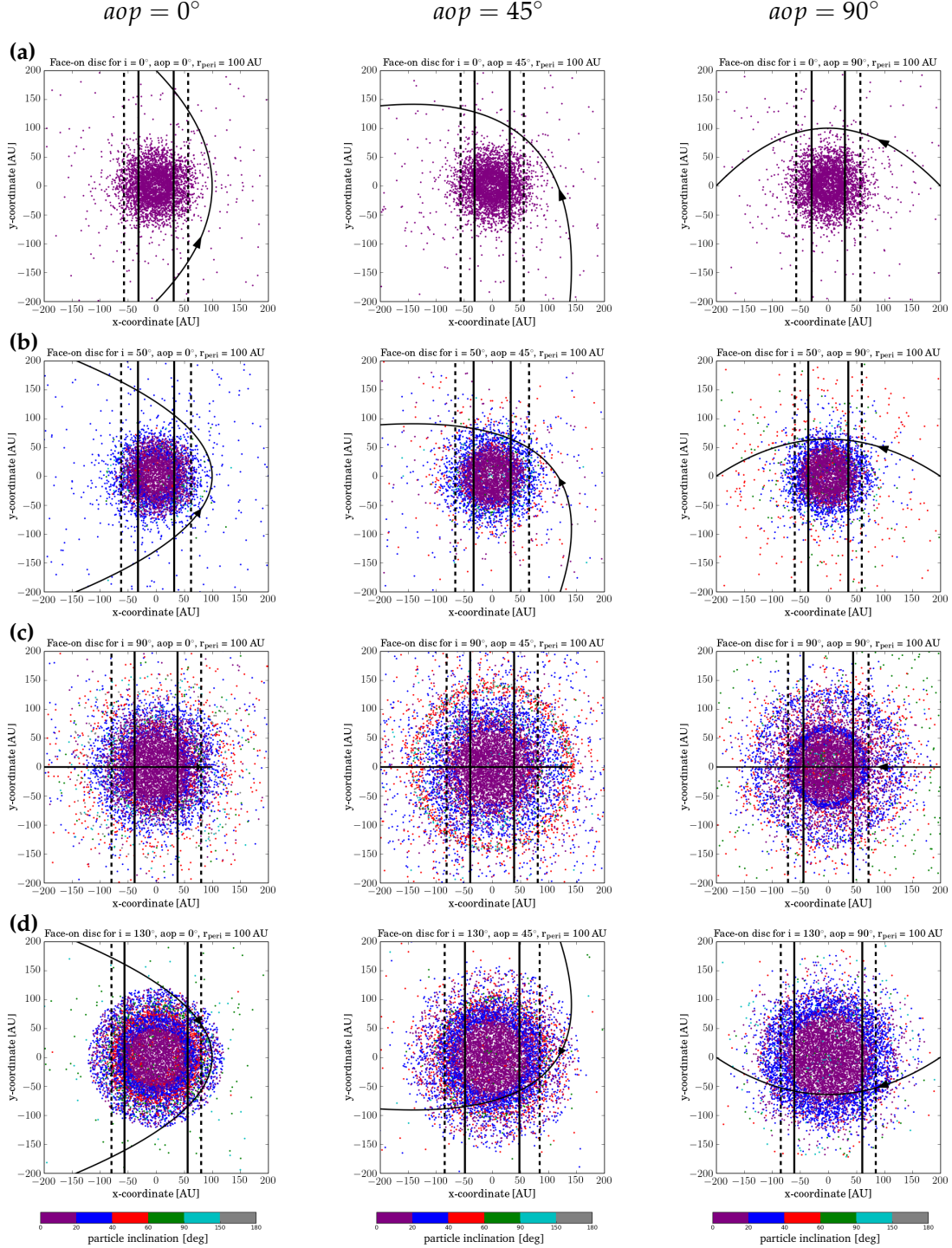


FIGURE 4.8: Face-on disc plots showing particle inclinations at the final time step after an encounter at $r_{\text{peri}} = 100$ AU, by a $1 M_{\odot}$ perturber on different orientations ($aop = 0^\circ, 45^\circ, 90^\circ$) and orbital inclinations (a) $i = 0^\circ$, (b) $i = 50^\circ$, (c) $i = 90^\circ$ and (d) $i = 130^\circ$. Vertical solid black line indicates the disc size from steepest gradient in long term averaged surface density profile. Vertical dashed black line indicates the disc size from steepest gradient in projected surface density profile. The different colors indicate **particle inclinations**, the values for which can be found in the legend.

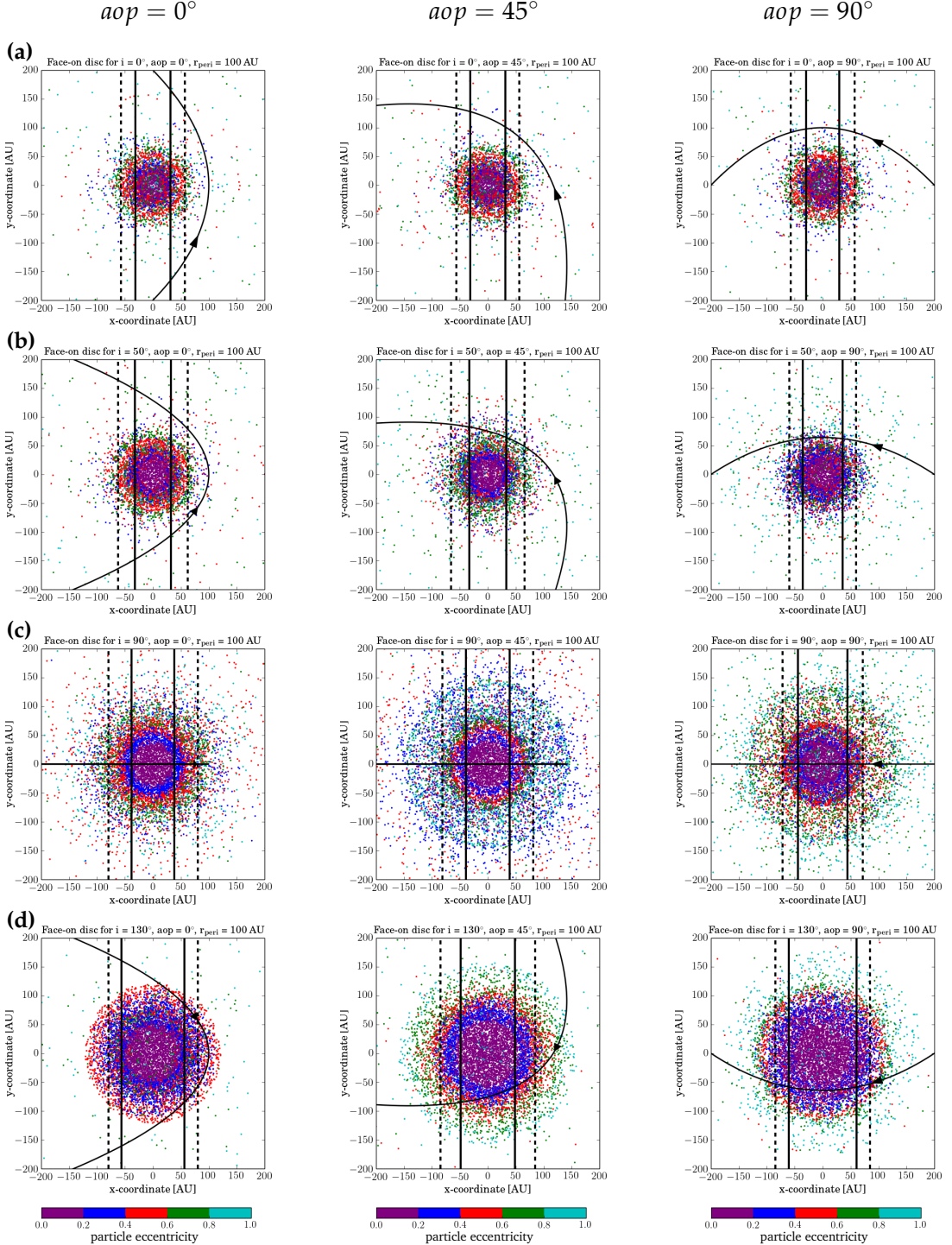


FIGURE 4.9: Face-on disc plots showing particle eccentricities at the final time step after an encounter at $r_{peri} = 100$ AU, by a $1 M_\odot$ perturber on different orientations (**a**) $i = 0^\circ$, (**b**) $i = 50^\circ$, (**c**) $i = 90^\circ$ and (**d**) $i = 130^\circ$. Vertical solid black line indicates the disc size from steepest gradient in long term averaged surface density profile. Vertical dashed black line indicates the disc size from steepest gradient in projected surface density profile. The different colors indicate **particle eccentricities**, the values for which can be found in the legend.

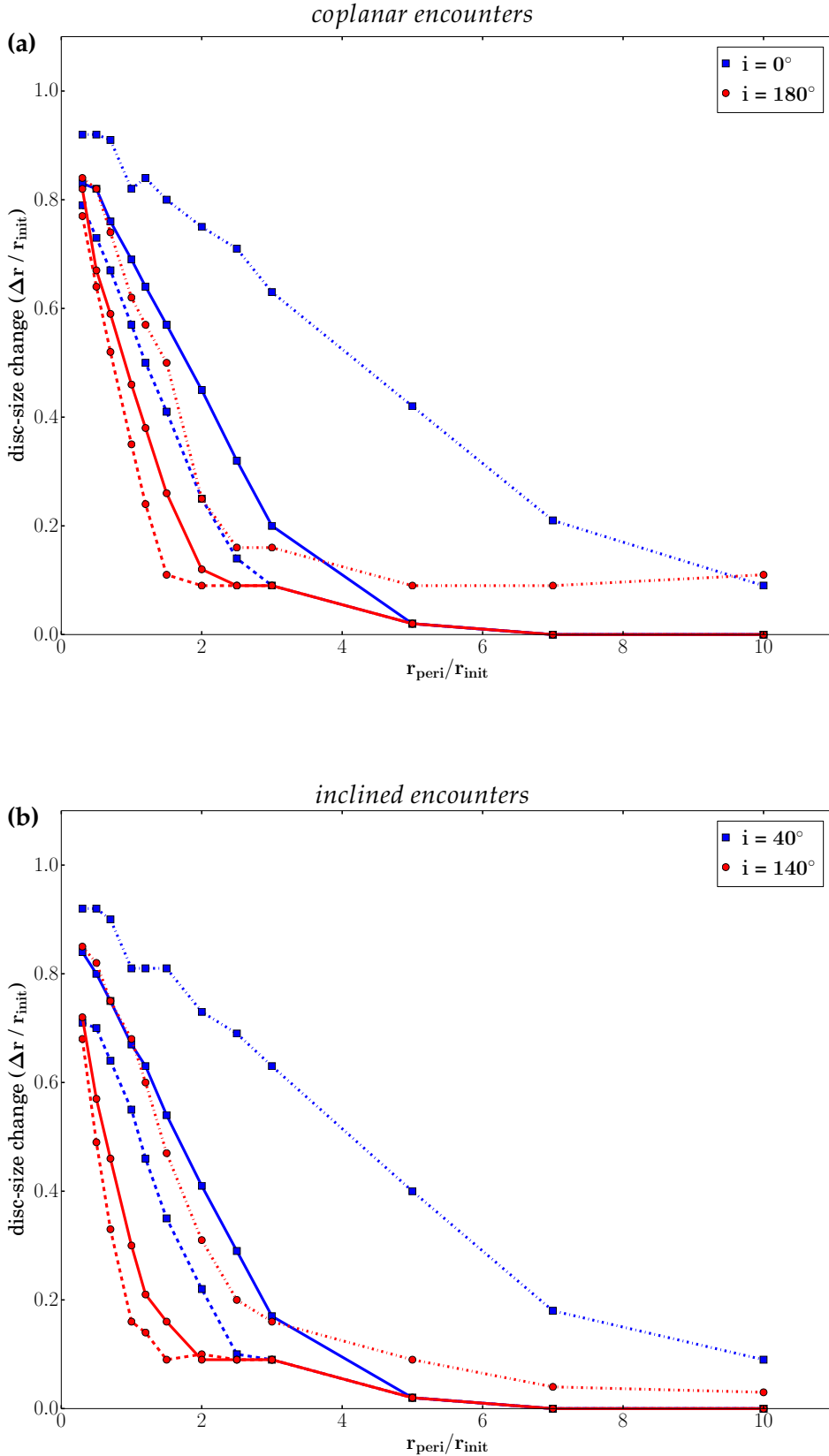


FIGURE 4.10: Disc-size change versus periastron distance scaled to the initial disc size (100 AU) for $m_{12} = 0.3 M_\odot$ (dashed), $1.0 M_\odot$ (solid) and $20.0 M_\odot$ (dotted) after prograde (blue squares) and retrograde (red circles) (a) *coplanar* and (b) *inclined* encounters.

4.3 Dependence on mass ratio and periastron distance

Next, we investigate the dependence of the disc size on the mass ratio. Firstly, for mass ratios, $m_{12} = 0.3 M_{\odot}$ (dashed), $1.0 M_{\odot}$ (solid) and $20.0 M_{\odot}$ (dotted), Fig. 4.10a shows the disc-size change versus the periastron distance scaled to the initial disc size (100 AU) for parabolic, *coplanar*, prograde ($i = 0^\circ$, blue squares) and retrograde ($i = 180^\circ$, red circles) encounters and Fig. 4.10b shows a similar plot for parabolic, *inclined*, prograde ($i = 40^\circ$, blue squares) and retrograde ($i = 140^\circ$, red circles) encounters. Note that unlike in previous plots in § 4.1 & § 4.2, here the y-axis represents the disc-size change and not the final disc size.

As seen in these figures, we find a simple dependence of the disc size on the mass ratio and periastron distance for both coplanar as well as inclined encounters. A more massive perturber has a greater influence on the disc hence resulting in larger disc-size change. For example an inclined, prograde encounter ($i = 40^\circ$, blue squares) at $r_{\text{peri}} = 100$ AU and $m_{12} = 1$ (Fig. 4.10b, blue solid line) truncates roughly 67% of the initial 100 AU disc whereas for a higher mass ratio $m_{12} = 20$ (Fig. 4.10b, blue dotted line) which has a stronger influence, nearly 81% of the initial disc is truncated.

Further, we also study the dependence of the disc size on the periastron distance. Our studies indicate that the closer the encounter distance, the more significant is the disc truncation. For example, an inclined, prograde ($i = 40^\circ$, Fig. 4.10b), equal-mass ($m_{12} = 1$, solid line) penetrating encounter at $r_{\text{peri}} = 50$ AU truncates 80% of the initial 100 AU disc whereas a distant encounter at $r_{\text{peri}} = 300$ AU truncates only 17% of the initial disc, affecting mostly only the outer disc region.

For the case of coplanar, prograde encounters, using pure N-body simulations, Breslau et al. [2014] found a similar dependence of the final disc size (r_{final}) on the mass ratio (m_{12}) and periastron distance (r_{peri}) to be of the form

$$r_{\text{final}} = 0.28 \cdot r_{\text{peri}} \cdot m_{12}^{-0.32}. \quad (4.1)$$

Here we expand the parameter range to study the dependence of the disc size on the mass ratio and periastron distance for both inclined and retrograde encounters.

Figure 4.11 shows the face-on view (at the final time step) of initial 100 AU discs for different mass ratios ($m_{12} = 0.5, 5, 20$) after an encounter at $r_{\text{peri}} = 100$ AU with a perturber on orbits with different inclinations. In this figure, one can compare the fate of the disc due to encounters with different mass perturbers as well as the influence of prograde coplanar ($i = 0^\circ$, Fig. 4.11a) & inclined ($i = 40^\circ$, Fig. 4.11b) and retrograde inclined ($i = 140^\circ$, Fig. 4.11c) & coplanar ($i = 180^\circ$, Fig. 4.11d) encounters. As seen in these plots, the more massive the perturber, the more influence it has on the disc particles. For example, an encounter on an orbital inclination of $i = 40^\circ$ (Fig. 4.11b)

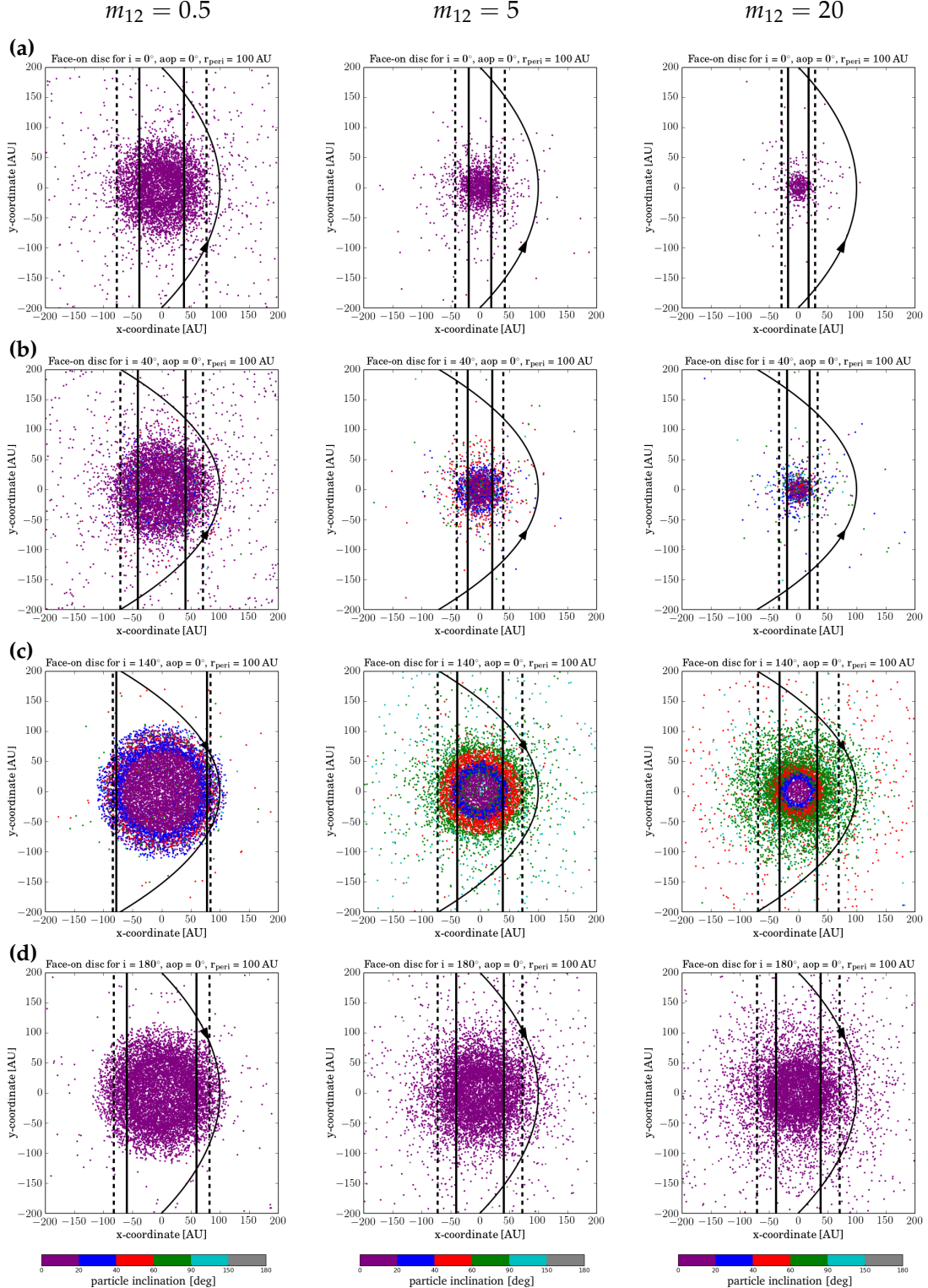


FIGURE 4.11: Face-on disc plots for an initial 100 AU disc for different mass ratios ($m_{12} = 0.5, 5, 20$) at the final time step after encounters at $r_{\text{peri}} = 100$ AU on orbital inclinations (a) $i = 0^\circ$, (b) $i = 40^\circ$, (c) $i = 140^\circ$, (d) $i = 180^\circ$. Vertical solid black line indicates the disc size from steepest gradient in long term averaged surface density profile. Vertical dashed black line indicates the disc size from steepest gradient in projected surface density profile.

at $r_{\text{peri}} = 100$ AU due to a massive perturber $M_2 = 20 M_\odot$ destroys most of the disc, leading to a final disc size of 19 AU whereas a perturber with $M_2 = 0.5 M_\odot$ leads to a disc size of 41 AU.

Figure 4.12 shows the face-on view (at the final time step) of initial 100 AU discs around a $1 M_\odot$ star after an encounter with a $1 M_\odot$ perturber on different orbital inclinations at different periastron distances. In this figure, one can compare the fate of the disc due to a penetrating ($r_{\text{peri}} = 50$ AU), grazing ($r_{\text{peri}} = 100$ AU) and distant ($r_{\text{peri}} = 200$ AU) encounter as well as the influence of prograde coplanar ($i = 0^\circ$) & non-coplanar ($i = 40^\circ$) and retrograde coplanar ($i = 180^\circ$) & non-coplanar ($i = 140^\circ$) encounters. The closer the perturber approaches the disc, the stronger is the disc truncation. For example, an equal-mass encounter on an orbital inclination of $i = 40^\circ$ (Fig. 4.12b) at a distance $r_{\text{peri}} = 50$ AU, penetrating through the initial 100 AU disc, destroys most of the disc leading to a final disc size of 20 AU whereas a distant encounter at $r_{\text{peri}} = 200$ AU affects mostly the outer disc particles, truncating the disc to 59 AU.

We find a similar dependence of disc size on mass ratio and periastron distance for the other cases of $aop = 45^\circ$ & 90° .

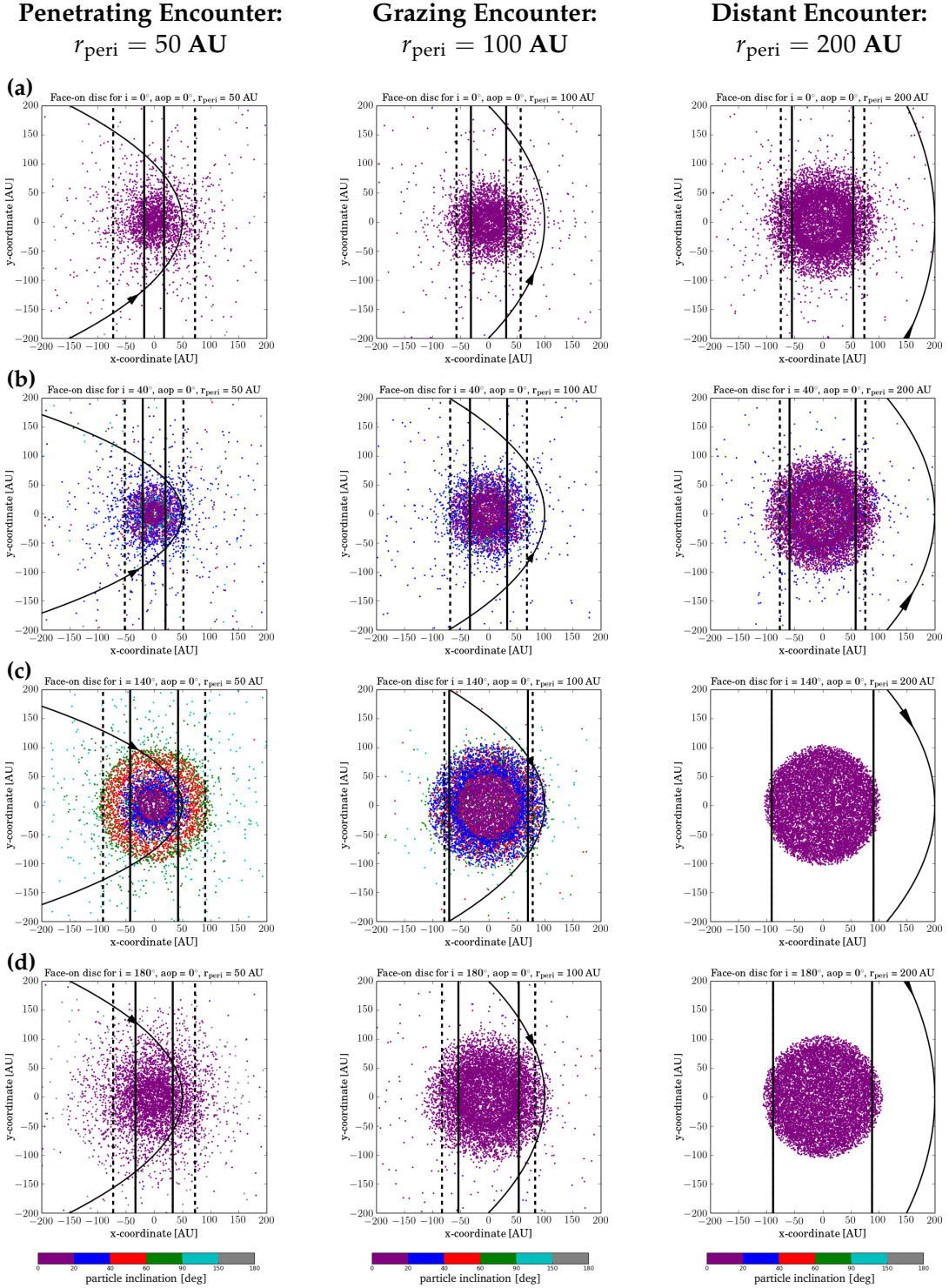


FIGURE 4.12: Face-on disc plots at the final time step for an initial 100 AU disc around a $1 M_\odot$ star after an encounter by a $1 M_\odot$ perturber at orbital inclinations (a) $i = 0^\circ$, (b) $i = 40^\circ$, (c) $i = 140^\circ$, (d) $i = 180^\circ$ at different periastron distances ($r_{\text{peri}} = 50, 100, 200 \text{ AU}$). Vertical solid black line indicates the disc size from steepest gradient in long term averaged surface density profile. Vertical dashed black line indicates the disc size from steepest gradient in projected surface density profile.

4.4 Dependence on initial disc size

Next we want to see how the results depend on the initial disc size. In their studies for coplanar, prograde encounters, Breslau et al. [2014] have already indicated that the final disc size is independent of the initial disc size. It is always the periastron distance and the mass ratio that determine the final disc size (see equation 4.1). In order to verify this result for the coplanar, prograde case and to study the dependence for the inclined and retrograde cases, a similar set of simulations as described in § 3.1, was performed for an initial disc size (r_{init}) of 200 AU.

As stated before, in the studies where viscous forces and self-gravity can be neglected, the fly-by can be treated as a three-body encounter for each particle. This basically implies that the fate of individual particles is independent of the remaining disc. Therefore, in this case the final disc size is independent of the initial disc size. This is confirmed by our simulation results as shown in Fig. 4.13 where the final disc size for an initial 100 AU disc (blue squares) are the same within the simulation error, as those for the disc with an initial size of 200 AU (red diamonds), as long as the final disc size is smaller than 100 AU.

Here, the resulting disc sizes obtained from the steepest gradient in the surface density after coplanar, prograde ($i = 0^\circ$, Fig. 4.13a) and inclined, retrograde ($i = 120^\circ$, Fig. 4.13b) encounters for an initial disc size of 200 AU are compared to the case of an initial 100 AU disc. It is seen that the dependence of the final disc size on the mass ratio, periastron distance and orbital inclination is the same irrespective of the initial disc size. The final disc size and the periastron distance can be scaled to an arbitrary initial disc size.

For example, as seen in Fig. 4.13a, for the coplanar, prograde ($i = 0^\circ$), equal-mass case ($m_{12} = 1$), for $r_{\text{init},1} = 100$ AU an encounter at $r_{\text{peri},1} = 200$ AU = $2 \cdot r_{\text{init},1}$ gives a disc size $r_{\text{disc},1} = 50$ AU = $0.5 \cdot r_{\text{init},1}$ whereas for $r_{\text{init},2} = 200$ AU an encounter at the same relative periastron distance $r_{\text{peri},2} = 2 \cdot r_{\text{init},2} = 400$ AU gives a resulting disc size $r_{\text{disc},2} = 100$ AU = $0.5 \cdot r_{\text{init},2}$. These results are confirmed using our simulations.

This is also valid for the inclined and retrograde encounters (Fig. 4.13b). For example, for the inclined, retrograde ($i = 120^\circ$) case of $m_{12} = 0.3$, for $r_{\text{init},1} = 100$ AU an encounter at $r_{\text{peri},1} = 100$ AU = $r_{\text{init},1}$ gives a disc size $r_{\text{disc},1} = 70$ AU = $0.7 \cdot r_{\text{init},1}$ whereas for $r_{\text{init},2} = 200$ AU an encounter at the same relative periastron distance $r_{\text{peri},2} = r_{\text{init},2} = 200$ AU gives a resulting disc size $r_{\text{disc},2} = 140$ AU = $0.7 \cdot r_{\text{init},2}$. Thus, our simulation results can be generalized to arbitrary initial disc sizes.

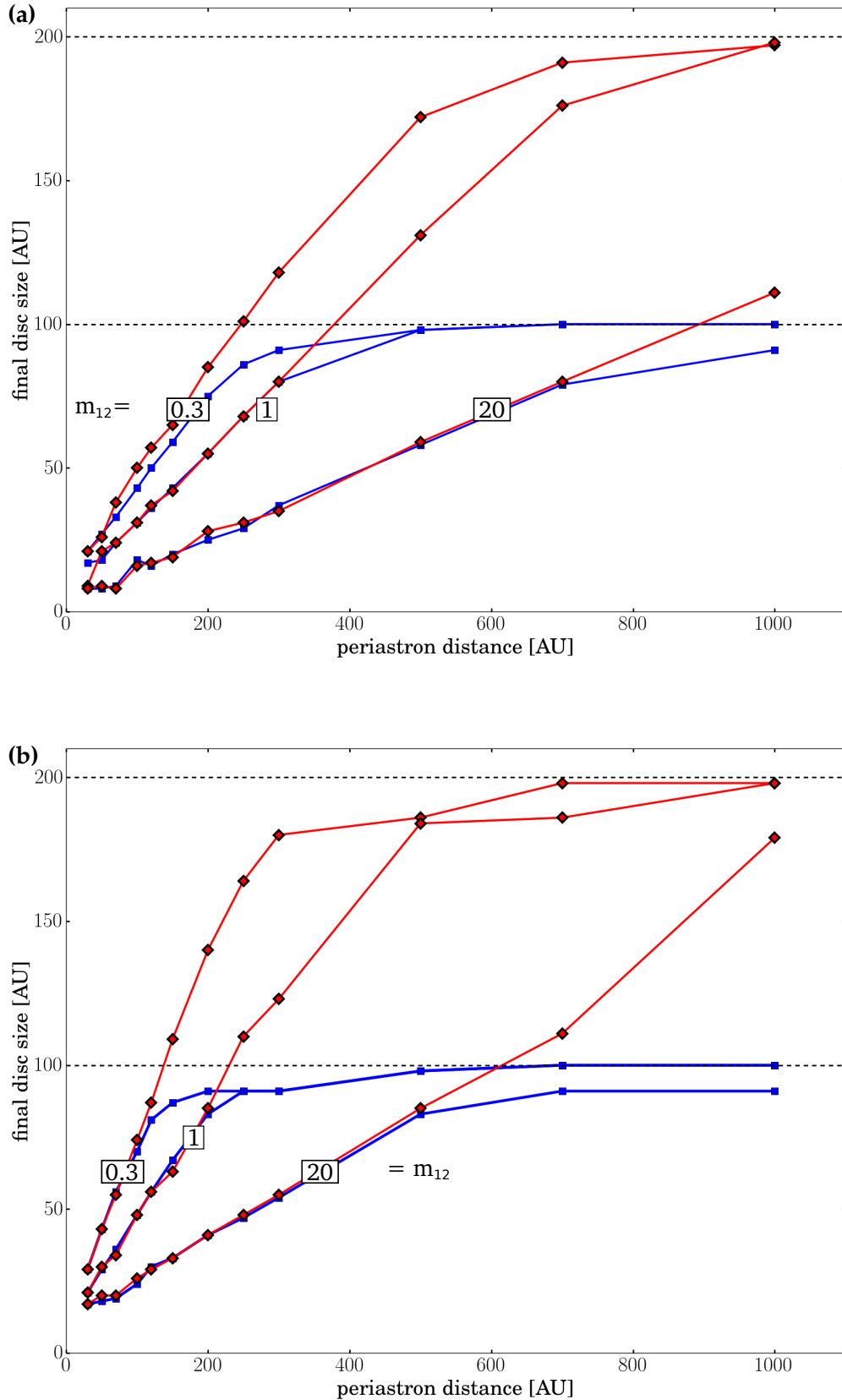


FIGURE 4.13: Final disc size versus periastron distance for different mass ratios (m_{12} , in boxes) for a disc with an initial 100 AU radius (blue squares) and 200 AU radius (red diamonds) around a $1 M_\odot$ star on a (a) coplanar prograde ($i = 0^\circ$) and (b) inclined retrograde ($i = 120^\circ$) orbit.

Chapter 5

Discussion

5.1 Limitations of the model

Some assumptions have been made for the studies described in this thesis. First, the discs are modelled using pure N-body methods and the effects due to viscosity and self-gravity have been neglected. Viscosity enables recircularisation of the remaining disc material after the encounter on long timescales [Clarke and Pringle, 1993]. However, this does not affect the disc size because recircularisation by viscosity is only efficient in the inner disc regions ($< 20 - 30$ AU) on the timescales considered here ($\sim 10^3$ years). The disc size reduces to such small radii only in case of penetrating encounters ($r_{\text{peri}} < r_{\text{init}}$) which are relatively rare in most star clusters. Scally and Clarke [2001] and Olczak et al. [2006] have shown that less than 5 - 10 % of the stars undergo encounters closer than 100 AU in clusters like the ONC. Another effect of viscosity seen on different timescales, is that of disc spreading where matter moves outwards up to a few 100 AU due to redistribution of angular momentum in a highly viscous gaseous disc. On these long time scales (> 0.5 Myr) this means that discs can have a larger size than immediately after the encounter. However, it has been studied that material at such large radii are usually affected by distant encounters resulting in a truncated disc which nullifies the effects of disc spreading [Rosotti et al., 2014]. Viscosity effects are not well constrained by observations so far.

The studies done here are restricted to low-mass thin discs where $m_{\text{disc}} \ll M_*$ ($m_{\text{disc}} \approx 0.01 M_*$, Andrews et al. [2013]). In this case, the influence of the particles on each other (self-gravity) can be neglected. The approximation of restricted three-body encounters is hence valid in case of low-mass thin discs. The presented studies may not apply to massive discs since in those cases viscosity and self-gravity effects become much stronger. Self-gravity becomes important only for cases where

$m_{\text{disc}} > 0.1 - 0.2 M_*$. However, even in these cases self-gravity mainly affects the inner disc regions. It is also important to note that massive discs ($m_{\text{disc}} > 0.1 M_*$) can become unstable to axisymmetric perturbations according to the disc stability criterion. In this case, the Toomre instability parameter Q becomes less than 1 (as discussed in § 2.2), which could trigger gravitational instabilities in the disc. Hence in case of massive discs these additional effects should also be taken into account while determining the disc size.

In order to simplify the investigation done here, only one of the stars is surrounded by a disc. In reality, in many cases, at least initially both stars will be surrounded by a disc. The disc can be replenished due to mass transfer between the two discs which could then in turn affect the disc size. However, it has been shown that most of transferred mass is usually transported in the inner regions of the disc and the captured material would have very little influence on the disc size [Pfalzner et al., 2005a]. Hence the assumption of a star-disc encounter works well for the low-mass thin discs modelled in these studies.

In our investigations, the numerical simulations are performed using 10 000 tracer particles. Several previous studies found that this proves to be a sufficient resolution for investigations of global properties like the disc size. In their studies, Kobayashi and Ida [2001] and Pfalzner [2003] have already shown that increasing the number of particles to $\sim 50\,000$ lead to similar results for disc masses and sizes. However, better resolution and higher particle number are important for example, for studies related to disc instabilities where several hundred thousand particles are required to obtain the necessary resolution.

The disc size definition used here would not necessarily define an absolute limit for the matter bound to the star, since the steepest gradient in the surface density distribution used to define the disc size could span some range. There is a small fraction of disc material outside this limit which is still bound to the star. In case of an initial r^{-1} distribution, the mass density of the bound particles outside the determined disc size is less than 15 % of the total mass density of bound particles. The here defined disc sizes can be used to determine the radius within which enough material would be available for the formation of planetary systems.

In case of distant encounters, the estimated disc size is mostly a result of redistribution of the disc material as compared to significant truncation for the grazing or penetrating encounters. Since most of the outer disc particles are on highly inclined and/or highly eccentric orbits (as seen in Figures 4.3 & 4.4) for distant encounters, it is rather difficult to estimate the disc size accurately for these cases. These particles on highly inclined and/or eccentric orbits can then be useful to understand the fate of Sedna-like objects in our solar system.

In this work only parabolic encounters are considered, as they are the most destructive type of encounters due to the longer interaction time compared to the hyperbolic ($e_p > 1$) ones [Clarke and Pringle, 1993, Pfalzner et al., 2005a]. It has been studied by Vincke and Pfalzner [subm] that the parabolic encounters mainly dominate in low-mass clusters and clusters like the ONC whereas hyperbolic encounters are predominant in denser clusters like the Arches cluster. Although the hyperbolic encounters would lead to larger disc sizes compared to the parabolic ones, the dependence of the final disc size on the orbital inclinations for the hyperbolic encounters would be interesting to compare with the parabolic ones. Effects due to hyperbolic encounters on the disc size will be investigated in a follow-up study. These results can also be applied directly to cluster simulations to determine the disc size distribution in different cluster environments.

The effect of multiple encounters on the disc size either due to stars captured during fly-bys or due to binary companions also needs to be investigated. Both these cases could lead to smaller disc sizes in comparison to single encounters, depending on the orbital properties of the captured or binary companion.

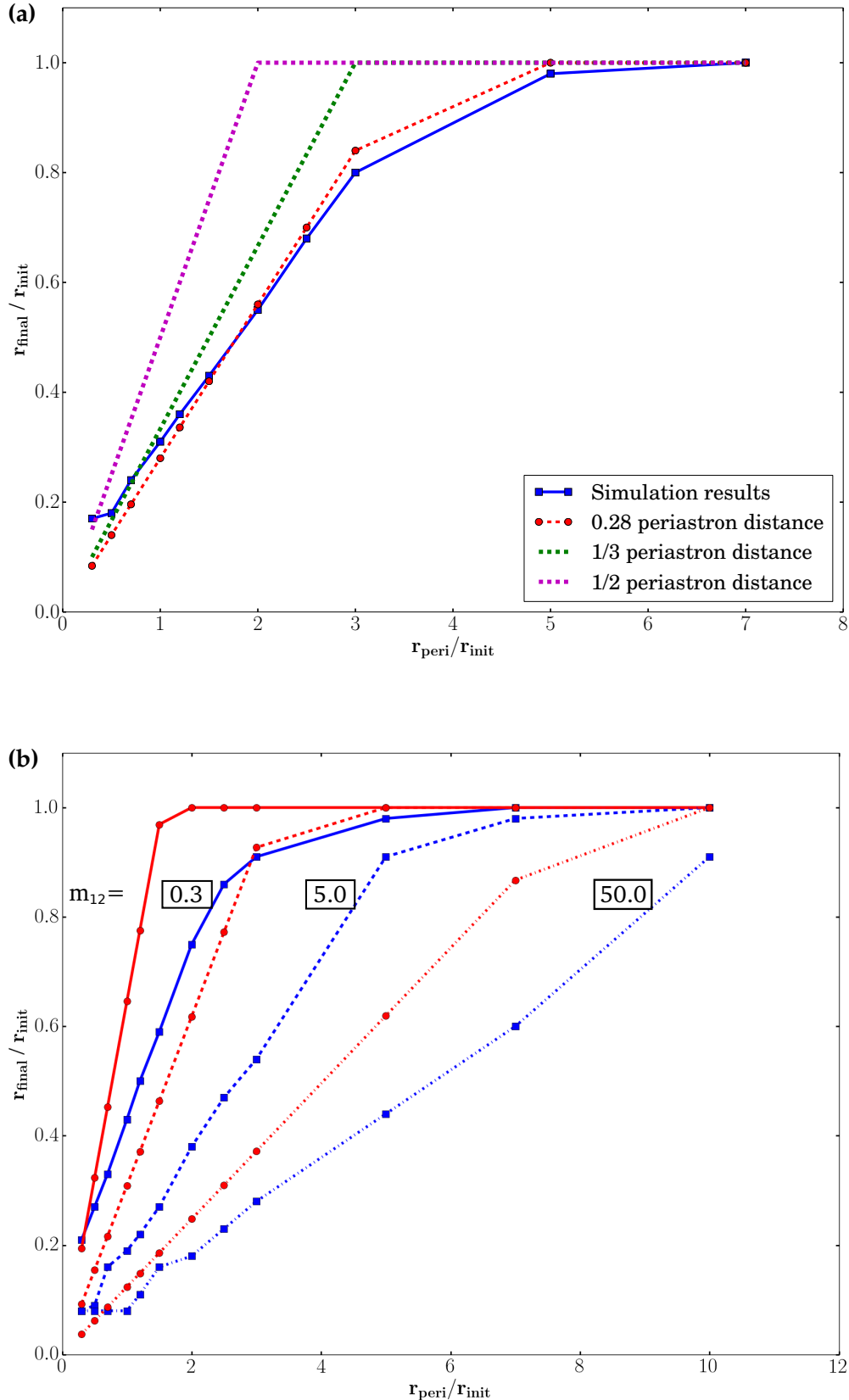


FIGURE 5.1: Final disc size from our simulation versus periastron distance scaled to the initial disc size (100 AU) for a coplanar encounter with (a) an equal-mass perturber compared to 1/2 (magenta), 1/3 (green) of the periastron distance and disc size defined by Breslau et al. [2014] (red). (b) compared to disc size determined by de Juan Ovelar et al. [2012] (red) for perturbers with mass equal to $0.3 M_{\odot}$ (solid), $5.0 M_{\odot}$ (dashed) and $50.0 M_{\odot}$ (dotted).

5.2 Comparisons to previous work

Firstly, for the case of coplanar, prograde encounters all the results obtained from our simulations confirm the results obtained by Breslau et al. [2014], who used the same disc size definition. Next, we compare our numerical results obtained using the here defined disc size to the previously used approximations for disc size definitions discussed in § 2.3.2. Comparison of our results to those obtained using the 1/2 and 1/3 periastron distance prove to be valid only for the equal-mass case, since these studies mainly focused on this type of encounter. Since the results obtained using our disc size definition are limited to the initial disc size ($r_{\text{init}} = 100$ AU), for all these comparisons, we consider the final disc sizes only within 100 AU, obtained using different disc size definitions.

Figure 5.1a shows comparisons of the final disc radii obtained here to those obtained using 1/2 (magenta), 1/3 (green) periastron distance and the disc size definition by Breslau et al. [2014] (red) for the equal-mass case. The disc sizes estimated using 1/2 periastron distance are much bigger than the numerical results. For example, for an equal-mass encounter at $r_{\text{peri}} = 200$ AU, our disc size definition gives a disc size of 55 AU whereas there is no change in the initial disc size using 1/2 periastron distance. Disc sizes estimated using 1/3 periastron distance work when the final disc sizes lie within the range 0.2 - 0.4 r_{init} for very close or grazing encounters which covers the extent of our solar system for which the criterion was proposed by Kobayashi and Ida [2001].

The disc sizes estimated using our disc size definition of the steepest gradient in the surface density distribution are much smaller than the analytical upper limit derived by de Juan Ovelar et al. [2012] using the disc mass loss from Olczak et al. [2006] (as discussed in § 2.3.2). Figure 5.1b shows comparisons of the disc radii obtained here to those obtained using the upper limit by de Juan Ovelar et al. [2012]. In case of distant encounters even for cases where the mass loss is less significant, there could still be a change in the disc size due to loss of angular momentum and redistribution of particles in the disc. Hence the actual final disc size would be much lower than the analytical upper limit. For example, for $m_{12} = 5$ and $r_{\text{peri}} = 300$ AU, the disc size determined using our disc size definition (dashed blue line) is 54 AU whereas that obtained from the upper limit (dashed red line) is ≈ 92 AU which gives a difference of nearly 38 %.

Figure 5.2 shows the final disc sizes for an initial 100 AU disc after an equal-mass encounter by a perturber on orbits with different inclinations. In order to indicate the difference in the disc sizes depending on the inclination of the perturber orbit, our numerical results (squares) are compared to the disc sizes obtained using 1/3 periastron distance (solid grey) [Kobayashi and Ida, 2001] and the analytical upper limit (dashed

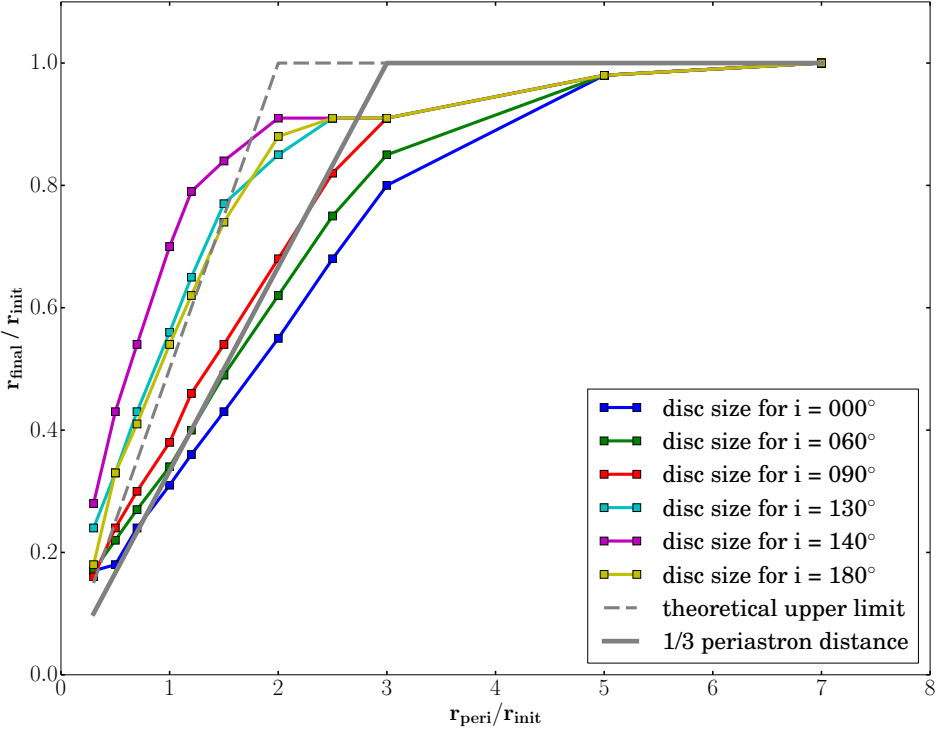


FIGURE 5.2: Final disc size versus periastron distance scaled as to the initial disc size (100 AU) for an equal-mass encounter by a perturber on orbits with different inclinations. Solid grey line indicates the disc size estimated using $1/3$ periastron distance. Dashed grey line indicates the disc size estimated using the analytical upper limit from de Juan Ovelar et al. [2012].

grey) [de Juan Ovelar et al., 2012]. The upper limit can be applied only in cases for prograde encounters ($i < 90^\circ$). In cases of retrograde encounters ($i > 90^\circ$) the disc sizes obtained using the steepest gradient in the surface density profile are larger than this upper limit. The dependence of the disc size on orbital inclinations is already explicitly discussed in § 4.1. Even though in this study it is confirmed that the coplanar prograde encounters are the strongest, it is important to note that mostly even inclined and retrograde encounters have a strong effect on the disc size.

In our studies, we find a nearly linear dependence of the disc size on the orbital inclination for the prograde encounters but it is more complex in case of retrograde encounters. Depending on the mass ratio and periastron distance, we find a peak for the disc size after an encounter with a perturber on an orbit with inclinations in the range $i = 140^\circ - 160^\circ$ (a detailed discussion can be found in § 4.1.2). Pfalzner et al. [2005b] found a similar behavior in case of effects on the disc-mass loss and angular momentum transfer due to inclined encounters. Their studies indicate a minimum in the relative mass loss and angular momentum loss for encounters with a perturber on orbital inclinations in the range 120° to less than 180° .

Chapter 6

Summary and Conclusion

Depending on the cluster density, stellar encounters might have a strong effect on protoplanetary discs in star cluster environments - the dominant place of star formation. Particularly the disc size might be strongly influenced by the presence of other cluster members [Vincke et al., 2015]. Most of the investigations so far have considered the effect of parabolic, coplanar encounters on the disc size. However, inclined encounters are the much more common situation in star clusters. In this thesis, the effect of fly-bys on the disc size with an emphasis on inclined and retrograde encounters has been investigated.

The parameter study covers encounters at orbital inclinations from $0^\circ - 180^\circ$ for different mass ratios in the range $m_{12} = 0.3 - 50$, at periastron distances from 30 - 1000 AU and for different orbital orientations (angle of periastron) with the periastron in the disc plane ($aop = 0^\circ$) and periastron outside the disc plane ($aop = 45^\circ, 90^\circ$).

The results from this extensive parameter study are summarized as follows,

- Our studies confirm the results from Breslau et al. [2014] for disc sizes after coplanar, prograde encounters.
- The results obtained here show, for the first time, that the coplanar, prograde encounters have the strongest effect on the **disc size**, in comparison to the inclined and retrograde encounters. Similar influence of coplanar, prograde encounters have already been studied in case of disc-mass loss and angular momentum loss [Clarke and Pringle, 1993, Pfalzner et al., 2005b].
- Although parabolic prograde encounters are the most destructive encounters, retrograde encounters also have a significant effect on the disc size. Hence the effect of retrograde encounters on disc-mass loss and angular momentum change should be studied.

- Even inclined encounters mostly have a strong influence on the disc size.
- The more massive the perturber, the stronger is the effect on disc size. The difference between the disc size due to prograde and retrograde encounters decreases with an increase of the perturber mass.
- Penetrating encounters destroy most of the disc whereas distant encounters mainly have a strong influence in the outer regions of the disc. The difference between the disc size due to prograde and retrograde encounters increases with an increase in the periastron distance.
- The disc size due to an encounter by a perturber on different orbital orientations (aop) differs by $\leq 10\%$. A change in the orientation of the perturber orbit mostly has a strong effect on outer discs particle inclinations and eccentricities which depends on the periastron distance, mass ratio and orbital inclination.

There have been studies related to the effect of stellar encounters on the solar birth environment and on dynamics of highly eccentric and inclined objects in our solar system [Adams and Laughlin, 2001, García-Sánchez et al., 2001, Rickman et al., 2004, Morbidelli and Levison, 2004, Adams, 2010, Bailer-Jones, 2015, Mamajek et al., 2015, Jilkova et al., 2015]. The studies done in this thesis could prove to be resourceful for further investigations to understand the influence of the solar birth environment on the formation of our solar system. For example, from the results obtained here, for an initial 100 AU disc and considering an equal-mass perturber, close stellar fly-bys at an encounter distance of $\approx 100 - 150$ AU would result in a solar-system size disc of $\approx 30 - 50$ AU. Considering the fact that inclined encounters can lead to particles on highly inclined and/or eccentric orbits, the implications of these encounters for bodies like Sedna [Brown et al., 2004] and 2012 VP₁₁₃ [Trujillo and Sheppard, 2014] on highly inclined orbits and other such trans-Neptunian objects (TNOs) in our solar system will further be investigated in a follow up study. Our studies also indicate that the thin disc structure transforms in to a torus-like structure due to particles on inclined and eccentric orbits after an encounter (see Figures 4.3 & 4.4). Thus, the here obtained results can also be useful to study the possible effects due to stellar encounters in the solar neighbourhood which could have led to inclined and eccentric orbits of objects in the Oort cloud resulting in its spherical structure [Weissman, 1980, Duncan et al., 1987, Brasser et al., 2006, 2012, Higuchi and Kokubo, 2015].

The effects of stellar fly-bys studied here can also be applied to investigate the impact of such encounters on orbital properties of extrasolar planets that could lead to planets on wide orbits, systems on highly inclined orbits, planet-planet scattering, ejection or capture by the perturber [Malmberg et al., 2007, Spurzem et al., 2009, Malmberg et al.,

2011, Hao et al., 2013, Davies et al., 2014]. These studies could also be useful to understand the possible formation scenarios of the recently discovered extrasolar analogues of the Kupier belt [Acke et al., 2012, Currie et al., 2015].

The results obtained for the disc size due to encounters on parabolic orbits can be applied directly to cluster simulations to determine the disc size distribution in low-mass clusters and clusters like the Orion nebula cluster (ONC) in which parabolic encounters dominate. Similar methods can be used to investigate the effects of hyperbolic encounters which are found to be dominant in the denser clusters [Vincke and Pfalzner, subm]. These results can thus be used to determine the maximum extent of the potentially forming planetary systems in different cluster environments.

With the current ground-based and space-based missions providing a plethora of data, the work done here can prove to be a useful tool to trace back the possible encounter scenarios for the observed disc sizes and spatial scale of planetary systems.

Appendices

Appendix A

Numerical Recipe for star-disc encounters

The Runge-Kutta Cash-Karp Integrator

The work in this thesis is done by considering gravitational interactions between the two stars and each of the particles in a low-mass thin disc. This reduces the numerical effort to $2N + 1$ calculations (for interactions between the two stars and each of the N disc particles). In the star-disc encounter simulations the ordinary differential equations were solved using the Runge-Kutta Cash-Karp (RKCK) integrator as described in [Press et al., 1992]. The RKCK integrator is based on the Runge-Kutta method but with an extended adaptive stepsize control.

The Runge-Kutta methods propagate a solution over an interval by combining information from several Euler method steps and then using the information obtained to match a Taylor series expansion up to some higher order. The numerical errors introduced into the solution can be controlled by automatic changing of the fundamental stepsize (adaptive stepsize control). The approximation for y_{n+1} is given by a weighted average of approximated values of f_k at several time steps within the interval $(t_n, t_n + \Delta t)$ with intermediate values

$$k_i = f(t_n + c_i \Delta t, y_n + \sum_{j=1}^{i-1} a_{ij} k_j) \Delta t \quad \text{with } i = 1, \dots, s. \quad (\text{A.1})$$

The next coordinate of the phase space can then be interpolated by

$$y_{n+1} = y_n + \sum_{i=1}^s b_i k_i. \quad (\text{A.2})$$

One then needs to provide the number of stages s and the coefficients a_{ij} (for $1 \leq j < i \leq s$), b_i (for $i = 1, 2, \dots, s$) and c_i (for $i = 2, 3, \dots, s$).

The most often used is the fourth-order Runge-Kutta formula given as

$$\begin{aligned} k_1 &= \Delta t f(t_n, y_n) \\ k_2 &= \Delta t f\left(t_n + \frac{\Delta t}{2}, y_n + \frac{k_1}{2}\right) \\ k_3 &= \Delta t f\left(t_n + \frac{\Delta t}{2}, y_n + \frac{k_2}{2}\right) \\ k_4 &= \Delta t f(t_n + \Delta t, y_n + k_3) \\ y_{n+1} &= y_n + \frac{k_1}{6} + \frac{k_2}{3} + \frac{k_3}{3} + \frac{k_4}{6} + \mathcal{O}(h^5), \end{aligned} \quad (\text{A.3})$$

where k_i with $i = 1, 2, 3, 4$ are the intermediate steps and y_{n+1} is the approximation for the time step t_{n+1} . The Runge-Kutta method treats every step in the given sequence of steps in an identical manner. Although this method is computationally more expensive than the Euler method, it leads to much smaller errors and hence to stable orbits of the particles.

An adaptive timestep control is usually used to achieve some predetermined accuracy in the solution and to enhance the computational effort. Here the RKCK integrator is used, which combines the fifth- and fourth-order method to obtain an error estimate. It uses six function evaluations to calculate fourth- and fifth-order accurate solutions. The difference between these solutions then provides the error estimate of the fourth-order solution. If the error exceeds a specific value, the integration can be repeated with a smaller time step, which is derived from the error estimate.

The error estimate is given by

$$\Delta_i = z_{n+1} - y_{n+1} = \sum_{i=1}^6 (b_{zi} - b_{yi}) k_i, \quad (\text{A.4})$$

where Δ scales as $(\Delta t)^5$, z_{n+1} is the fifth-order solution and y_{n+1} is the fourth-order solution. If a step size Δt_1 is taken, which produces an error of Δ_1 , the step size Δt_0 that would produce another error Δ_0 can then be estimated as

$$\Delta t_0 = \Delta t_1 \left| \frac{\Delta_0}{\Delta_1} \right|^{1/5}. \quad (\text{A.5})$$

Δ_0 denotes the desired accuracy. Equation A.5 can then be used in two ways. If Δ_1 is larger than Δ_0 in magnitude, the equation tells how much to decrease the stepsize when retrying the present step whereas if Δ_1 is smaller than Δ_0 , the equation tells how much the step size can be safely increased for the next step. For the application of this method to the present work, the accuracy is adjusted to the strength of the particle interactions,

which is in the performed simulations given by the nearness of the particles relative to the stars. For example, close particles require a smaller global time step. It is important to note that reduction in the time step size increases the accumulation of errors due to larger number of integration steps and hence does not always increase the accuracy.

Appendix B

Disc sizes after encounter by a perturber on an orbit with $aop = 0^\circ$

Here, the values for the final disc sizes for an initial 100 AU disc around a $1 M_\odot$ star for different perturber masses in the range $0.3 M_\odot - 50 M_\odot$ listed in different tables is presented. Every table contains the final disc size for different periastron distances (r_{peri}) in the range 30 AU - 1000 AU and for different inclinations of the perturber orbit in the range $0^\circ - 180^\circ$. The effect of orbital inclinations as discussed in § 4.1 can hence be compared for the different parameters studied. Here the orbital orientation (aop) is fixed to 0° .

TABLE B.1: Final disc sizes [AU] after encounter by a $0.3 M_{\odot}$ perturber at different periastron distances (r_{peri}) [AU] and for different orbital inclinations.

TABLE B.2: Final disc sizes [AU] after encounter by a $0.5 M_{\odot}$ perturber at different periastron distances (r_{peri}) [AU] and for different orbital inclinations.

TABLE B.3: Final disc sizes [AU] after encounter by a $1 M_{\odot}$ perturber at different periastron distances (r_{peri}) [AU] and for different orbital inclinations.

TABLE B.4: Final disc sizes [AU] after encounter by a $2 M_{\odot}$ perturber at different periastron distances (r_{peri}) [AU] and for different orbital inclinations.

TABLE B.5: Final disc sizes [AU] after encounter by a $5 M_{\odot}$ perturber at different periastron distances (r_{peri}) [AU] and for different orbital inclinations.

TABLE B.6: Final disc sizes [AU] after encounter by a $10 M_{\odot}$ perturber at different periastron distances (r_{peri}) [AU] and for different orbital inclinations.

TABLE B.7: Final disc sizes [AU] after encounter by a $20 M_{\odot}$ perturber at different periastron distances (r_{peri}) [AU] and for different orbital inclinations.

r_{peri}	0°	10°	20°	30°	40°	50°	60°	70°	80°	90°	100°	110°	120°	130°	140°	150°	160°	170°	180°
030	8	8	8	8	8	8	8	8	8	8	17	18	15	19	17	17	17	16	
050	8	8	8	8	8	8	8	8	8	10	11	18	20	18	20	25	22	18	
070	9	8	9	11	10	10	10	11	16	9	17	19	19	24	25	28	36	30	26
100	18	18	17	19	19	16	17	18	16	17	20	22	24	29	32	34	50	39	38
120	16	16	17	20	19	19	19	21	21	22	21	25	30	35	40	33	61	46	43
150	20	21	19	20	19	21	24	24	22	23	26	28	33	41	53	54	76	54	50
200	25	24	26	25	27	27	29	29	30	29	34	33	41	50	69	84	84	65	75
250	29	30	30	31	31	33	35	36	36	36	39	42	47	58	80	84	86	84	84
300	37	37	36	36	37	37	41	41	41	44	45	50	54	67	84	90	84	84	84
500	58	58	58	60	60	61	63	64	66	68	71	76	83	88	91	91	91	91	91
700	79	78	80	80	82	82	83	84	86	89	91	91	91	91	96	97	97	97	97
1000	91	91	91	91	91	91	91	91	91	91	91	91	91	97	97	97	97	97	97

TABLE B.8: Final disc sizes [AU] after encounter by a $50 M_{\odot}$ perturber at different periastron distances (r_{peri}) [AU] and for different orbital inclinations.

Appendix C

Disc sizes after encounter by a perturber on an orbit with $aop = 45^\circ$

Here, the values for the final disc sizes for an initial 100 AU disc around a $1 M_\odot$ star for different perturber masses in the range $0.3 M_\odot - 50 M_\odot$ listed in different tables is presented. Every table contains the final disc size for different periastron distances (r_{peri}) in the range 30 AU - 1000 AU and for different inclinations of the perturber orbit in the range $0^\circ - 180^\circ$. The effect of orbital inclinations as discussed in § 4.1 can hence be compared for the different parameters studied. Here the orbital orientation (aop) is fixed to 45° .

TABLE C.1: Final disc sizes [AU] after encounter by a $0.3 M_{\odot}$ perturber at different periastron distances (r_{peri}) [AU] and for different orbital inclinations.

TABLE C.2: Final disc sizes [AU] after encounter by a $0.5 M_{\odot}$ perturber at different periastron distances (r_{peri}) [AU] and for different orbital inclinations.

TABLE C.3: Final disc sizes [AU] after encounter by a $1 M_{\odot}$ perturber at different periastron distances (r_{peri}) [AU] and for different orbital inclinations.

TABLE C.4: Final disc sizes [AU] after encounter by a $2 M_{\odot}$ perturber at different periastron distances (r_{peri}) [AU] and for different orbital inclinations.

TABLE C.5: Final disc sizes [AU] after encounter by a $5 M_{\odot}$ perturber at different periastron distances (r_{peri}) [AU] and for different orbital inclinations.

TABLE C.6: Final disc sizes [AU] after encounter by a $10 M_{\odot}$ perturber at different periastron distances (r_{peri}) [AU] and for different orbital inclinations.

TABLE C.7: Final disc sizes [AU] after encounter by a $20 M_{\odot}$ perturber at different periastron distances (r_{peri}) [AU] and for different orbital inclinations.

r_{peri}	0°	10°	20°	30°	40°	50°	60°	70°	80°	90°	100°	110°	120°	130°	140°	150°	160°	170°	180°
030	8	8	8	8	8	8	8	8	8	8	8	8	11	16	17	18	16	18	
050	8	8	8	8	8	8	8	8	8	8	8	18	18	22	21	27	23	21	
070	8	8	16	9	10	9	10	9	11	10	11	19	19	19	25	26	28	28	28
100	17	19	19	18	21	18	19	16	19	19	16	23	25	24	31	41	35	39	38
120	18	16	16	19	20	19	21	20	21	20	22	21	28	29	33	39	40	42	42
150	19	20	19	21	21	24	20	25	25	24	28	29	30	32	42	44	52	49	50
200	24	25	24	25	26	29	28	28	31	31	32	35	39	41	50	73	59	78	75
250	28	29	30	31	31	31	33	36	37	39	39	41	45	50	56	84	84	84	82
300	36	36	35	37	37	37	39	44	41	44	45	49	53	58	66	84	84	84	84
500	58	58	59	59	59	60	64	66	67	68	72	74	81	86	91	91	91	91	91
700	79	79	80	79	81	83	84	86	87	90	90	91	91	91	91	29	97	91	91
1000	91	91	91	91	91	91	91	91	91	91	91	91	91	91	97	97	97	97	97

TABLE C.8: Final disc sizes [AU] after encounter by a $50 M_{\odot}$ perturber at different periastron distances (r_{peri}) [AU] and for different orbital inclinations.

Appendix D

Disc sizes after encounter by a perturber on an orbit with $aop = 90^\circ$

Here, the values for the final disc sizes for an initial 100 AU disc around a $1 M_\odot$ star for different perturber masses in the range $0.3 M_\odot - 50 M_\odot$ listed in different tables is presented. Every table contains the final disc size for different periastron distances (r_{peri}) in the range 30 AU - 1000 AU and for different inclinations of the perturber orbit in the range $0^\circ - 180^\circ$. The effect of orbital inclinations as discussed in § 4.1 can hence be compared for the different parameters studied. Here the orbital orientation (aop) is fixed to 90° .

TABLE D.1: Final disc sizes [AU] after encounter by a $0.3 M_{\odot}$ perturber at different periastron distances (r_{peri}) [AU] and for different orbital inclinations.

TABLE D.2: Final disc sizes [AU] after encounter by a $0.5 M_{\odot}$ perturber at different periastron distances (r_{peri}) [AU] and for different orbital inclinations.

TABLE D.3: Final disc sizes [AU] after encounter by a $1 M_{\odot}$ perturber at different periastron distances (r_{peri}) [AU] and for different orbital inclinations.

TABLE D.4: Final disc sizes [AU] after encounter by a $2 M_{\odot}$ perturber at different periastron distances (r_{peri}) [AU] and for different orbital inclinations.

TABLE D.5: Final disc sizes [AU] after encounter by a $5 M_{\odot}$ perturber at different periastron distances (r_{peri}) [AU] and for different orbital inclinations.

TABLE D.6: Final disc sizes [AU] after encounter by a $10 M_{\odot}$ perturber at different periastron distances (r_{peri}) [AU] and for different orbital inclinations.

TABLE D.7: Final disc sizes [AU] after encounter by a $20 M_{\odot}$ perturber at different periastron distances (r_{peri}) [AU] and for different orbital inclinations.

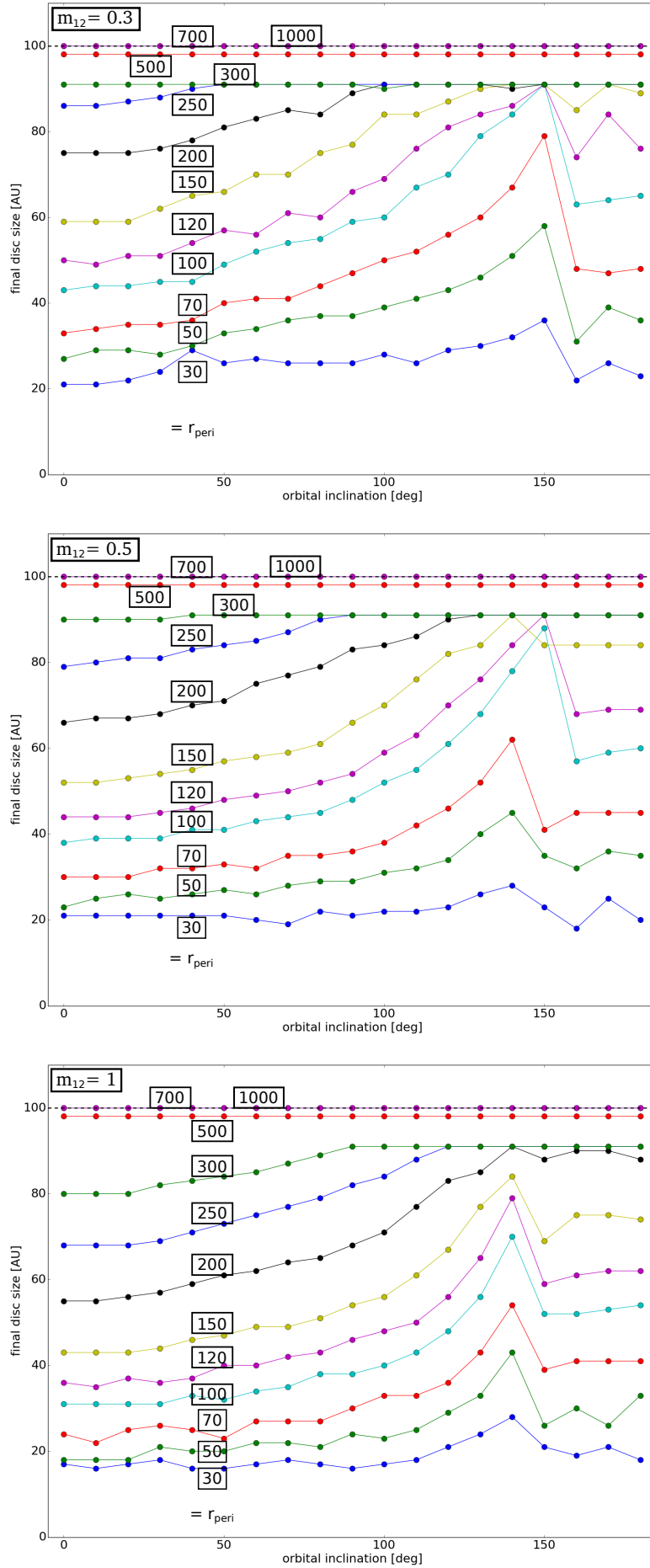
r_{peri}	0°	10°	20°	30°	40°	50°	60°	70°	80°	90°	100°	110°	120°	130°	140°	150°	160°	170°	180°
030	8	8	8	8	8	8	8	8	8	8	8	17	17	19	17	17	17	17	
050	8	8	8	9	8	9	8	9	8	8	9	9	18	23	26	24	19	19	
070	8	8	16	16	17	12	12	12	10	10	13	16	18	21	26	31	31	29	
100	14	16	18	19	18	18	19	18	19	19	17	22	21	26	32	38	39	38	
120	17	16	19	19	22	20	21	19	21	21	23	22	27	29	35	43	40	44	
150	18	21	19	22	22	22	25	22	25	25	27	28	29	34	42	64	52	51	
200	25	25	23	26	27	26	29	28	31	32	31	34	40	42	53	81	77	63	
250	30	31	31	30	31	33	33	38	37	39	40	43	48	52	59	84	84	83	
300	36	36	36	38	38	38	40	41	42	44	49	49	54	61	69	84	87	84	
500	58	58	59	60	60	61	63	65	67	71	72	77	84	90	91	91	91	91	
700	79	80	80	81	81	82	84	86	88	91	91	91	91	91	91	91	91	97	
1000	91	91	91	91	91	91	91	91	91	91	91	91	91	97	97	97	97	97	

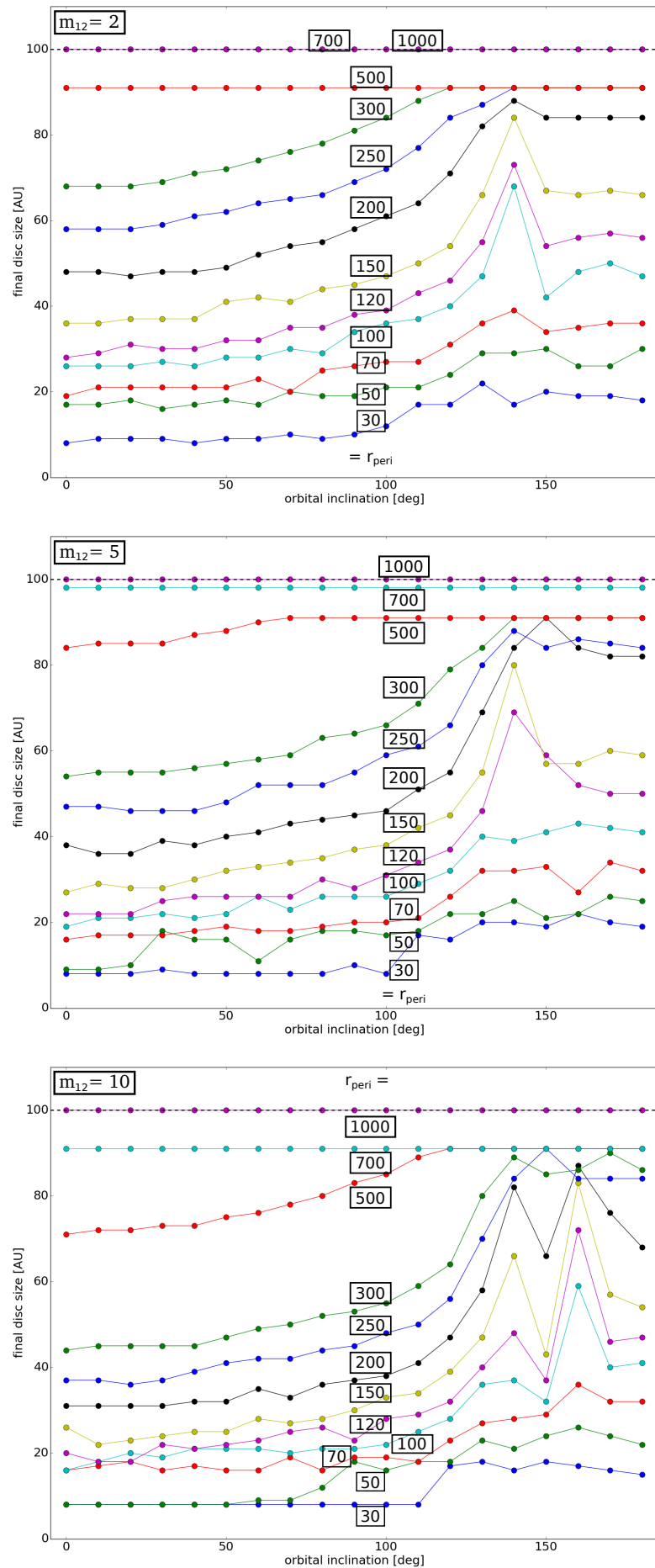
TABLE D.8: Final disc sizes [AU] after encounter by a $50 M_{\odot}$ perturber at different periastron distances (r_{peri}) [AU] and for different orbital inclinations.

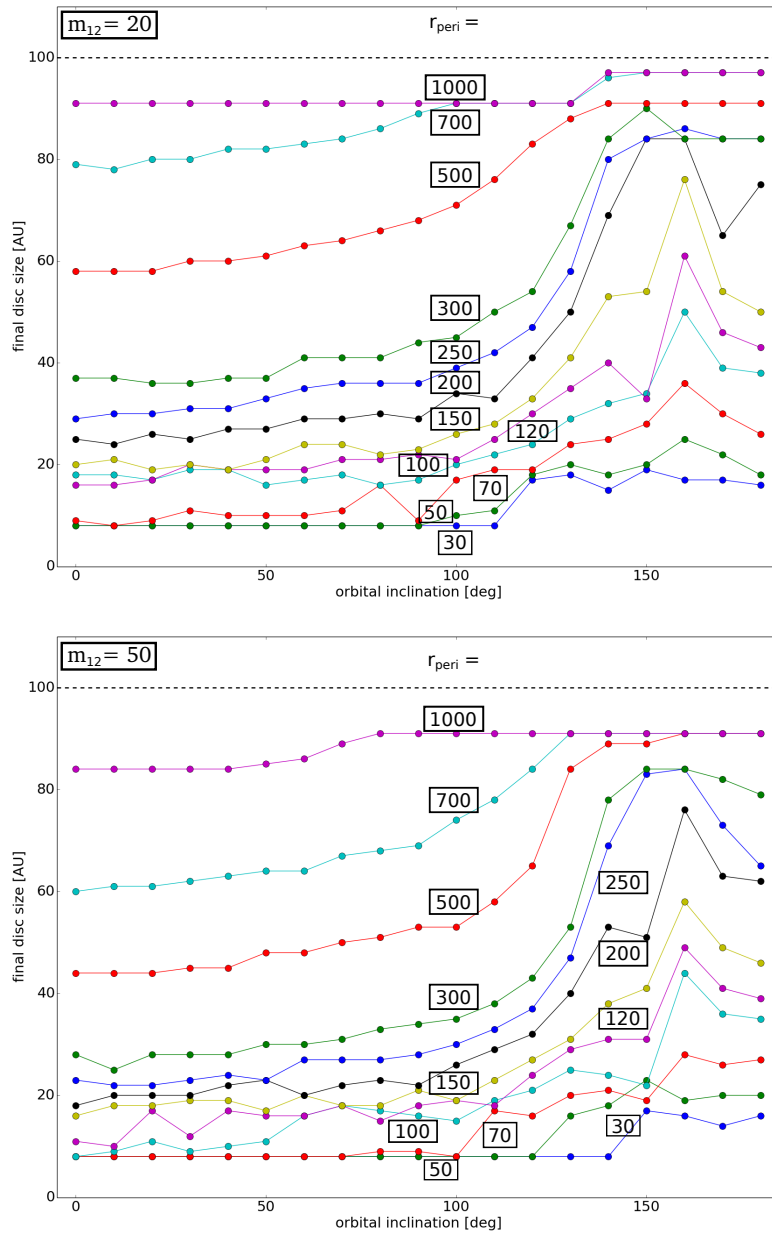
Appendix E

Comparison of disc sizes as a function of perturber orbital inclinations

For every mass ratio (m_{12}) in the range 0.3 - 50, we present the plots for the final disc size [AU] estimated using the steepest gradient in the surface density distribution versus the perturber orbital inclination in the range $0^\circ - 180^\circ$ for different periastron distances (r_{peri}) [AU, in boxes] for a disc with initially 100 AU (dotted) radius. The effect of orbital inclinations on final disc sizes can hence be compared for the different mass ratios. Here for comparison the results are shown only for the case of perturber orbit with $aop = 0^\circ$.







Bibliography

- B. Acke, M. Min, C. Dominik, B. Vandenbussche, B. Sibthorpe, C. Waelkens, G. Olofsson, P. Degroote, K. Smolders, E. Pantin, M. J. Barlow, J. A. D. L. Blommaert, A. Branderker, W. De Meester, W. R. F. Dent, K. Exter, J. Di Francesco, M. Fridlund, W. K. Gear, A. M. Glauser, J. S. Greaves, P. M. Harvey, T. Henning, M. R. Hogerheijde, W. S. Holland, R. Huygen, R. J. Ivison, C. Jean, R. Liseau, D. A. Naylor, G. L. Pilbratt, E. T. Polehampton, S. Regibo, P. Royer, A. Sicilia-Aguilar, and B. M. Swinyard. Herschel images of Fomalhaut. An extrasolar Kuiper belt at the height of its dynamical activity. *A&A*, 540:A125, April 2012. doi: 10.1051/0004-6361/201118581.
- F. C. Adams. The Birth Environment of the Solar System. *ARA&A*, 48:47–85, September 2010. doi: 10.1146/annurev-astro-081309-130830.
- F. C. Adams and G. Laughlin. Constraints on the Birth Aggregate of the Solar System. *Icarus*, 150:151–162, March 2001. doi: 10.1006/icar.2000.6567.
- F. C. Adams, D. Hollenbach, G. Laughlin, and U. Gorti. Photoevaporation of Circumstellar Disks Due to External Far-Ultraviolet Radiation in Stellar Aggregates. *ApJ*, 611:360–379, August 2004. doi: 10.1086/421989.
- F. C. Adams, E. M. Proszkow, M. Fatuzzo, and P. C. Myers. Early Evolution of Stellar Groups and Clusters: Environmental Effects on Forming Planetary Systems. *ApJ*, 641:504–525, April 2006. doi: 10.1086/500393.
- P. André. The Initial Conditions for Protostellar Collapse: Observational Constraints. In J. Bouvier and J.-P. Zahn, editors, *EAS Publications Series*, volume 3 of *EAS Publications Series*, pages 1–38, 2002. doi: 10.1051/eas:2002043.
- P. Andre, D. Ward-Thompson, and M. Barsony. From Prestellar Cores to Protostars: the Initial Conditions of Star Formation. *Protostars and Planets IV*, page 59, May 2000.
- P. André, J. Di Francesco, D. Ward-Thompson, S.-I. Inutsuka, R. E. Pudritz, and J. E. Pineda. From Filamentary Networks to Dense Cores in Molecular Clouds: Toward a

- New Paradigm for Star Formation. *Protostars and Planets VI*, pages 27–51, 2014. doi: 10.2458/azu_uapress_9780816531240-ch002.
- S. M. Andrews and J. P. Williams. Circumstellar Dust Disks in Taurus-Auriga: The Submillimeter Perspective. *ApJ*, 631:1134–1160, October 2005. doi: 10.1086/432712.
- S. M. Andrews and J. P. Williams. High-Resolution Submillimeter Constraints on Circumstellar Disk Structure. *ApJ*, 659:705–728, April 2007a. doi: 10.1086/511741.
- S. M. Andrews and J. P. Williams. A Submillimeter View of Circumstellar Dust Disks in ρ Ophiuchi. *ApJ*, 671:1800–1812, December 2007b. doi: 10.1086/522885.
- S. M. Andrews, K. A. Rosenfeld, A. L. Kraus, and D. J. Wilner. The Mass Dependence between Protoplanetary Disks and their Stellar Hosts. *ApJ*, 771:129, July 2013. doi: 10.1088/0004-637X/771/2/129.
- P. J. Armitage. Dynamics of Protoplanetary Disks. *ARA&A*, 49:195–236, September 2011. doi: 10.1146/annurev-astro-081710-102521.
- P. J. Armitage. Physical processes in protoplanetary disks. *ArXiv e-prints*, September 2015.
- Philip J. Armitage. *Astrophysics of Planet Formation*. Cambridge University Press, 2009. ISBN 9780511802225. URL <http://dx.doi.org/10.1017/CBO9780511802225>. Cambridge Books Online.
- C. A. L. Bailer-Jones. Close encounters of the stellar kind. *A&A*, 575:A35, March 2015. doi: 10.1051/0004-6361/201425221.
- J. Bally, R. K. Mann, J. Eisner, S. M. Andrews, J. Di Francesco, M. Hughes, D. Johnstone, B. Matthews, L. Ricci, and J. P. Williams. ALMA Observations of the Largest Protoplanetary Disk in the Orion Nebula, 114-426: A CO Silhouette. *ArXiv e-prints*, June 2015.
- S. V. W. Beckwith, A. I. Sargent, R. S. Chini, and R. Guesten. A survey for circumstellar disks around young stellar objects. *AJ*, 99:924–945, March 1990. doi: 10.1086/115385.
- M. T. Beltran and W. J. de Wit. Accretion disks in luminous young stellar objects. *ArXiv e-prints*, September 2015.
- R. Brasser, M. J. Duncan, and H. F. Levison. Embedded star clusters and the formation of the Oort Cloud. *Icarus*, 184:59–82, September 2006. doi: 10.1016/j.icarus.2006.04.010.

- R. Brasser, M. J. Duncan, H. F. Levison, M. E. Schwamb, and M. E. Brown. Reassessing the formation of the inner Oort cloud in an embedded star cluster. *Icarus*, 217:1–19, January 2012. doi: 10.1016/j.icarus.2011.10.012.
- A. Breslau, M. Steinhausen, K. Vincke, and S. Pfalzner. Sizes of protoplanetary discs after star-disc encounters. *A&A*, 565:A130, May 2014. doi: 10.1051/0004-6361/201323043.
- M. E. Brown, C. Trujillo, and D. Rabinowitz. Discovery of a Candidate Inner Oort Cloud Planetoid. *ApJ*, 617:645–649, December 2004. doi: 10.1086/422095.
- R. Cesaroni, D. Galli, G. Lodato, C. M. Walmsley, and Q. Zhang. Disks Around Young O-B (Proto)Stars: Observations and Theory. *Protostars and Planets V*, pages 197–212, 2007.
- E. I. Chiang and P. Goldreich. Spectral Energy Distributions of T Tauri Stars with Passive Circumstellar Disks. *ApJ*, 490:368–376, November 1997.
- C. J. Clarke. The photoevaporation of discs around young stars in massive clusters. *MNRAS*, 376:1350–1356, April 2007. doi: 10.1111/j.1365-2966.2007.11547.x.
- C. J. Clarke and J. E. Pringle. Accretion disc response to a stellar fly-by. *MNRAS*, 261: 190–202, March 1993.
- C. J. Clarke, I. A. Bonnell, and L. A. Hillenbrand. The Formation of Stellar Clusters. *Protostars and Planets IV*, page 151, May 2000.
- Thayne Currie, Carey M. Lisse, Marc Kuchner, Nikku Madhusudhan, Scott J. Kenyon, Christian Thalmann, Joseph Carson, and John Debes. Direct Imaging and Spectroscopy of a Young Extrasolar Kuiper Belt in the Nearest OB Association. *The Astrophysical Journal Letters*, 807(1):L7, 2015. URL <http://stacks.iop.org/2041-8205/807/i=1/a=L7>.
- M. B. Davies, F. C. Adams, P. Armitage, J. Chambers, E. Ford, A. Morbidelli, S. N. Raymond, and D. Veras. The Long-Term Dynamical Evolution of Planetary Systems. *Protostars and Planets VI*, pages 787–808, 2014. doi: 10.2458/azu_uapress_9780816531240-ch034.
- M. de Juan Ovelar, J. M. D. Kruijssen, E. Bressert, L. Testi, N. Bastian, and H. Cánovas. Can habitable planets form in clustered environments? *A&A*, 546:L1, October 2012. doi: 10.1051/0004-6361/201219627.
- C. P. Dullemond and J. D. Monnier. The Inner Regions of Protoplanetary Disks. *ARA&A*, 48:205–239, September 2010. doi: 10.1146/annurev-astro-081309-130932.

- C. P. Dullemond, D. Hollenbach, I. Kamp, and P. D'Alessio. Models of the Structure and Evolution of Protoplanetary Disks. *Protostars and Planets V*, pages 555–572, 2007.
- M. Duncan, T. Quinn, and S. Tremaine. The formation and extent of the solar system comet cloud. *AJ*, 94:1330–1338, November 1987. doi: 10.1086/114571.
- J. A. Eisner, R. L. Plambeck, J. M. Carpenter, S. A. Corder, C. Qi, and D. Wilner. Proplyds and Massive Disks in the Orion Nebula Cluster Imaged with CARMA and SMA. *ApJ*, 683:304–320, August 2008. doi: 10.1086/588524.
- B. Ercolano, C. J. Clarke, and A. C. Hall. The clearing of discs around late-type T Tauri stars: constraints from the infrared two-colour plane. *MNRAS*, 410:671–678, January 2011. doi: 10.1111/j.1365-2966.2010.17473.x.
- D. Fedele, M. E. van den Ancker, T. Henning, R. Jayawardhana, and J. M. Oliveira. Timescale of mass accretion in pre-main-sequence stars. *A&A*, 510:A72, February 2010. doi: 10.1051/0004-6361/200912810.
- A. S. Font, I. G. McCarthy, D. Johnstone, and D. R. Ballantyne. Photoevaporation of Circumstellar Disks around Young Stars. *ApJ*, 607:890–903, June 2004. doi: 10.1086/383518.
- J. García-Sánchez, P. R. Weissman, R. A. Preston, D. L. Jones, J.-F. Lestrade, D. W. Latham, R. P. Stefanik, and J. M. Paredes. Stellar encounters with the solar system. *A&A*, 379:634–659, November 2001. doi: 10.1051/0004-6361:20011330.
- U. Gorti and D. Hollenbach. Photoevaporation of Circumstellar Disks By Far-Ultraviolet, Extreme-Ultraviolet and X-Ray Radiation from the Central Star. *ApJ*, 690:1539–1552, January 2009. doi: 10.1088/0004-637X/690/2/1539.
- Jr. K. E. Haisch, E. A. Lada, and C. J. Lada. Disk Frequencies and Lifetimes in Young Clusters. *ApJ*, 553:L153–L156, June 2001. doi: 10.1086/320685.
- S. M. Hall. Circumstellar disc density profiles: a dynamic approach. *MNRAS*, 287:148–154, May 1997.
- S. M. Hall, C. J. Clarke, and J. E. Pringle. Energetics of star-disc encounters in the non-linear regime. *MNRAS*, 278:303–320, January 1996.
- W. Hao, M. B. N. Kouwenhoven, and R. Spurzem. The dynamical evolution of multiplanet systems in open clusters. *MNRAS*, 433:867–877, July 2013. doi: 10.1093/mnras/stt771.
- D. Harsono, J. K. Jørgensen, E. F. van Dishoeck, M. R. Hogerheijde, S. Bruderer, M. V. Persson, and J. C. Mottram. Rotationally-supported disks around Class I sources in

- Taurus: disk formation constraints. *A&A*, 562:A77, February 2014. doi: 10.1051/0004-6361/201322646.
- L. Hartmann. *Accretion Processes in Star Formation: Second Edition*. Cambridge University Press, 2009.
- C. Hayashi. Structure of the Solar Nebula, Growth and Decay of Magnetic Fields and Effects of Magnetic and Turbulent Viscosities on the Nebula. *Progress of Theoretical Physics Supplement*, 70:35–53, 1981. doi: 10.1143/PTPS.70.35.
- C. H. Heller. Encounters with Protostellar Disks. II. Disruption and Binary Formation. *ApJ*, 455:252, December 1995. doi: 10.1086/176573.
- A. Higuchi and E. Kokubo. Effect of Stellar Encounters on Comet Cloud Formation. *ArXiv e-prints*, July 2015.
- D. Hollenbach, D. Johnstone, S. Lizano, and F. Shu. Photoevaporation of disks around massive stars and application to ultracompact H II regions. *ApJ*, 428:654–669, June 1994. doi: 10.1086/174276.
- D. J. Hollenbach, H. W. Yorke, and D. Johnstone. Disk Dispersal around Young Stars. *Protostars and Planets IV*, page 401, May 2000.
- L. Jilkova, S. Portegies Zwart, T. Pijloo, and M. Hammer. How Sedna and family were captured in a close encounter with a solar sibling. *ArXiv e-prints*, June 2015.
- J. J. Jiménez-Torres, B. Pichardo, G. Lake, and H. Throop. Effect of different stellar galactic environments on planetary discs - I. The solar neighbourhood and the birth cloud of the Sun. *MNRAS*, 418:1272–1284, December 2011. doi: 10.1111/j.1365-2966.2011.19579.x.
- V. Joergens, M. Bonnefoy, Y. Liu, A. Bayo, S. Wolf, G. Chauvin, and P. Rojo. OTS 44: Disk and accretion at the planetary border. *A&A*, 558:L7, October 2013. doi: 10.1051/0004-6361/201322432.
- D. Johnstone, D. Hollenbach, and J. Bally. Photoevaporation of Disks and Clumps by Nearby Massive Stars: Application to Disk Destruction in the Orion Nebula. *ApJ*, 499:758–776, May 1998.
- S. J. Kenyon and L. Hartmann. Pre-Main-Sequence Evolution in the Taurus-Auriga Molecular Cloud. *ApJS*, 101:117, November 1995. doi: 10.1086/192235.
- H. Kobayashi and S. Ida. The Effects of a Stellar Encounter on a Planetesimal Disk. *Icarus*, 153:416–429, October 2001. doi: 10.1006/icar.2001.6700.

- C. M. Koepferl, B. Ercolano, J. Dale, P. S. Teixeira, T. Ratzka, and L. Spezzi. Disc clearing of young stellar objects: evidence for fast inside-out dispersal. *MNRAS*, 428:3327–3354, February 2013. doi: 10.1093/mnras/sts276.
- C. J. Lada. Star formation - From OB associations to protostars. In M. Peimbert and J. Jugaku, editors, *Star Forming Regions*, volume 115 of *IAU Symposium*, pages 1–17, 1987.
- C. J. Lada and E. A. Lada. Embedded Clusters in Molecular Clouds. *ARA&A*, 41:57–115, 2003. doi: 10.1146/annurev.astro.41.011802.094844.
- C. J. Lada and B. A. Wilking. The nature of the embedded population in the Rho Ophiuchi dark cloud - Mid-infrared observations. *ApJ*, 287:610–621, December 1984. doi: 10.1086/162719.
- CharlesJ. Lada. On the Road to Understanding Star Formation. In W. Wamsteker, M.S. Longair, and Y. Kondo, editors, *Frontiers of Space And Ground-Based Astronomy*, volume 187 of *Astrophysics and Space Science Library*, pages 235–247. Springer Netherlands. ISBN 978-94-010-4341-0. doi: 10.1007/978-94-011-0794-5_25. URL http://dx.doi.org/10.1007/978-94-011-0794-5_25.
- R. B. Larson. The physics of star formation. *Reports on Progress in Physics*, 66:1651–1697, October 2003. doi: 10.1088/0034-4885/66/10/R03.
- Z.-Y. Li, R. Banerjee, R. E. Pudritz, J. K. Jørgensen, H. Shang, R. Krasnopolsky, and A. Maury. The Earliest Stages of Star and Planet Formation: Core Collapse, and the Formation of Disks and Outflows. *Protostars and Planets VI*, pages 173–194, 2014. doi: 10.2458/azu_uapress_9780816531240-ch008.
- D. Malmberg, F. de Angeli, M. B. Davies, R. P. Church, D. Mackey, and M. I. Wilkinson. Close encounters in young stellar clusters: implications for planetary systems in the solar neighbourhood. *MNRAS*, 378:1207–1216, July 2007. doi: 10.1111/j.1365-2966.2007.11885.x.
- D. Malmberg, M. B. Davies, and D. C. Heggie. The effects of fly-bys on planetary systems. *MNRAS*, 411:859–877, February 2011. doi: 10.1111/j.1365-2966.2010.17730.x.
- E. E. Mamajek. Initial Conditions of Planet Formation: Lifetimes of Primordial Disks. In T. Usuda, M. Tamura, and M. Ishii, editors, *American Institute of Physics Conference Series*, volume 1158 of *American Institute of Physics Conference Series*, pages 3–10, August 2009. doi: 10.1063/1.3215910.

- E. E. Mamajek, S. A. Barenfeld, V. D. Ivanov, A. Y. Kniazev, P. Väisänen, Y. Beletsky, and H. M. J. Boffin. The Closest Known Flyby of a Star to the Solar System. *ApJ*, 800: L17, February 2015. doi: 10.1088/2041-8205/800/1/L17.
- R. K. Mann and J. P. Williams. Protoplanetary disk masses in the Orion nebula cluster. In *Astronomical Society of India Conference Series*, volume 4 of *Astronomical Society of India Conference Series*, page 35, 2012.
- R. K. Mann, S. M. Andrews, J. A. Eisner, J. P. Williams, M. R. Meyer, J. Di Francesco, J. M. Carpenter, and D. Johnstone. Protoplanetary Disk Masses in the Young NGC 2024 Cluster. *ApJ*, 802:77, April 2015. doi: 10.1088/0004-637X/802/2/77.
- M. J. McCaughrean and C. R. O'dell. Direct Imaging of Circumstellar Disks in the Orion Nebula. *AJ*, 111:1977, May 1996. doi: 10.1086/117934.
- A. Moór, Á. Kóspál, P. Ábrahám, D. Apai, Z. Balog, C. Grady, T. Henning, A. Juhász, C. Kiss, A. V. Krivov, N. Pawellek, and G. M. Szabó. Stirring in massive, young debris discs from spatially resolved Herschel images. *MNRAS*, 447:577–597, February 2015. doi: 10.1093/mnras/stu2442.
- A. Morbidelli and H. F. Levison. Scenarios for the Origin of the Orbits of the Trans-Neptunian Objects 2000 CR₁₀₅ and 2003 VB₁₂ (Sedna). *AJ*, 128:2564–2576, November 2004. doi: 10.1086/424617.
- Z. E. Musielak and B. Quarles. The three-body problem. *Reports on Progress in Physics*, 77(6):065901, June 2014. doi: 10.1088/0034-4885/77/6/065901.
- C. R. O'dell. Observational properties of the Orion Nebula proplyds. *AJ*, 115:263, January 1998. doi: 10.1086/300178.
- C. Olczak, S. Pfalzner, and R. Spurzem. Encounter-triggered Disk Mass Loss in the Orion Nebula Cluster. *ApJ*, 642:1140–1151, May 2006. doi: 10.1086/501044.
- E. C. Ostriker. Capture and induced disk accretion in young star encounters. *ApJ*, 424: 292–318, March 1994. doi: 10.1086/173890.
- J. E. Owen, B. Ercolano, C. J. Clarke, and R. D. Alexander. Radiation-hydrodynamic models of X-ray and EUV photoevaporating protoplanetary discs. *MNRAS*, 401: 1415–1428, January 2010. doi: 10.1111/j.1365-2966.2009.15771.x.
- J. E. Owen, C. J. Clarke, and B. Ercolano. On the theory of disc photoevaporation. *MNRAS*, 422:1880–1901, May 2012. doi: 10.1111/j.1365-2966.2011.20337.x.
- S. Pfalzner. Spiral Arms in Accretion Disk Encounters. *ApJ*, 592:986–1001, August 2003. doi: 10.1086/375808.

- S. Pfalzner. Angular Momentum Transfer in Star-Disk Encounters: The Case of Low-Mass Disks. *ApJ*, 602:356–362, February 2004. doi: 10.1086/381023.
- S. Pfalzner. Early evolution of the birth cluster of the solar system. *A&A*, 549:A82, January 2013. doi: 10.1051/0004-6361/201218792.
- S. Pfalzner and C. Olczak. Gravitational instabilities induced by cluster environment? The encounter-induced angular momentum transfer in discs. *A&A*, 462:193–198, January 2007. doi: 10.1051/0004-6361:20066037.
- S. Pfalzner, S. Umbreit, and T. Henning. Disk-Disk Encounters between Low-Mass Protoplanetary Accretion Disks. *ApJ*, 629:526–534, August 2005a. doi: 10.1086/431350.
- S. Pfalzner, P. Vogel, J. Scharwächter, and C. Olczak. Parameter study of star-disc encounters. *A&A*, 437:967–976, July 2005b. doi: 10.1051/0004-6361:20042467.
- A. Porras, M. Christopher, L. Allen, J. Di Francesco, S. T. Megeath, and P. C. Myers. A Catalog of Young Stellar Groups and Clusters within 1 Kiloparsec of the Sun. *AJ*, 126:1916–1924, October 2003. doi: 10.1086/377623.
- WH Press, SA Teukolsky, WT Vetterling, and BP Flannery. Numerical Recipes in FORTRAN, the Art of Scientific Computing, 2nd edn Cambridge University Press, 1992.
- J. E. Pringle. Accretion discs in astrophysics. *ARA&A*, 19:137–162, 1981. doi: 10.1146/annurev.aa.19.090181.001033.
- Á. Ribas, B. Merín, H. Bouy, and L. T. Maud. Disk evolution in the solar neighborhood. I. Disk frequencies from 1 to 100 Myr. *A&A*, 561:A54, January 2014. doi: 10.1051/0004-6361/201322597.
- H. Rickman, C. Froeschlé, C. Froeschlé, and G. B. Valsecchi. Stellar perturbations on the scattered disk. *A&A*, 428:673–681, December 2004. doi: 10.1051/0004-6361:20041109.
- G. P. Rosotti, J. E. Dale, M. de Juan Ovelar, D. A. Hubber, J. M. D. Kruijssen, B. Ercolano, and S. Walch. Protoplanetary disc evolution affected by star-disc interactions in young stellar clusters. *MNRAS*, 441:2094–2110, July 2014. doi: 10.1093/mnras/stu679.
- G. P. Rosotti, B. Ercolano, and J. E. Owen. The long-term evolution of photoevaporating transition discs with giant planets. *ArXiv e-prints*, September 2015.
- A. Scally and C. Clarke. Destruction of protoplanetary discs in the Orion Nebula Cluster. *MNRAS*, 325:449–456, August 2001. doi: 10.1046/j.1365-8711.2001.04274.x.
- N. I. Shakura and R. A. Sunyaev. Black holes in binary systems. Observational appearance. *A&A*, 24:337–355, 1973.

- A. Sicilia-Aguilar, L. W. Hartmann, G. Fürész, T. Henning, C. Dullemond, and W. Brandner. High-Resolution Spectroscopy in Tr 37: Gas Accretion Evolution in Evolved Dusty Disks. *AJ*, 132:2135–2155, November 2006. doi: 10.1086/508058.
- R. Spurzem, M. Giersz, D. C. Heggie, and D. N. C. Lin. Dynamics of Planetary Systems in Star Clusters. *ApJ*, 697:458–482, May 2009. doi: 10.1088/0004-637X/697/1/458.
- M. Steinhausen, C. Olczak, and S. Pfalzner. Disc-mass distribution in star-disc encounters. *A&A*, 538:A10, February 2012. doi: 10.1051/0004-6361/201117682.
- H. Störzer and D. Hollenbach. Photodissociation Region Models of Photoevaporating Circumstellar Disks and Application to the Proplyds in Orion. *ApJ*, 515:669–684, April 1999. doi: 10.1086/307055.
- I. Thies, P. Kroupa, and C. Theis. Induced planet formation in stellar clusters: a parameter study of star-disc encounters. *MNRAS*, 364:961–970, December 2005. doi: 10.1111/j.1365-2966.2005.09644.x.
- A. Toomre. On the gravitational stability of a disk of stars. *ApJ*, 139:1217–1238, May 1964. doi: 10.1086/147861.
- C. A. Trujillo and S. S. Sheppard. A Sedna-like body with a perihelion of 80 astronomical units. *Nature*, 507:471–474, March 2014. doi: 10.1038/nature13156.
- S. M. Vicente and J. Alves. Size distribution of circumstellar disks in the Trapezium cluster. *A&A*, 441:195–205, October 2005. doi: 10.1051/0004-6361:20053540.
- K. Vincke and S Pfalzner. Cluster dynamics largely shapes protoplanetary disc sizes. subm.
- K. Vincke, A. Breslau, and S. Pfalzner. Strong effect of the cluster environment on the size of protoplanetary discs? *A&A*, 577:A115, May 2015. doi: 10.1051/0004-6361/201425552.
- S. J. Weidenschilling. The distribution of mass in the planetary system and solar nebula. *Ap&SS*, 51:153–158, September 1977. doi: 10.1007/BF00642464.
- C. Weidner, P. Kroupa, and I. A. D. Bonnell. The relation between the most-massive star and its parental star cluster mass. *MNRAS*, 401:275–293, January 2010. doi: 10.1111/j.1365-2966.2009.15633.x.
- P. R. Weissman. Stellar perturbations of the cometary cloud. *Nature*, 288:242, November 1980. doi: 10.1038/288242a0.
- J. P. Williams and L. A. Cieza. Protoplanetary Disks and Their Evolution. *ARA&A*, 49: 67–117, September 2011. doi: 10.1146/annurev-astro-081710-102548.

H.-X. Zhang, Y. Gao, M. Fang, H.-B. Yuan, Y. Zhao, R. Chang, X. Jiang, X.-W. Liu, A. Luo, H. Ma, Z. Shao, and X. Wang. Evolutionary Stages and Disk Properties of Young Stellar Objects in the Perseus Cloud. *ArXiv e-prints*, June 2015.

